Helsinki University of Technology Doctoral Theses in Materials and Earth Sciences

Espoo 2005 TKK-ME-DT-3

STUDIES ON GAS-LIQUID MASS TRANSFER IN ATMOSPHERIC LEACHING OF SULPHIDIC ZINC CONCENTRATES

Doctoral Thesis

Toni Kaskiala

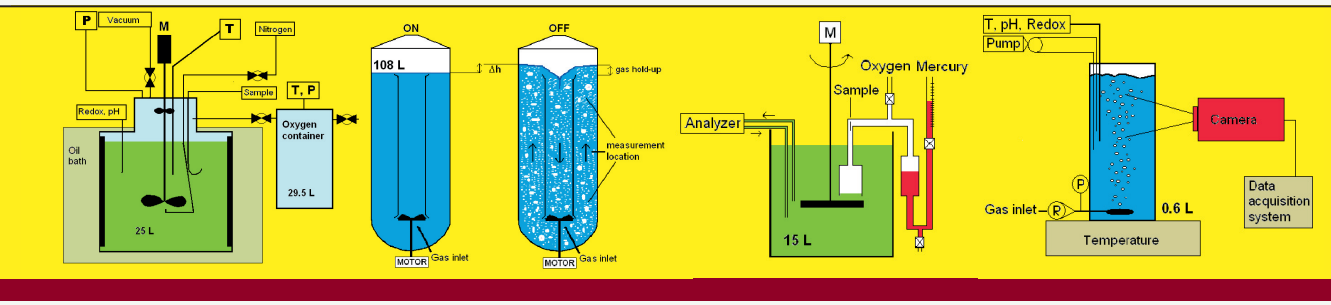

TEKNILLINEN KORKEAKOULU
TEKNISKA HÖGSKOLAN
HELSINKI UNIVERSITY OF TECHNOLOGY
TECHNISCHE UNIVERSITÄT HELSINKI
UNIVERSITE DE TECHNOLOGIE D'HELSINKI

Helsinki University of Technology Doctoral Theses in Materials and Earth Sciences
Laboratory of Materials Processing and Powder Metallurgy
Espoo 2005 TKK-ME-DT-3

STUDIES ON GAS-LIQUID MASS TRANSFER IN ATMOSPHERIC LEACHING OF SULPHIDIC ZINC CONCENTRATES

Toni Kaskiala

Dissertation for the degree of Doctor of Science in Technology to be presented with due permission of the Department of Materials Science and Engineering for public examination and debate in Auditorium 1 at Helsinki University of Technology (Espoo, Finland) on the 12th of May, 2005, at 12 noon.

Helsinki University of Technology
Department of Materials Science and Engineering
Laboratory of Materials Processing and Powder Metallurgy

Teknillinen korkeakoulu
Materiaalitekniikan osasto
Materiaalien valmistustekniikan ja jauhemetallurgian laboratorio

Helsinki University of Technology
Laboratory of Materials Processing and Powder Metallurgy
P.O. Box 6200
FI-02015 TKK

Available in pdf-format at http://lib.hut.fi/Diss/

Cover: Schematic pictures of the experimental setups from left modified autoclave, pilot water model, mass transfer equipment and bubble swarm system.

ISBN 951-22-7664-X
ISBN 951-22-7665-8 (electronic)
ISSN 1795-0074

HeSE print
Helsinki 2005

ABSTRACT

In this work, the mass transfer of oxygen in the atmospheric leaching process of zinc sulphide was investigated. Four new experimental apparatus items suitable for this purpose were designed and developed. The experiments conducted with the *water model* were focused on volumetric mass transfer, gas and liquid flow patterns, gas dispersion and bubble size. The effects of liquid properties and temperature on bubble size were examined with the *bubble swarm system*. Mass transfer coefficients, k_L, between oxygen and different liquids were measured with *mass transfer equipment*. Modified high-temperature and pressure *autoclave* was used to determine the oxygen consumption rates in leaching conditions. The experimental set-ups and program carried out are discussed and the errors and problems associated with the techniques reviewed.

The results revealed, amongst other occurrences, that the non-coalescence of bubbles occurs and the bubble size is controlled by the formation and breakage close to the impeller. According to the experiments, it seems to be possible to control the foaming and the surface aeration by adjusting the liquid volume and gas flow rate in the process. Too much liquid in the process increases the foaming, while too little increases the surface aeration. Furthermore, increasing the gas flow rate decreases foaming. Gas hold-up increased with mixing speed, while increasing the gas flow rate decreased the power consumption, as expected. Experimentally determined volumetric mass transfer values, k_La, varied between $(2.17\text{-}12.00)\times10^{-3}$ 1/s and mass transfer values, k_L, between $(13.81\text{-}19.24)\times10^{-5}$ m/s with oxygen and pure water. On the other hand, k_L values between oxygen and process solutions varied between $(1.5\text{-}11.32)\times10^{-5}$ m/s. Increasing electrolyte content decreased the mass transfer values notably, sulphuric acid and zinc sulphate additions having a stronger effect than sodium chloride. Both the determined mass transfer parameters were also strongly dependent on the mixing intensity. The oxygen consumption rate in the process solution varied between 0.018-0.075 mmol/(m^2s). Increasing the pressure and mixing intensity increased the oxygen consumption rate significantly, but temperature did not have a similar effect. Decreasing the dissolved zinc content in the solution increased the oxygen consumption rate significantly, whereas increasing the amount of concentrate only slightly increased the consumption rate. The experimental results of this work provide additional data for the improvement of existing leaching models, as well as the development of new ones.

KEYWORDS: leaching, atmospheric, zinc, sulphidic, concentrate, gas, bubble, interface, solubility, dissolution, mass transfer, coefficient, diffusion.

PREFACE

The research work presented in this thesis was carried out at Helsinki University of Technology (HUT), Laboratory of Materials Processing and Powder Metallurgy during years 2001-2005. I would like to express my sincere gratitude to my Professor *Michael Gasik* for the possibility to work and study in this laboratory and for all the support and confidence in me during the research. I am also truly thankful to the *staff of our Laboratory* for the pleasant working atmosphere, and especially *Sami Saarela, Janne Oksanen, Lauri Aspola, Kirsi Anttola* and *Tiia Juhala* for their assistance in conducting the experiments. I wish to gratefully acknowledge my supervisor Docent *Ari Jokilaakso* and Docent *Pekka Taskinen* and Dr. *Panu Talonen* for the supporting discussions during the work and useful comments and suggestions on the manuscript.

I would also like to thank my friends and colleagues *Rodrigo Grau, Luis Rudolphy, Nóra Schreithofer* and *Justin Salminen* at HUT for their help, support and coffee breaks during these years. A special thanks goes to my room-mate and colleague and most of all a friend *Jarmo Ylikerälä* for providing an encouraging working ambient. Facing the difficulties of the science together with you was always full of laughter and joy. Also for the *staff of the mechanical workshop* and laboratory engineer *Markku Kaskiala* for helping me to build all the experimental setups, I am truly thankful.

The financial support from of the *Outokumpu Oyj Foundation, Magnus Ehrnrooth Foundation* and *Cultural Foundation of Finland* is also acknowledged.

I am truly grateful for the following organized and less organized groups; *Pihkut, Töölönlahden valaat, Isännät, Tetrat, Rikos- ja rangaistuspotku, Levottomat Jalat, Pallo Hukassa 99, Kiffen, Ohari, Urheiluseura Jääahmat, Vuorenvarmat, Toisen aallon ratsastajat, Ilvesveikot* and *Pro Unicum Society* for the physical and spiritual support in so many different ways.

Profesor *Juan Yianatos*, estoy muy agradecido por la posibilidad de trabajar en U.T.F.S.M en Valparaíso, Chile. Su sincera pasión, dedicación a la ciencia y educación será siempre un buen ejemplo a mí. Estoy contento de haber conocido a un amigable grupo de laboratorio. Muchas gracias a todos mis amigos en Chile, especialmente a *Nicolas Bergh, Jorge Moltedo, Pascale Mansuy y Romina Bucarey*, por la hospitalidad y amabilidad que siempre recibí. También quiero expresar mi gratitud a todas las uvas del valle central que me apoyaron cuando estuve perdido en la selva de la ciencia.

Lämpimimmät kiitokset kuuluvat *vanhemmilleni* kaikesta tuesta ja poikkeuksellisesta kärsivällisyydestä kaikkien näiden opiskeluvuosien ajan. Kiitos Äiti! Vaimolleni *Katille* olen kiitollinen kaikesta siitä avusta, rohkaisusta, ruuasta ja rakkaudesta, jota olen työn valoisina ja synkkinä hetkinä saanut. Sinun lämpimässä ja ymmärtäväisessä seurassasi on kaikki niin paljon helpompaa.

In loving memory of *Ari*, whose courage and determination can be read between the lines of this book.

Espoo, April 2005, Toni Kaskiala

CONTENTS

LIST OF SYMBOLS AND ABBREVIATIONS

Symbol	Definition	Unit
A	Area	m^2
B	energy of translation	kJ
C	concentration	mol/m^3
D	diffusion coefficient	m^2/h
F	Helmholtz energy	kJ/mol
G	Gibbs energy	kJ/mol
H	Henry's law constant	bar or atm
J	mass transfer flux	mol/m^2s
K	overal mass transfer coefficient,	m/s
K	constant	-
M	molarity	mol/dm^3
M	molecular weight	g/mol
N	Avogadro's number	$6.023x10^{23}$
N	mass transfer rate	mol/m^3s
P	power	W
P_i	pressure of gas i	bar
R	gas constant	J/Kmol
T	temperature	K, °C
V	volume	m^3
V	velocity	m/s
W	work	W
a	interfacial area per liquid volume	m^2/m^3
a_i	activity of substance i	-
a_i^o	standard activity of substance i	-
b	stoichiometric coefficient	-
c	concentration	mol/dm^3, g/dm^3
d	diameter	m, mm
e	electronic charge	$1.602x10^{-19}$ C
f	fugacity	-
g	gas	-
g	acceleration of gravity	kgm/s^2
j	solvent	
k	equilibrium constant, constant	mol/kg, -
k	Boltzmann's constant	$1.38x10^{-23}JK^{-1}$
k_L	liquid side mass transfer coefficient	m/s
k_G	gas side mass transfer coefficient	m/s
k_La	liquid side volumetric mass transfer coefficient	s^{-1}
l	liquid	-
m	molality	mol/kg H_2O
n	gas amount	mol
r	radius	m
s	solid, solute	
t	time	s
x	mol fraction	-
w	water, work	-, J

α	phase	-
β	phase	-
δ	boundary layer	m
ε	hold-up	%
ϕ	fugacity coefficient	-
γ	activity coefficient	J/m^2 or N/m
λ	interaction parameter	-
μ	chemical potential of substance i	J/mol
μ	dynamic viscosity	Ns/m^2, kg/ms
ν	interaction parameter	-
ν	gas flow rate	dm^3/min
ν	kinematic viscosity	m^2/s
ρ	density	kg/m^3
σ	surface area	m^2
σ	surface tension	N/m
τ	ion	mol
τ	torque	Nm
θ	exposure time	s
ψ	electrostatic potential	V
*	saturated gas	
$_0$	initial, zero	
$_0$	orifice	
$_e$	effective	
$_G$	gas	
$_L$	liquid	
$_s$	salt	
$_s$	superficial	

CHAPTER 1 INTRODUCTION

Hydrometallurgy is a specialized branch of extractive metallurgy dealing with metal recovery from ores, concentrates, and other metallurgical intermediate products by aqueous methods. The present annual world production of iron, steel, aluminium, copper, zinc, lead, nickel and magnesium is close to 1 billion tonnes PAL (2001). Based on current trends, metals are likely to remain one of the primary materials of choice for several decades to come. Most metals and their alloys are synthesized from sulphide, oxide and halide sources. The energy required for the production of metals is obtained mainly from carbon, hydrocarbons, and oxygen. The reactants and energy sources often contain many additional elements, such as sulphur, phosphorous, nitrogen, halogens and other metals. The process industries spend an estimated $500 billion annually worldwide in conceptual design, process engineering, detailed engineering, construction, start-up, plant operations, and maintenance for chemical, refining, polymer and power plants.

Metallic zinc is principally produced by two routes; hydrometallurgically, by electrolytic deposition from aqueous solutions, or pyrometallurgically, by reduction to metallic forms at a temperature so high that the metal is distilled off and subsequently recovered by condensation FUGLEBERG (1999). Zinc, which was formerly produced by pyrometallurgical processes, is now mainly produced using a roast-leach electrowinning process. The production is thus more efficient with respect to manpower, energy and pollution abatement. Furthermore, low-grade complex ores can be leached CORRIOU ET AL (1988).

The direct atmospheric leaching process for sulphidic zinc concentrates uses a relatively new technology, which is already utilised at both elevated and atmospheric pressures. However, the disadvantage of pressure leaching is normally associated with complicated process maintenance and equipment.

The leaching of zinc concentrates was investigated in order to increase the capacity of zinc production without roaster expansion or an increase of sulphuric acid production TAKALA (1999). At Boliden Kokkola Oy, this technology at atmospheric pressures has been utilized since 1998; expansion for the accommodation of this process was finished at the end of 2001. The expansion increased the production of the plant by up to 275 000 tons per year, making it the second largest plant in Europe and among the sixth largest in the world.

The objective in direct leaching is to obtain the zinc in solution directly from the sulphidic form from zinc sulphide concentrate. The concentrate, together with the slurry from the conversion process and acid from the electrolysis, is fed to the reactors where the leaching takes place by injecting oxygen into the slurry. Extraction of Zn well above 98% can be reached with a number of available concentrates FUGLEBERG (1998). The dissolved iron from conversion and from the concentrate is precipitated as jarosite. The sulphur concentrate is separated from the slurry by flotation and stored separately from the jarosite residue.

1.1 REASONS FOR THE THESIS

In the atmospheric leaching of sulphidic zinc concentrates, the oxygen acts as an oxidant in the dissolution. Injection and dispersion of oxygen into solution requires a significant effort. The availability of oxygen for reactions has an important effect on the kinetics of the whole process. DREISINGER AND PETERS (1987) found that in the oxygen absorption, ferrous oxidation by dissolved oxygen controlled the overall rate of leaching during the early stages of the process. Also, ADAMS AND MATHEW (1981) stated that, in moderately agitated stirred tank reactors, the reaction is likely to be limited by gas diffusion into the aqueous phase. In addition, the lack of poorly soluble oxygen in the solution is emphasized at atmospheric pressures.

Measurements or investigations of oxygen solubility in water and aqueous solutions have been carried out for many decades and the factors affecting the solubility are well known. Gas-liquid mass transfer is also well researched and several correlations for the mass transfer coefficient have been reported. However, as KASTANEK ET AL. (1993) stated, "Neither a comprehensive theory of bubble dispersion formation nor appropriate quantitative relations for hydrodynamic parameters of bubble beds has yet been developed for systems in which the liquid phase is formed by aqueous solutions of electrolytes."

It should also be stressed that none of the overall correlations for volumetric mass transfer coefficients k_La has universal applicability MOO-YOUNG AND BLANCH (1987). Therefore, to explain further the gas-liquid mass transfer phenomena it is important to study the behaviour of coefficients k_L and a independently FUKUMA ET AL. (1987).

For the new leaching process studied, no suitable correlations for gas mass transfer exist. Therefore, it was found crucial to define experimentally the gas-liquid mass transfer in direct atmospheric leaching of sulphuric zinc concentrates. The experimental results of this work provide additional data for the improvement of existing leaching models and the development of new ones.

A better understanding of the oxygen use may result in small improvements in process optimization and notable annual savings in chemicals and energy costs.

CHAPTER 2 THEORETICAL PART

2.1 ZINC PRODUCTION

Zinc is the fourth most-used metal in the world today, with a metal production of a million tonnes a year IZA (2004). The productivity of zinc mines has doubled over the past 30 years, together with metal and zinc demand, see Figure 1.

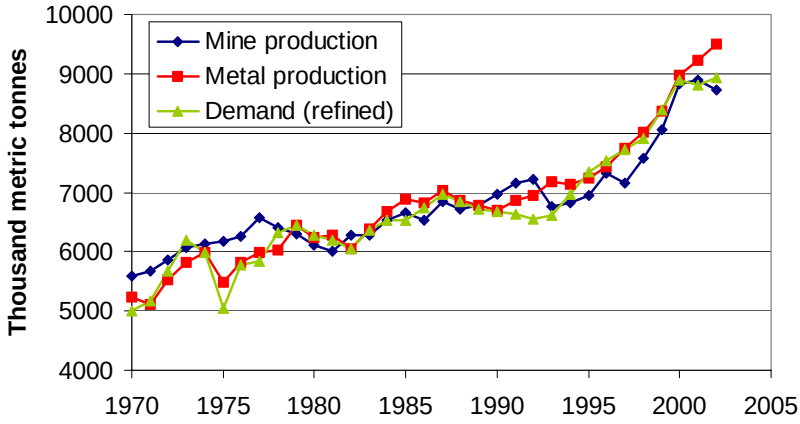

Figure 1 Zinc mine and metal production and refined zinc demand 1970-2002, IZA (2004)

Over half of the zinc is used for the galvanisation of other metals and in alloys such as brass. Approximately 70% of the produced zinc originates from primary resources and 30% from secondary IZA (2004).

The process industries spend an estimated $500 billion annually world-wide in conceptual design, process engineering, detailed engineering, construction, start-up, plant operations, and maintenance for chemical, refining, polymer and power plants. The present annual world production of iron/steel, aluminium, copper, zinc, lead, nickel and magnesium is close to 1 billion tonnes. Based on current trends, metals are likely to remain one of the primary materials of choice for several decades to come. Most metals and their alloys are synthesized from oxide, sulphide, and halide sources.

Metallic zinc is produced principally by two methods, pyro- or hydrometallurgically. Pyrometallurgically, the sulphidic zinc concentrate is roasted into ZnO and hydrometallurgically the concentrate is leached into solution. Hydrometallurgy is a specialized branch of extractive metallurgy dealing with metal recovery from ores, concentrates, and other metallurgical intermediate products by aqueous methods. The total energy consumption of the hydro- and pyrometallurgical alternatives are not significantly

different. In hydrometallurgy, the lower operating temperatures (and associated slower reaction rates) are compensated with larger volumes. Nickel, cadmium, copper, gold, silver, cobalt, uranium, vanadium, aluminium, magnesium, beryllium and zinc, for example, are produced hydrometallurgically AROMAA (1990) and BEVER (1986). Zinc appears in small amounts everywhere in nature and is considered an element essential for plants and animals. Like other metals, zinc is produced from minerals; altogether 55 different zinc minerals are known. The economical and most important ones are presented in Table I KIRK-OTHMER (1998) and HALAVAARA (1996).

Table I Eight different zinc minerals Kirk-Othmer (1998) and Halavaara (1996)

Name	Chemistry	Zinc content (wt -%)
Sphalerite	α-ZnS	38-67
Wurtzite	β- ZnS	48-67
Hemimorphite	$Zn_4[Si_2O_7](OH)_2H_2O$	54.2
Smithsonite	$ZnCO_3$	52.0
Hydrozincite	$Zn_5(OH)_6[CO_3]_2$	56.0
Zincite	ZnO	80.3
Willemite	$Zn_2[SiO_4]$	58.5
Franklinite	$(Zn,Fe,Mn)(Fe,Mn)_2O_4$	15-20

About 90 % of world zinc is produced from sulphidic zinc, mostly Sphalerite KIRK-OTHMER (1998). Zinc content in the ore varies between 2-12 % with an average of 4 % TAKALA (1999).

2.2 ATMOSPHERIC DIRECT LEACHING AS A PART OF ZINC PROCESS

Boliden Kokkola Oy in Finland started in 1969 and has been utilising the direct atmospheric leaching process for zinc production since 1998 TAKALA (1999). Factory combines the conventional roasting – leaching – solution purification – electrowinning process with direct leaching. The expansion of the direct leaching process during year 2001 increased the production of the plant by up to 275 000 tonnes per year and, furthermore, made it the second largest plant in Europe and the sixth largest in the world. The flow sheet of Boliden Kokkola Oy illustrates the use of pyro- and hydrometallurgical applications and parallel processing of zinc concentrate by roasting and direct leaching, see Figure 2.

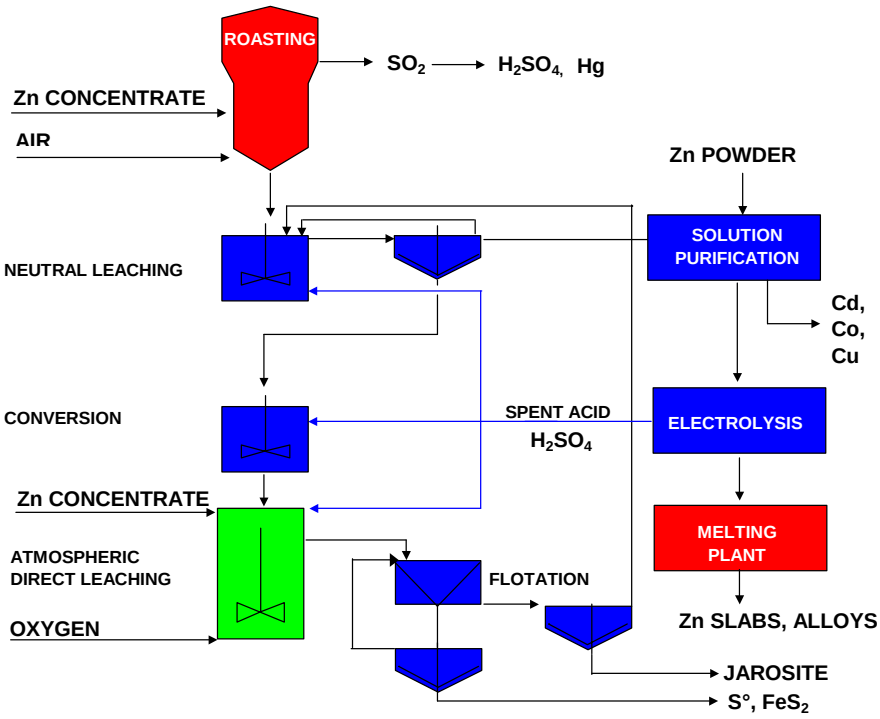

Figure 2 The flow sheet of the Boliden Kokkola Oy plant

Roasting is carried out in two parallel fluidized bed furnaces at about 920-960 ºC NYBERG (2004). The combustion air is blown through tuyeres in a grid and further through the fluid bed of material being roasted on the grid. The concentrate is fed onto the top of the bed. The oxygen reacts with the metal sulphides to produce oxides, which are soluble in sulphuric acid solution TAKALA (1999). The gases from the roaster are cooled in a waste-heat boiler and cleaned of dust in cyclones and electrostatic precipitators. The sulphur burns to sulphur dioxide SO_2, which is made into sulphuric acid at the separate plant. Mercury is removed from the gases before the acid production.

Practically all the iron is combined with zinc to give zinc ferrite $ZnO{\cdot}Fe_2O_3$ FUGLEBERG (1999). The solution containing dissolved zinc is removed to solution purification and the undissolved zinc ferrite is further leached in the conversion process and iron precipitated as complex compound called jarosite.

The new concentrate, together with the slurry from the conversion process and acid from the electrolysis, is fed to the direct leaching, where oxygen in used as an oxidizer. Pyrite FeS_2 and elementary sulphur S°, which does not dissolve at leaching temperatures below 100°C, are removed by flotation and iron is precipitated as jarosite FUGLEBERG (1998) and TAKALA (1999). The solution is circulated back to neutral leaching.

The solution purification is primarily for removing the impurities interfering with the electrolysis. All metals more noble than zinc, such as Cu, Co, Ni and Cd, are precipitated in a three-stage cementation. In the electrowinning, the zinc is reduced from the purified solution on aluminium cathodes as metallic zinc and the released sulphuric acid is used in

the leaching stages. Metallic zinc is stripped from the cathodes, melted and cast into different shapes and sent to customers.

2.3 LEACHING PROCESS

The oldest patents found by literature research concerning leaching of zinc were written in the early 20th Century EVANS (1907 AND 1909) and WILLIAMS AND BRANDLEY (1911). Zinc leaching has been investigated increasingly since the late fifties FORWARD AND VELTMAN (1959). During the late seventies and through the eighties, zinc leaching became popular; BJORLING (1973) made the following predictions: "It is inevitable that hydrometallurgical methods for treatment of low-grade ores and concentrates must take over an increasing part of the extraction of non-ferrous metals". During the past seven years, new interest has been shown in these methods, partly for environmental reasons and partly because of the availability of smaller and poorer concentrates.

Direct leaching methods result in the conversion of the sulphur in the feed to the elemental form, rather than to sulphur dioxide, decoupling zinc production from acid production BUBAN ET AL. (2000), BJORLING (1973).

Leaching sulphuric zinc as a sulphate is the most common alternative and has been used as an industrial scale application since 1981 PARKER AND ROMANCHUK (1980) and PARKER (1981). In a second plant, opened in 1983, and in a third opened in 1993 XUEZHONG AND LAND (1998), direct leaching can be operated with elevated pressures at 140-150 ºC, when reaction rates are higher compared to atmospheric pressures below 100 ºC. Conversion times for pressurized alternatives can be several times faster (2-5 h) than at atmospheric pressures (20-30 h) FUGLEBERG (1999). As a relatively new process, the atmospheric direct leaching of sulphuric zinc concentrates started operating in 1998 at Boliden Kokkola Oy.

Comparisons of direct leaching in elevated and atmospheric pressures have been made BUBAN ET AL. (2000) and, depending on the perspective, more suitable technology can be chosen. Maintenance of the pressurized equipment is more difficult and has greater explosion risks CHENG ET AL. (1994), FUGLEBERG (1999), whereas it also has a faster and higher overall recovery then at atmospheric pressures BUBAN ET AL (2000). Economically, pressurised technology is more favourable, according to BUBAN ET AL. (2000) or, according to TAKALA (1999), atmospheric is more favourable. However, both technologies are in use around the world.

At atmospheric pressures, the sulphuric zinc dissolves mainly with strong oxidizers. Leaching with sulphuric acid solutes has been very common, but also investigations have been made for using hydrogen chloride (HCl) AWAKURA (1986), LOTENS AND WESKER (1987) LOCHMANN AND PEDLÍK (1995), chlorous acid (HClO), nitric acid (HNO_3) BJORLING (1973), hydrogen peroxide (H_2O_2) LOTENS AND WESKER (1987), BALAZ AND EBERT (1991), dinitrogen oxide (NO_2), hydrogen nitride (HNO_3) LU AND XIE (1998) and injecting mixed gas (SO_2/O_2) ADAMS AND MATTHEW (1981), NAMI (1988), FERRON (2000), ZHANG (2000), or hydrogen sulphide (H_2S) and activated carbon CORRIOU ET AL. (1988). The addition of hydrogen sulphide inhibits the dissolution of the zinc sulphide, while the addition of activated carbon accelerates this dissolution by removal of hydrogen sulphide. Leaching with bacteria is also possible,

however, with long conversion times FOWLER AND CRUNDWELL (1999). A mixture of sulphuric acid and sodium chloride (NaCl) solution brought advantages when chloride ions prevented the large sulphur crystals to form.

2.3.1 Dissolution of sulphidic zinc concentrate

Zinc concentrate normally contains approximately 50% zinc, 30% sulphur and 5-15% iron. In zinc mineral sphalerite iron occurs mainly as sulphides replacing zinc in the crystal (Zn,Fe)S. When zinc sulphides are leached in sulphuric acid solution in oxidizing conditions in atmospheric reactors, the total reaction equation can be written following FERRON (2000) AND TAKALA (1999):

$$ZnS + H_2SO_4 + 0.5O_2 = ZnSO_4 + H_2O + S° \quad (1)$$

Iron acts as intermediary in the zinc sulphide leaching between the atmospheric oxygen and the mineral, and has an important catalytic role in the process. Ferric ions offer an efficient oxidant at moderate temperatures and suitable concentrations BJORLING (1973). The leaching rate due to direct oxygen leaching compared to iron is slow and therefore neglected, which was also observed by DREISINGER AND PETERS (1987). The oxidation is slow if the concentration of acid-soluble iron in the solution is insufficient AU-YEUNG AND BOLTON (1986), which is due to the acid-soluble iron providing the oxidizing transport:

$$2FeSO_4 + H_2SO_4 + 0.5O_2 \rightarrow Fe_2(SO_4)_3 + H_2O \quad (2)$$

$$ZnS + Fe_2(SO_4)_3 \rightarrow ZnSO_4 + 2FeSO_4 + S° \quad (3)$$

Usually the concentrate contains small amounts of other sulphides, enabling zinc to be replaced by any of the following in the formula: Fe, Pb, Cu, Cd, Ca. Other sulphides either precipitate or are separated in electrowinning.

The thermodynamic driving force of a dissolution reaction is the potential difference between the anodic and cathodic reactions PESONEN (2000). In the zinc leaching process, the potential difference is the equilibrium potential of a sulphide and the redox-potential of the solution. When the anodic and cathodic reactions are in equilibrium the state of the system can be described by mixed potential BOCKRIS AND KHAN (1993). Ferric-ions absorb on the concentrate surfaces and a simple oxidising-reduction (anodic and cathodic) reaction occurs as follows:

Anode: $S^{2-} \rightarrow 2e^- + S°$ (4)

Cathode: $2Fe^{3+} + 2e^- \rightarrow 2Fe^{2+}$ (5)

$$0.5O_2 + 2H^+ + 2e^- \rightarrow H_2O \quad (6)$$

Oxygen is also capable of oxidising zinc sulphide directly (6), but the oxygen concentration in the solution is too low so the cathodic reaction (5) with ferric iron prevails DREISING AND PETERS (1987). As the anodic dissolution reaction proceeds, a product

layer is formed. Elementary sulphur S^o either moves to solution or stays as a product layer on the mineral surface. Other products in the solution are zinc sulphate, iron(II)sulphate, iron(III)sulphate, iron(II) and iron(III) complexes and sulphides H_2S, HS^- and S^{2-}. According to thermodynamic calculations, the stable conditions for the listed phases are below pH value 2.4, as can be seen in the Eh-pH-diagram POURBAIX (1966) in Figure 3.

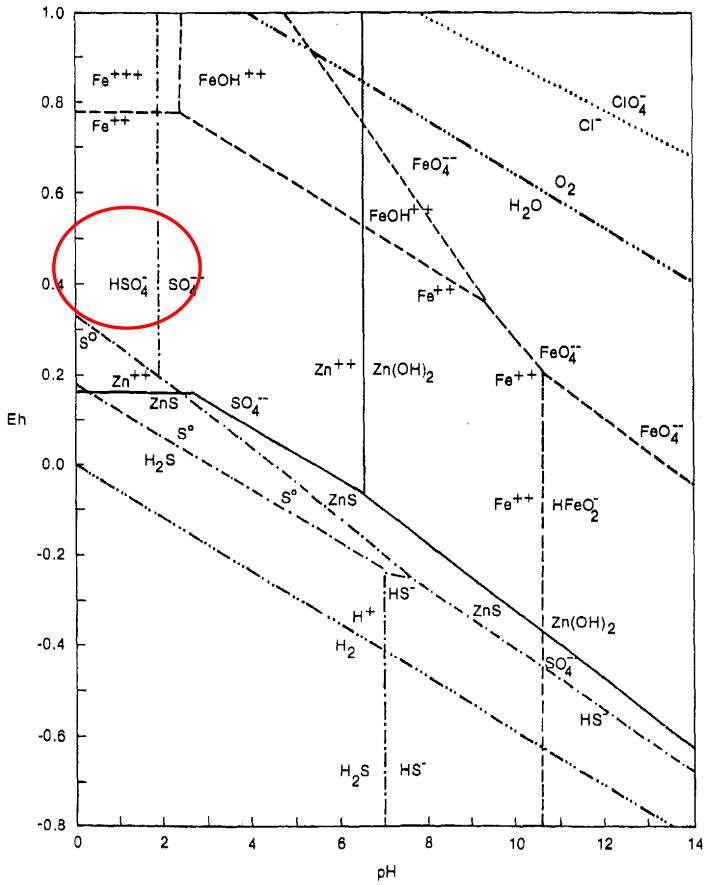

Figure 3 Pourbaix-diagram for aqueous sphalerite in 25 °C, 0.25 M Fe and 0.05 M Zn Pourbaix (1966) (Process conditions circled)

2.3.2 The shrinking-core model

According to several authors CRUNDWELL (1987), DREISINGER (1989), HALAVAARA (1996), HOLMES (2000), LOCHMANN AND PEDLIK (1995) and UUSIPAAVALNIEMI ET AL (1996), the sulphide mineral follows the shrinking-core model. In this model, the particle remains constant, but the area of the surface where the reaction takes place decreases with time CRUNDWELL (1987) and LOCHMANN AND PEDLIK (1995). The dissolution occurs first on the surface of the mineral, and then continues by diffusion through this layer, see Figure 4.

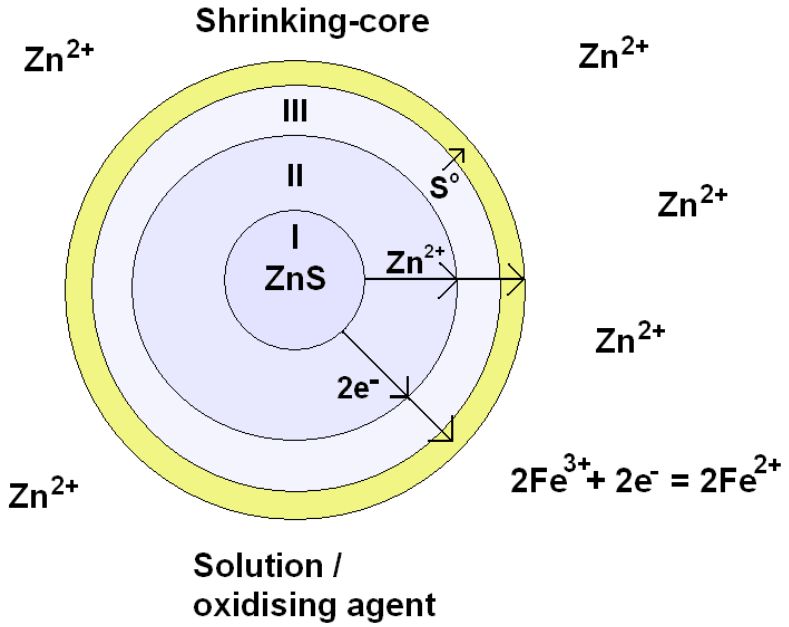

Figure 4 A simplified shrinking-core model of the oxidative dissolution of zinc sulphide.

The core, *phase I*, consists of the original zinc sulphide. As the dissolution begins, the zinc ions from *phase I* move to the solution and in *phase II* a zinc deficient sulphide is formed. A higher potential is needed for the dissolution through *phase II* than initially in *phase I*. As the dissolution continues, a layer, *phase III*, of zinc-deficient sulphide with elemental sulphur is formed and this layer has a yet higher dissolution potential. The *outermost layer* is of pure elemental sulphur, formed because all the zinc ions have moved to the solution. For dissolution to continue after each step, an increasing potential is required and the layers formed have to allow both mass and charge transfer through them. As the sulphur layer grows, it becomes more impenetrable and eventually the dissolution ceases PESONEN (2000). Electrochemically, the elemental sulphur is almost inert and does not react; it is also a poor conductor AROMAA (1990).

The dissolution rate of a sulphide mineral is affected both by charge transfer and mass transfer through the reaction product layer on the surface of the mineral. The mass transfer of ions is affected by the porosity, thickness and other structural factors and charge transfer, i.e., negative electrons and positive holes, as well as by electrical conductivity and thickness of the layer. The dissolution of sulphuric zinc concentrate takes a combination of the following kinetic steps RYTIOJA (1997):

1. The mass transfer of reagents and products between liquid-solid interface.
2. The diffusion of reagents and products through the product layer between the unreact core and particle surface.
3. Chemical reactions.
4. Charge transfer reactions.

If the mass transfer through the liquid-solid interface is ignored, the dissolution can be classified according to diffusion or reaction as the limiting factor. The possible controlling factors are the reactions on the surface or diffusion of reacting species through the porous product layer, or a combination of them.

In the early stages of the dissolution, the rate-limiting step for the dissolution is the charge transfer reaction; the shrinking-core model for spherical geometry adopts the following form LOCHMANN AND PEDLIK (1995) and BOBECK AND SU (1985):

$$k_c t_c = 1 - (1 - X)^{\frac{1}{3}}, \tag{7}$$

where X is the conversion degree given by $1-(r/r_o)^3$, t_c the reaction time elapsed and k_c the reaction rate coefficient controlled by surface reaction. The coefficient k_c is defined as follows RYTIOJA 1997:

$$k_c = \frac{Mbc_a}{\rho_s r_0} k_s, \tag{8}$$

where M is the molecular weight of the sulphide mineral, b the stoichiometric coefficient, c_a the concentration of Fe^{3+}, ρ_s the specific density of mineral, r_0 the initial radius of the particle and k_s the reaction rate for surface reaction.

If the product layer stays on the surface and the diffusion rate decreases, the reaction becomes diffusion controlled and the shrinking-core model acquires the following form NEOU-SYNGOUNA (1990) and BOBECK AND SU (1985):

$$k_d t_d = 1 - \frac{2}{3} X - (1 - X)^{\frac{2}{3}}, \tag{9}$$

where t_d is the time elapsed and k_d the reaction rate coefficient controlled by diffusion and defined as follows:

$$k_d = \frac{2Mbc_a}{\rho_s r_0^2} D_e \tag{10}$$

where D_e is the effective diffusion coefficient.

If the controlling factor is a combination of electrochemical surface reaction and diffusion through the product layer, the total time of dissolution is a sum of times: $t = t_c + t_d$. The shrinking-core model acquires the form HALAVAARA (1996), RASTAS (1986) and BOBECK AND SU (1985):

$$\frac{Mbc_a k_s D_e}{\rho_s r_0^2} t = \frac{D_e}{r_0}\left[1 - (1 - X)^{\frac{1}{3}}\right] + \frac{k_s}{2}\left[1 - \frac{2}{3} X - (1 - X)^{\frac{2}{3}}\right] \tag{11}$$

CRUNDWELL (1987) and DREISINGER ET AL. (1990) suggest that the sphalerite dissolution, sulphuric acid with ferric sulphate, obeys the reaction controlled shrinking-core mechanism. Also PALENCIA PEREZ (1990) supports the same theory following

experiments carried out using ferric sulphide and ferric chloride media. Kinetic studies of sphalerite leaching under oxidising conditions below the melting point of sulphur (119 °C) have shown that initially the reaction is under reaction control, whereas after about 50-70% leaching the development of a porous layer of sulphur brings the reaction under diffusion control ARAUCO AND DOYLE (1986), BOBECK AND SU (1985), LOCHMANN AND PEDLIK (1995), HALAVAARA (1996), AALTONEN (2002).

2.3.3 Factors affecting zinc sulphides oxidation

Increasing the temperature increases the reaction rate constant k_c values significantly after temperatures of approximately 80 °C, as can be seen from the experimental results of HALAVAARA (1996) in Figure 5.

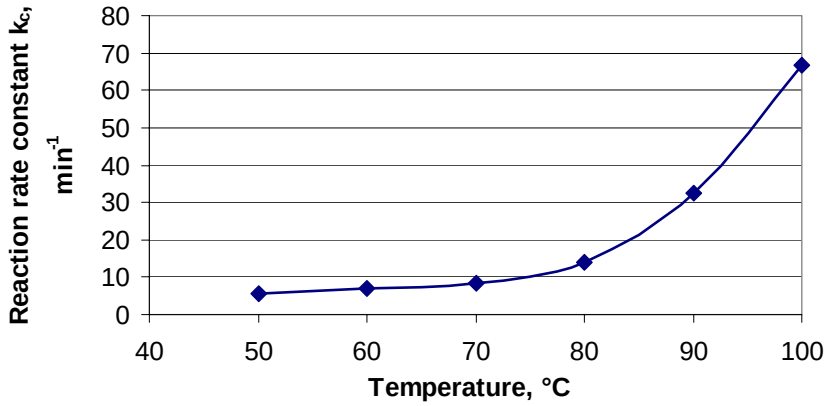

Figure 5 Experimental values for reaction rate constant k_c in sulphuric zinc leaching, Halavaara (1996)

The activation energies calculated from the reaction rates (angular coefficient) gave values 29.5 kJ/mol for the temperature range 50-80 °C and 74.4 kJ/mol for the temperature range 80-100 °C. The activation energy E_a of the reaction represents the effect of temperature on the rate of reaction. This relation between temperature and the rate of reaction is given by the Arrhenius equation:

$$k_c = Ae^{\frac{-E_a}{RT}}, \tag{12}$$

where A is the pre-exponential factor, k_c the rate constant of the reaction, R the molar gas constant and T the absolute temperature. The logarithmic values of the equation (12) describe well the two different types of controlling factors at temperatures <70 °C and >80 °C, see Figure 6.

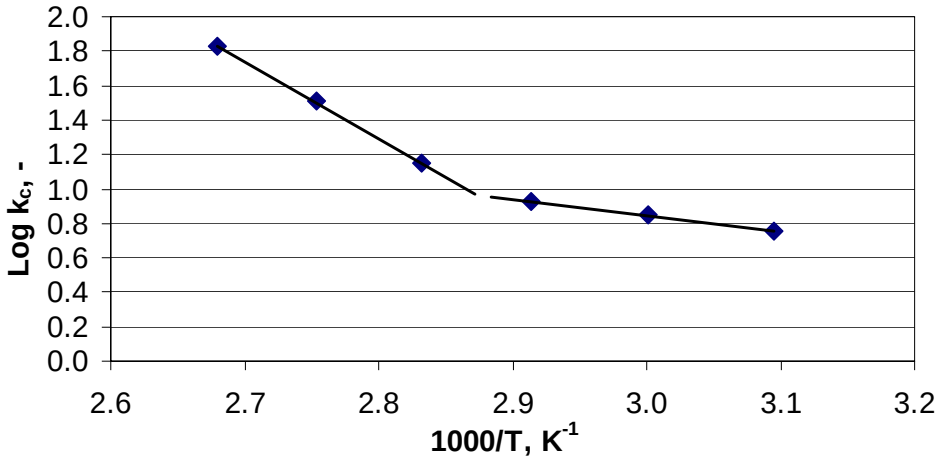

Figure 6 Logarithmic values for reaction rate constant k_c in sulphuric zinc leaching, Halavaara (1996)

The higher the activation energy, the greater the effect temperature has on the rate of reaction. Diffusion is moderately dependent on temperature, and the activation energies for diffusion through liquid film are 4.2-12.6 kJ/mol., whereas for chemical reactions the values are greater than 40 kJ/mol. HALAVAARA (1996) and are therefore highly dependent on temperature. When the rate-limiting step is diffusion through a porous layer, the apparent activation energies lie between these two values. The activation energy values for the zinc sulphide dissolution found in the literature are listed in Table II.

Table II Activation energies for the dissolution of zinc sulphide according to different sources

Source	T (°C)	$[Fe^{3+}]$	$[H_2SO_4]$	E_a (kJ/mol)
Halavaara (1996)	50-80	0.3 M	0.25 M	29.5
Halavaara (1996)	80-100	0.3 M	0.25 M	74.4
Palencia Perez (1990)	50-90	0.3 M	0.3 M	41-72
Crundwell (1987)	78	0.5 M	0.1 M	46
Verbaan and Crundwell (1986)	25-85	0.4 M	0.1 M	56.64

The amount of iron in sphalerite mineral has been shown to have an increasingly strong effect on the rate of dissolution BOBECK AND SU (1985), HALAVAARA (1996), VERBAAN AND MULLINGER (1980), AALTONEN (2002). The different concentrate

composition was found to affect the dissolution only at the early stages of the conversion KANTANEN (1996).

PALENCIA PEREZ AND DUTRIZAC (1991) found the dissolution rate to increase with more efficient stirring. However, HALAVAARA (1996) AND AALTONEN (2002) did not find a significant increase in dissolution rate with stirring.

KAMMEL ET AL. (1987) reported an increase in zinc extraction by grinding sphalerite to a smaller particle size. Grinding increased not only the surface area, but also the amount of lattice defects in the mineral, which can affect both the conductivity and stability of the crystals. BALAZ AND EBERT (1991) found also mechanical activation by grinding to increase the rate of dissolution of sphalerite in hydrogen peroxide.

At lower temperatures, an elemental sulphur layer does not immediately block the surface of the particle. However, at temperatures above the melting point of sulphur, 119 °C, the diffusion limiting layer appears even faster. The sulphur layer can be affected by the use of surface-active substances, such as lignosulphonate or quebracho, which cause the sulphur to form droplets on the surface HALAVAARA (1996). LOCHMANN AND PEDLÍK (1995) found that the use of 1 g/l lignosulphonate in solution increased conversion significantly by transforming the surface sulphur into porous form, which was also noticed by OWUSU ET AL. (1995) and OWUSU (1992). OWUSU (1992) reported in their research: "when 0.3 g/L or more of ligninsulphonate was added to the solution the contact angle between liquid sulphur and the same solution increased from 80±5° to 148±5°. As a result, the work of adhesion between liquid sulphur and zinc sulphide falls from 63.7 mJ/m^2 to about 5.3 mJ/m^2". The results indicated that adsorption of ligninsulphonate occurs on both the mineral aqueous and the sulphur-aqueous interfaces.

2.3.4 The oxidation of ferrous iron

The oxidation of Fe(II) in acidic aqueous sulphate solutions with dissolved molecular oxygen is commonly employed in many hydrometallurgical processes such as leaching. In the direct leaching conditions, ferrous ion is oxidised by oxygen MATHEWS AND ROBINS (1972), VERBAAN AND CRUNDWELL (1986) as follows:

$$4Fe^{2+} + 4H^{+} + O_2 = 4Fe^{3+} + 2H_2O \quad (13)$$

Different reaction paths *a, b* and *c* have been proposed. Path (I-IV)*a* by MATHEWS AND ROBINS (1972) being:

Ia $Fe^{2+} + O_2 \leftrightarrow FeO_2^{2+}$

IIa $FeO_2^{2+} + Fe^{2+} + H_2O \rightarrow 2Fe^{3+} + OH^- + O_2H^-$

IIIa $O_2H^- + H^+ \rightarrow H_2O_2$

IVa $H_2O_2 \rightarrow H_2O + 0.5O_2$

Path (I-III)*b* consists of three steps MATHEWS AND ROBINS (1972):

Ib $Fe^{2+} + O_2 \leftrightarrow FeO_2^{2+}$

IIb $Fe^{2+} + H_2O \leftrightarrow FeOH^{+} + H^{+}$

IIIb $2H_2O + FeO_2^{2+} + FeOH^{+} \rightarrow 2Fe^{3+} + 5OH^{-}$

RÖNNHOLM ET AL. (2002) proposed a congestive reaction mechanism (I-VI)*c*, according to which the oxidation proceeds through the formation of an intermediate peroxide complex between dissolved oxygen and ferrous ions, and the cleavage of the O-O-bond of the complex:

Ic $O_2 + Fe^{2+} \leftrightarrow (Fe\text{-}O\text{-}O^*)^{2+}$

IIc $(Fe\text{-}O\text{-}O^*)^{2+} + Fe^{2+} \leftrightarrow (Fe\text{-}O\text{-}O\text{-}Fe)^{4+}$

IIIc $(Fe\text{-}O\text{-}O\text{-}Fe)^{4+} + Fe^{2+} \leftrightarrow (Fe_2\text{-}O)^{4+} + (O\text{-}Fe)^{2+}$

IVc $(O\text{-}Fe)^{2+} + Fe^{2+} \leftrightarrow (Fe_2\text{-}O)^{4+}$

Vc $(Fe_2\text{-}O)^{4+} + H_3O^{+} \leftrightarrow OH^{-} + H_2O + 2Fe^{3+}$

VIc $H_3O^{+} + OH^{-} \leftrightarrow 2H_2O$

where $(Fe\text{-}O\text{-}O^*)^{2+}$ is an intermediate complex and the overall reaction formula (13). Steps Ic-IIc were assumed to be rate limiting, while steps IIIc-Vc merged into a pseudo-step. The overall rate of the ferrous ion oxidation has been described by several authors, see Table III.

Table III Rate equations for the oxidation of ferrous iron in H_2SO_4 by molecular oxygen

References	Rate equation, *r*	T (°C)	E_a (kJ/mol)
Mathews & Robins (1972)	$k\cdot[Fe^{2+}]^{1.84}\cdot[O_2]^{1.01}\cdot[H^{+}]^{-0.25}$	20-80	73.7
Chmielewski & Charewicz (1984)	$k\cdot[Fe^{2+}]^2\cdot p(O_2)$	50-130	56.9
Iwai et al. (1982)	$k_1\cdot[Fe^{2+}]^2\cdot p(O_2) +$ $k_2[SO_4^{2-}]\cdot[Fe^{2+}]^2\cdot p(O_2)$	70-90	51.6 (1) 94.4 (2)
Verbaan & Crundwell (1986)	$k\cdot[Fe^{2+}]^2\cdot[O_2]\cdot[H^{+}]^{-0.36}$	25-85	68.6

According to several authors, the oxidation of ferrous iron is of second order with respect to $[Fe^{2+}]$ AWAKURA (1986), IWAI ET AL. (1982), POHJOLA (1997), VERBAAN AND CRUNDWELL (1986) and with low ferrous concentrations of first

order with respect to [Fe^{2+}] CHMIELEWSKI AND CHAREWICZ (1984). IWAI ET AL. (1982) stated that the addition of ferric sulphate to the solution causes retardation in the oxidation reaction of [Fe^{2+}], which may be due to the decrease in the [SO_4^{2-}] ion activity through the formation of [Fe^{3+}] sulphate-complexes.

The dependency of the rate constant upon the concentration of sulphuric acid appears to increase the concentration less and to be independent of the concentration above 1 mol/dm^3 AWAKURA (1986), IWAI ET AL (1982), POHJOLA (1997) and CHMIELEWSKI AND CHAREWICZ (1984).

Oxidation of ferrous iron was found to be concentration in power -0.245 with respect to [H^+] MATHEWS AND ROBINS (1972), -0.36 VERBAAN AND CRUNDWELL (1986) and -0.6 AWAKURA (1986).

Oxidation rates in the presence of sulphates are far greater than without them. Cupric and zinc sulphate increases the kinetics of [Fe^{2+}] oxidation with dissolved molecular oxygen AWAKURA (1986) and MATHEWS AND ROBINS (1972). It is likely that the catalysis with copper is carried out through the cupric-cuprous redox couple DREISINGER AND PETERS (1987).

ADAMS AND MATTHEW (1981) stated that significant extractions of zinc and iron were achieved only within a very narrow temperature range, with dissolution maxima occurring at about 85 °C when using oxygen enriched with 10-12% sulphur dioxide. NAMI (1988) determined optimum amount of sulphur dioxide to increase the rate of dissolution to be equal or less than 2% in the gas mixture.

Considering the direct leaching conditions, approximations for the reaction rate constant are difficult to estimate. The ferrous iron-oxidation rate values found ranged from 4 to 22 ($dm^3 \cdot mol^{-1} \cdot min^{-1}) \cdot 10^{-3}$, taking into account the conditions closest to the direct sulphuric zinc concentrates leaching. The values of measured activation energies E_a vary between 51.6-73.7 (kJ/mol), which indicates that the ferrous iron-oxidation rate is limited by the chemical reaction. The values for the reaction rate constant k in different conditions were reported by different authors, see Table IV.

Table IV Ferrous iron-oxidation reaction rate constant k ($dm^3 \cdot mol^{-1} \cdot min^{-1}$) $\cdot 10^{-3}$ according to authors listed in left column

Author	P (bar)	T (°C)	$FeSO_4$ (mol/l)	H_2SO_4 (mol/l)	k $*10^{-7}$ (dm^3/mol Pa·min)
Iwai et al. (1982)	1	80	0.2	1	4.07
Iwai et al. (1982)	1	90	0.2	1	7.22
Pohjola (1997)	5-7	80	0.2	0.5	10.5
Pohjola (1997)	5-40	80	0.2	0.5	19.5
Verbaan& Crundwell (1986)	1	60	0.4	0.25	≅3
Verbaan & Crundwell (1986)	3	80	0.4	0.25	≅22
Verbaan & Crundwell (1986)	4.5	70	0.4	0.25	≅60
Vracar (1997)	10	50	0.18	<0.5	≅30

2.3.5 Ferric iron precipitation

The iron in the solution has the ability/tendency to form complex compounds called jarosites. The most favourable conditions for the precipitation of jarosites lie in the range 90-100 °C and pH in the range 1-2.5 HALAVAARA (1996). In the later stages of leaching, the iron is removed from the process when dissolved ferric iron precipitates as jarosite through the addition of ammonia (NH_4^+) TAKALA (1999). Overall reactions for the formation of jarosites can be written as KNUUTILA (1985), ARAUCO AND DOYLE (1986):

$$3Fe_2(SO_4)_3 + Me_2SO_4 + 12H_2O \rightarrow Me_2Fe_6(SO_4)_4(OH)_{12} + 6H_2SO_4 \quad (14),$$

where Me: NH_4^+, Na^+, K^+, Rb^+, Ag^+, Ti^+ and H_3O^+. Losses of divalent metals to alkali jarosites increase with increasing divalent metal concentrations, increasing pH or decreasing the Fe(III) concentration. Losses vary according to the metal in question, but rarely exceed 3% ARAUCO AND DOYLE (1986), HARVEY AND YEN (1998). The descending order for losses is:

$$Fe^{3+} > Cu^{2+} > Zn^{2+} > Co^{2+} > Ni^{2+} > Mn^{2+} > Cd^{2+}.$$

Precipitation of ferric iron can occur also as a Plumbojarosite as follows:

$$3Fe_2(SO_4)_3 + MeSO_4 + 12H_2O \rightarrow MeFe_6(SO_4)_4(OH)_{12} + 6H_2SO_4 \quad (15),$$

where Me: Pb^{2+} and Hg^{2+}. Other options available for the treatment of the ferrite residue are hematite or goethite or smelting processes. Advantages of removing iron as a jarosite are the high recovery from various concentrates and the ability to utilise heavy metal containing acids.

It is complicated to determine the kinetics of jarosite precipitation for process solutions because of the various metal ions available. According to TEIXEIRA (1986), the effects of temperature and seeding indicated that the precipitation reaction rate is controlled by a chemical reaction step occurring on the surface of the jarosite crystals. The effects of the chemical variables were explained in terms of mechanisms of adsorption, leading to an adequate correlation of the experimental rate data with the following semi-empirical model:

$$\frac{-d\left[Fe^{3+}\right]}{dt} = 6.4 \cdot 10^{-4} \frac{\left[Fe^{3+}\right]^{0.86}}{\left[H^+\right]^{0.63}\left[NH_4^+\right]^{1.8}} \quad (16)$$

The measurements were made in specified laboratory conditions, which, however, can give an estimation of the time scale and the effect of concentrations when the direct leaching conditions are borne in mind.

RASTAS (1986) and UUSIPAAVALNIEMI ET AL. (1996) determined the empirical equation for the precipitation of jarosite as follows:

$$\frac{-d\left[Fe^{3+}\right]}{dt} = k(T)\left[Fe^{3+}\right]^{\alpha}\left[H_2SO_4\right]^{\beta}\left[A^+\right]^{\gamma}\left[A - jar\right]^{\delta} \quad (17)$$

where the concentrations of ferric ion, sulphuric acid, cation A and jarosite are in brackets and the Greek characters α, β, δ and γ represent empirical constants that have been determined for different jarosites. The values of the exponents were determined as follows: $\alpha \cong$ 1.9-2.4 (Na, K, NH_4), $\beta \cong$ -3.5 to –2.2, $\gamma \cong$ 0.5-0.7 (Na, NH_4), $\gamma \cong$ -0.2 (K) and $\delta \cong$ 0.8-1.4 (Na, K, NH_4). The value of the coefficient k depends on temperature and varies between 1.0 and 1.7 $(g/l)^{1-\alpha-\beta-\delta-\gamma}\ h^{-1}$ at 95 °C.

2.4 GAS-LIQUID MASS TRANSFER

Mass transfer between gas and liquid is a basic fundamental phenomenon in process engineering. Chemical engineering operations can be divided into three different transfer phenomena: momentum, heat and mass transfer, which are presented with the same basic relation between driving force and resistance:

$$\text{Flux} = \frac{\text{driving force}}{\text{resistance}}$$

The basic equation to present mass transfer between gas and liquid can be written as:

$$\frac{\partial C}{\partial t} + v_L \nabla C = D\nabla^2 C + R\,, \tag{18}$$

where C is the concentration of absorpted gas A, t time, v_L liquid velocity, D (m^2/s) diffusion coefficient of gas A and R the consumption of gas A in reaction when present MERCHUK (1983). Since Equation 18 cannot generally be solved analytically and the boundary values are undefined, several models for mass transfer at the gas-liquid interface have been proposed. These models simplify the microscopic phenomena at the interface. The assumptions of the models include values known as the parameters (in this case, for example, time and distance).

The well-known Fick's law for molecular diffusion J_A (mol/m^2s) can be written as follows:

$$J = -D\left(\frac{dC}{dx}\right) \cong \frac{D}{\delta}(C_G - C_L) \tag{19}$$

The driving force of the molecular diffusion is the concentration difference between gas C_G and liquid C_L side of the interface over the thickness dx or δ (m) of the layer. The mass transfer coefficient K (m/s) is defined dividing the diffusion coefficient D by the thickness of the interface δ as follows:

$$K = \frac{D}{\delta} \tag{20}$$

The mass transfer coefficient K can be divided into gas k_G and liquid k_L side mass transfer coefficients (Equations 21 and 22):

$$k_G = \frac{D_G}{\delta_G} \tag{21}$$

$$k_L = \frac{D_L}{\delta_L}\,. \tag{22}$$

Combining Equations 19 and 20 gives the rewritten mass transfer flux of gas *A* through interface:

$$J_A = K(\Delta C), \tag{23}$$

where the mass transfer coefficient *K* consists of both gas and liquid side transfer coefficients as follows:

$$\frac{1}{K} = \frac{1}{Ek_G} + \frac{1}{k_L}, \tag{24}$$

where *E* is the angular coefficient in the saturation curve. If $k_G E << k_L$, the gas side mass transfer controls the total transfer. It is commonly accepted CUSSLER (1997) that the greater resistance for mass transfer is on the liquid side and $k_L << k_G E$, see Figure 7 for a schematic picture of the gas-liquid interface.

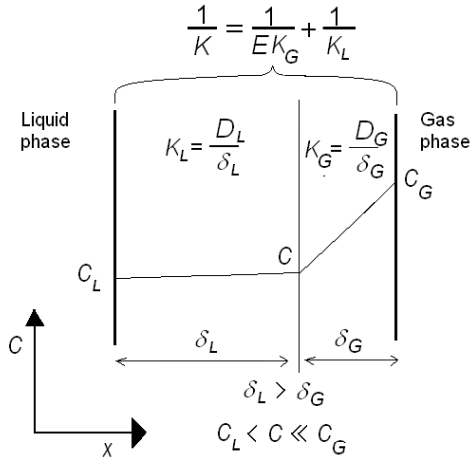

Figure 7 Schematic presentation of the gas-liquid interface, concentrations and the mass transfer coefficients K, k_L and k_G

This implies that $K \approx k_L$ and the formula of Fick's law (19) for gas and liquid mass transfer flux can be written as:

$$J \cong \frac{D_L}{\delta_L}(\Delta C) \cong k_L(C - C_L), \tag{25}$$

where the driving force is the concentration difference between saturated concentration of the gas in the bulk liquid C_L and concentration *C* in the liquid at the gas-liquid interface. If gas dissolves in the liquid without reacting, it is found experimentally that the rate of absorption of gas *A* is given as follows DANCKWERTS (1967):

$$N_A = k_L \frac{A}{V}\Delta C = k_L a \Delta C, \tag{26},$$

where N (mol/m^{3}s) is the mass transfer rate and a (m^2/m^3) is the gas-liquid interfacial area A per unit volume of fluid V. In experimental determinations, the parameters k_L and a are often combined as the volumetric liquid mass transfer coefficient k_La, which is usually presented as a function of process parameters.

2.4.1 Models

The film model, proposed by WHITMAN (1923), pictures a stagnant film of thickness δ at the surface of the liquid next to the gas. While the rest of the liquid is kept uniform in composition by agitation, the concentration in the film falls from C_0 at its surface to C_L at its inner edge; there is no convection in the film so dissolved gas crosses the film by molecular diffusion alone, see Figure 8.

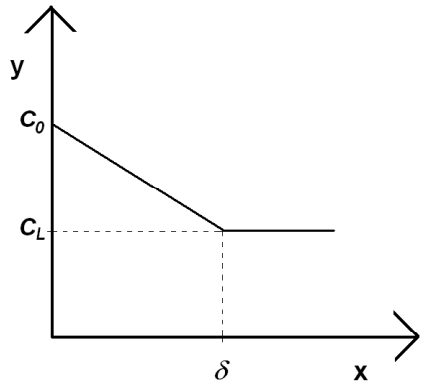

Figure 8 Concentration change in film model

In the film model, the constant boundary concentrations at the boundary layer are: $x = 0 \Rightarrow C = C_0$ and $x = \delta \Rightarrow C = C_L$. The concentration as a linear relation across the layer $0 \le x \le \delta$ can be written as:

$$C = -(C_0 - C_L)\frac{x}{\delta} + C_0 \qquad (27).$$

The molecular diffusion flux can be written as Equation (19):

$$J = -D\left(\frac{dC}{dx}\right)_{x=0} = \frac{D_L}{\delta}(C_0 - C_L),$$

while the film model leads to:

$$k_L = \frac{D_L}{\delta}.$$

The assumption of a stagnant, laminar-flow film next to the boundary in which the mass transfer resistance is highest is not appropriate under many practical flow conditions, which require the application of the Fick´w law for unsteady-state diffusion given below MOO-YOUNG AND BLANCH (1987):

$$\frac{\partial C}{\partial t} = D\frac{\partial^2 C}{\partial x^2} \tag{28},$$

where chemical reactions are neglible. To solve this equation, simplifying assumptions must be made, especially with regard to fluid behaviour. HIGBIE (1935) solved this problem according to his penetration model, which assumes that every element of surface is exposed to the gas for the same length of time, θ, before being replaced by liquid of the bulk composition. The model assumes that the composition of the film does not stay stagnant as in the film model MERCHUK (1983). During this short time, the element of liquid absorbs the same amount of gas per unit area as though it were stagnant and infinitely deep. The exposure time of θ is determined by the hydrodynamic properties of the system and is the only parameter required to account for their effect on the transfer coefficient k_L. Using appropriate boundary conditions: when $x = 0$ then $C = C_0$ at $0 < t < \theta$ and when $x > 0$ then $C = C_L$ at $t = 0$ and when $0 < t < \theta$ then $x = \infty$ and $C = C_L$, he deduced that the mass transfer coefficient takes the form:

$$k_L = 2\sqrt{\frac{D}{\pi\theta}} \tag{29}.$$

Mass transfer is dependent on the physical properties of the liquid and also the dynamics of the liquid, e.g., contact time θ.

DANCKWERTS (1951) questioned the hypothesis of a constant exposure time and postulated a random continuous renewal of surface elements at the interface according to his “surface renewal” as a more realistic situation. He introduced the statistical parameter *s* and found that:

$$k_L \propto \sqrt{sD} \tag{30}.$$

The difference from the penetration model is the contact time, which is not constant but can change. Mathematically, the difference is the boundary value of the contact time, which is not limited in the surface renewal model MERCHUK (1983).

TOOR AND MARCHELLO (1958) proposed a film-penetration model, in which a stagnant film of definite thickness exists at the surface, but is replaced piecewise from time to time by liquid having the bulk composition. If all the parameters are kept constant, then models correlate with the equation as follows:

$$k_L = \alpha D^n, \tag{31},$$

where the value *n* gets the following values: *n = 1* in the film model, *n = 0.5* represents both penetration and surface renewal model and the film-penetration model can get values $0.5 < n < 1$. Experimentally determined values were found as well between $0.5 < n < 1$ LEKHAL (1997). See also Table V of the collected data of the models.

Table V Collected data of the Film, Penetration and Surface removal models

Model	Film	Penetration	Surface removal
Presented	Whitman (1923)	Higbie (1935)	Danckwerts (1951)
Coefficient k_L	$k_L = \frac{D}{\delta}$	$k_L = \sqrt{\frac{4D}{\pi\theta}}$	$k_L = \sqrt{sD}$
Time dependence	No	Constant	Functional
Boundary conditions	$x = 0 \Rightarrow C = C_0$ $x = \delta \Rightarrow C = C_L$	When $x = 0$ and $t = 0$ then $C = C_L$ or $0 < t < \theta$ then $C = C_0$. When $x = \infty$ and $0 < t < \theta$ then $C = C_L$	When $x = 0$ and $t = 0$ then $C = C_L$. or $0 < t < \infty$ then $C = C_0$. When $x = \infty$ and $0 < t < \infty$ then $C = C_L$

2.4.2 Factors affecting gas-liquid mass transfer

The processes are usually operated according to optimum temperature, pressure, mixing, concentrations and the way of introducing the substances. To understand the hydrodynamic factors affecting the mass transfer rate, Equation (26) is divided into the following parts: volumetric liquid mass transfer coefficient k_La, liquid mass transfer coefficient k_L, gas-liquid interfacial area per liquid volume a, concentration driving force ΔC, superficial gas and liquid velocity Vs, and gas hold-up ε see Figure 9.

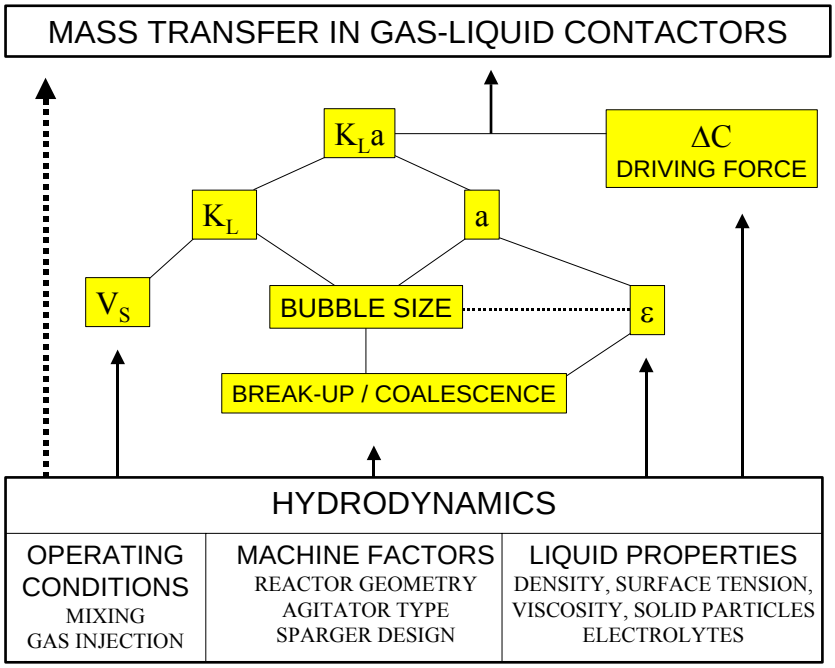

Figure 9 Relationship between the various factors affecting the mass transfer rates in a gas-liquid reactor

The overall mass transfer rate is complex and influenced by a number of physical parameters, operating conditions and machine factors WALTER AND BLANCH (1986). Each term has a special effect on and is therefore discussed separately.

2.4.2.1 Volumetric liquid mass transfer coefficient, $\mathbf{k_La}$

In experimental determinations, the parameters k_L and a are often combined as the volumetric liquid mass transfer coefficient k_La, which is usually presented as a function of process parameters. In practice, it is usually not possible to determine k_L and a separately by measurements of physical absorption, but it is possible in the case of k_La DANCKWERTS (1967), where process parameters represent operating parameters such as power input P, volume V_L and gas superficial flow rate υ_G. Volumetric liquid mass transfer coefficient k_La values are often presented to within a ±30% error level as follows VAN´T RIET (1979) and ZHU ET AL. (2001):

$$k_La = \kappa\left(\frac{P}{V_L}\right)^{\alpha}\upsilon_G^{\beta}, \tag{32}$$

where κ is constant and α and β are exponents. The values for α and β show a great variation: $0.4<\alpha<1$ and $0<\beta<0.7$. It is not unusual for the κ value to remain unmentioned VAN´T RIET (1979).

The volumetric mass transfer coefficient increases significantly when ion concentration in the solution is raised. The addition of electrolyte increases the gas hold-up, due to its influence on decreasing bubble size and the non-coalescence effect at both low and high pressures WILKINSON ET AL. (1994). Once a limit for non-coalescence concentration has been reached, the increase is much smaller. The distinction depends on P/V and υ_G. It increases at higher P/V values, hence the k_La´s for ionic solutions are more dependent on P/V than those for pure water VAN´T RIET (1979).

Volumetric mass transfer correlations are also dependent on the reactor type applied. For example, LETZEL ET AL. (1999) proved an increase of k_La with increasing pressure by the increase in total gas hold-up. Therefore, with high reactors, the hydrostatic pressure can be assumed to have an effect on k_La. VAN´T RIET (1979) and NIENOW (1996), on the subject of correlation with P/V, stated that there is no influence of stirrer geometry and the number of stirrers on mass transfer in non-viscous systems. However, ZHU ET AL. (2001) were able to increase the mass-transfer rate 17% by changing the impeller.

According to HIRAOKA ET AL. (2001), the k_La value decreased with increasing the liquid viscosity and increased with temperature. ZHU AND WU (2002) stated also increasing of k_La value with increasing temperature between approximately 25-60 °C and decreasing of k_La value with increasing temperature between approximately 60-80 °C.

According to HARNBY ET AL. (1997) and YANG ET AL. (2001), solid particles can have an opposing effect on gas-liquid mass transfer, k_La. High concentrations of fine particles increase the apparent viscosity, decreasing k_L and a. Very small particles, which stay at the interface, can decrease interface mobility, decreasing the change of coalescence, thereby increasing a, but decreasing k_L. However, small particles could also give premature film rupture, thus enchanting coalescence and decreasing a. Larger particles could collide with bubbles and distort them until they break, thereby increasing k_L and a. RAUTIO (1996) found experimentally that increasing solid concentrations of up to 10 vol-% decreased k_La values by 30% compared to pure water and, with 40 vol-% of solid, the decreasing was already 60% smaller.

It should also be stressed that none of the overall correlations for k_La has universal applicability MOO-YOUNG AND BLANCH (1987). Therefore, to explain further the gas-liquid mass transfer phenomena, it is important to study the behaviour of k_L and a independently FUKUMA ET AL. (1987).

2.4.2.2 Liquid side mass transfer coefficient, $\mathbf{k_L}$

The liquid side mass transfer coefficient, k_L, measures the rate at which molecules move through an interfacial boundary layer.

- Temperature (viscosity, density, surface tension)
- Mixing conditions (stirrer and reactor)
- Size of the molecules
- Surface active substances

Increasing the mass transfer coefficient is possible by either reducing the size of the boundary layer or increasing the rate at which molecules move through the boundary layer. Increasing the turbulence decreases the boundary layer. Increasing the temperature increases the diffusivity and reduces the boundary layer MERCHUK (1983) and TEKIE ET AL. (1997). An increase in temperature results in an increase in k_L CALBERBANK AND MOO-YOUNG (1961). Numerous studies on mass transfer in the bubble column have revealed that the mass-transfer coefficient k_L depends mainly on the mean bubble size, physical properties of the liquid medium, and the diffusivity of the absorbing gas component in the liquid medium SADA ET AL (1986).

The bubble size influences significantly the value of the mass transfer coefficient, k_L. According to KASTANEK ET AL. (1993), it is possible to distinguish between the effect of so-called tiny bubbles, $d_s < 0.002$ m, and of large bubbles, $d_s > 0.002$ m. For tiny bubbles, values increase rapidly with bubble size from constant initial value $k_L = 1\times10^{-4}$ m/s corresponding to $d_s \leq 0.0008$ m to $k_L \cong 5\times10^{-4}$ m/s corresponding to $d_s \cong 0.002$ m. In the region of large bubbles, values of the mass transfer coefficient decrease slightly PEDERSEN (2001) with increasing bubble diameter to the value of $k_L \cong (3\text{-}4)\times10^{-4}$ m/s. The bubble-size effect should be employed with caution, especially if bubble size is decreased with the use of a surface active agent (e.g., electrolytes, polymers, antifoams, oils, alcohol and small particles) when the k_L is influenced strongly by interfacial phenomena as well. Since the addition of surface active substances reduces the rate of renewal of the surface elements at the interface, it negatively affects the mass transfer from the bubbles KASTANEK ET AL. (1993). In general though, surface active agents increase a by increasing ε_G and decreasing d_b, by an even larger factor, so that k_La usually increases, though occasionally it has been found to decrease HARNBY ET AL. (1997) and YOSHIDA (1988).

Several correlations for the mass transfer coefficient in mechanically agitated reactors exists in the literature, as in, for example:

DANCKWERTS (1951):

$$k_L = 0.42\left(\frac{\mu_L g}{\rho_L}\right)^{\frac{1}{3}}\left(\frac{D_L\rho_L}{\mu_L}\right)^{\frac{1}{2}} \quad (33).$$

CALDERBANK AND MOO-YOUNG (1961):

$$k_L = 0.42\left(\frac{(\rho_L-\rho_G)\mu_L g}{\rho_L^{\,2}}\right)^{\frac{1}{3}}\left(\frac{D_L\rho_L}{\mu_L}\right)^{\frac{1}{2}} \qquad d_b > 2.5\text{mm}, \quad (34).$$

$$k_L = 0.31\left(\frac{(\rho_L-\rho_G)\mu_L g}{\rho_L^{\,2}}\right)^{\frac{1}{3}}\left(\frac{D_L\rho_L}{\mu_L}\right)^{\frac{1}{2}} \qquad d_b < 2.5\text{mm} \quad (35).$$

For bubble columns the correlation for k_L was proposed as follows by AKITA AND YOSHIDA (1974):

$$k_L = (D_L d_b)^{\frac{1}{2}}\left(\frac{\rho_L}{\gamma}\right)^{\frac{3}{8}} \quad (36).$$

According to several authors, k_L values between oxygen and water at STP ranged between (1-6)×10^{-4} m/s. CALDERBANK AND MOO-YOUNG (1961) reported, for example, the exact value of 1.35×10^{-4} (m/s).

2.4.2.3 Specific gas-liquid interface area, **a**

The value of a can be evaluated from the mean gas hold-up, ε_G, and the volume surface mean bubble diameter, $d_,$ as follows FUKUMA ET AL. (1987):

$$a = \frac{6\varepsilon_G}{d_b} \quad (37).$$

The total gas-liquid interfacial area in liquid volume a is determined by the size, shape and number of the bubbles. Factors affecting the size of the bubbles include:

- stirring speed and type of the impeller
- reactor design
- the way the substances are introduced
- medium composition (e.g., the presence of surface active agents)

The interfacial area can be increased by creating smaller bubbles or increasing the number of bubbles. For a given volume of gas, a greater interfacial area, *a*, is provided if the gas is dispersed into many small bubbles rather than a few large ones. The stirrer and the mixing intensity play a major role in breaking up the bubbles. Reactor design effects the gas dispersion, hold-up and residence time of the bubbles. Baffles are used to create turbulence and shear, which break up the bubbles.

The properties of the medium also affect significantly the bubble sizes and coalescence and therefore the interfacial area. When the solution contains electrolytes, it was found that electrolytes decrease the dissolved gas concentration, which in turn decreases the strength of the attraction between bubbles mediated by micro bubbles; this inhibits coalescence WEISSENBORN AND PUHG (1996). SADA ET AL. (1986 AND 1987) showed that, with particles finer that 10 μm, the bubble coalescence was hindered and the bubble interfacial area and hold-up was increased; with particles larger than 50 μm, the effects were the opposite. O'CONNOR ET AL. (1990) reported bubble size increased with the particle size of the ore, pulp density and air flow rate. An increase in temperature reduced bubble size, as did reduced viscosity.

In the literature, there are several correlations for bubble sizes, which can be divided into categories of bubbles generated at an orifice and bubbles far from the orifice. Previous studies by JAMIALAHMADI ET AL. (2001) on the mechanism of bubble formation show that, depending on the controlling mechanisms, one can distinguish between:

- surface tension controlled by bubble detachment diameter;
- viscous drag controlled by bubble detachment diameter; and
- liquid inertia controlled by bubble diameter.

The surface tension and viscous forces are two major contributing forces influencing the bubble diameter during its formation. JAMIALAHMADI ET AL. (2001) observed that the surface tension is one of the major parameters contributing to the bubble volume, and that it should be taken into consideration even at high gas flow rates. On the other had, the viscous force is only important at high gas flow rates and can be ignored at low flow rates. The orifice diameter d_0 influences the bubble size strongly only at very low gas-flow rates, where the bubble size is found by equating surface tension KOMAROV AND SANO (1998) and buoyancy forces MOO-YOUNG AND BLANCH (1987):

$$d_b = \left[\frac{6\sigma d_0}{g(\rho_L - \rho_G)} \right]^{\frac{1}{3}} \tag{38}$$

The gas rates for which this equation is valid are too small to be of practical interest. At high gas-flow rate, in the case of liquids with low viscosity, the effect of surface tension is generally considered negligible. In the region of the tank away from the orifice, the bubble size may vary, depending on the liquid properties and the liquid motions generated by the rising gas stream. If the power input from the gas phase is insufficient to generate turbulence in the liquid phase, the bubble size in the tank will be that of bubbles formed at the orifice, and may increase with liquid height in the tank due to bubble coalescence. Once the liquid is in turbulent motion, however, bubble break-up will also occur, and equilibrium between coalescence and break-up will determine the mean bubble size.

In the case of preheated gas injection, KOMAROV AND SANO (1998) found a decrease in the bubble diameter was associated with increasing temperature.

A correlation between the oxygen solubility and transition concentration suggested that dissolved gas concentration has an important influence on the interaction between two bubbles, but a contribution due to the Gibbs-Marangoni effect and surface elasticity cannot be ruled out WEISSENBORN AND PUHG (1996).

LIN ET AL. (1998) stated that increasing pressure decreases bubble size and hold-up. For fixed pressure and gas velocity the temperature effect on gas hold-up is complex, but an increase in temperature generally increases the gas hold-up. This general trend is due to the dominant role of the associated reduction in liquid viscosity and surface tension, which leads to smaller bubble size. The associated gas density often plays a secondary role. ZOU ET AL. (1988) stated that the hold-up of the air water systems increases slowly at temperature $T < 75$ °C and remarkably at $T > 75$ °C and is related to the vapour pressure of the gas.

2.4.2.4 The diffusional driving force, ΔC

The driving force is the gradient between the concentration of the substance at the boundary layer and in the bulk liquid (average concentration). Factors affecting this gradient include:

- the solubility of the gas
- metabolic activity

Higher solubilities can be achieved by increasing the partial pressure of the gas. The presence of one solute may affect the solubility of another. The *salting-out effect* is the reduction of the solubility of a gas in water when such a salt is added ATKINS (1994). Solubility has a minimum point as a function of temperature. In case of water, the minimum is close to the boiling point of water. Solubility is dependent on, for example, temperature, pressure, salts present and chemical reactions. Chapter 2.4 discusses gas solubilities in more detail.

Metabolic activity, on the other hand, uses the substrate and therefore decreases the concentration in the bulk liquid (C), again increasing the driving force across the boundary layer.

When it comes to determining the rate-limiting step for bubble dissolution, there are different opinions. YUNG (1989) showed by means of three-component gas bubble tests that solubility is the major effect that causes bubble dissolution in the early time of the dissolution process. For intermediate and longer times, the rate of diffusion interacts with the solubility to control the rate of bubble shrinkage. On the other hand, WEINBERG (1981) assumed that the rate-limiting step for bubble dissolution is diffusion of gas in the fluid rather than interfacial mass transport.

2.5 SOLUBILITY OF GASES IN LIQUIDS

The solubility of a particular solute in a solvent is the maximum amount of solute that will dissolve in a specified amount of solution or solvent. It represents the saturated level of the solution where no more solute will dissolve within the solution. This saturated condition is a physical equilibrium between the solute and solvent and the solution. Unsaturated solutions are those that are below the solubility limits of the solute in that solvent, while supersaturated solutions are above the solubility limits. Supersaturated solutions are nonstable. Such solutions will have the excess solute crystallise out with any disturbance of the supersaturated solution establishing a saturated solution NARITA (1983).

Measurements or investigations of oxygen solubility in water and aqueous solutions have been done for many decades BOHR (1910), BRUHN ET AL (1967), CHRISTOFF (1906), GEFFCKEN (1904), HAYDUK (1991), KLYUEVA (1967), NARITA (1983), TROMAN'S (1998A, 1998B, 2000A AND 2000B), TURCHINOV (1967), WEISENBERGER AND SCHUMPE (1996), KASKIALA (2001A, 2001B AND 2002), KASKIALA AND SALMINEN (2002) and SALMINEN AND KASKIALA (2003) and the factors affecting the solubility are well known.

Models and theories based on different assumptions for estimating the activities in solutions have been created ZHIBAO (2001). Theories for aqueous solutions with strong electrolytes have been presented by, for example, DEBYE-HÜCKEL (1923), PITZER (1973) and CHEN (2002).

Modelling of oxygen solubility in aqueous solutions can be found FOGG AND GERARD (1991) and CLEGG AND BRIMBLECOMBE (1990) and SALMINEN (1998) and TROMAN´S (1998A, 1998B, 2000A, 2000B) and NARITA (1983) and SIPPOLA (1992).

2.5.1 Thermochemical calculations

The equilibrium between molecular oxygen in the gas phase $O_2(g)$ and oxygen dissolved in water $O_2(aq)$ is given by the following equation:

$$k = \frac{\left[\gamma c_{aq}\right]}{\left[\phi P_{o_2}\right]} = \frac{\left[\mathrm{O}_2\right]_{aq}}{\left[\mathrm{O}_2\right]_g}, \tag{39}$$

where k is the equilibrium constant and $[O_2]_{ag}$ and $[O_2]_g$ represent the activity of $(O_2)_{aq}$ and fugacity of $(O_2)_{g,}$ respectively. When c_{aq} is proportional to P_{O2}, the solute exhibits a Henry-type behaviour with a proportional Henry´s law constant H equilibrium; the constant may be rewritten as:

$$k = \frac{1}{H}\left(\frac{\gamma}{\phi}\right) = \frac{[O_2]_{aq}}{[O_2]_g}, \tag{40}$$

when γ and ϕ are close to unity such that γ/ϕ=1, then $k=1/H$. This situation is expected to prevail at low-solute concentrations and moderate partial pressures of oxygen TROMAN´S (1998B).

At any temperature T, k is related to the standard molar chemical potentials μ^o_{aq} and μ^o_g of the aqueous and gaseous oxygen species, respectively, at temperature T and to the overall change in standard chemical free energy of the reaction (ΔG^o) via Equation (41) leading to Equation (42).

$$\Delta G^o = \mu^o_{aq} - \mu^o_g = -RT \ln k \tag{41}$$

$$k = \exp\left\{\frac{\mu^o_g - \mu^o_{aq}}{RT}\right\} = \exp\left\{\frac{-\Delta G^o}{RT}\right\} \tag{42}$$

Through thermodynamic calculations, it is possible to calculate the equilibrium constants for gases and electrolytes in liquids KASKIALA AND SALMINEN (2002) and SALMINEN AND KASKIALA (2003).

The computer aided multi-component calculation methods for multiphase systems, including gas solubility, have been developed in recent years ERIKSSON AND HACK (1990), ROINE (1999), KOUKKARI ET AL. (2000), SALMINEN ET AL. (2000).

2.5.2 Gas solubility at elevated temperatures

The gas-liquid equilibrium of oxygen is described by Henry's law, the linear relationship of which is valid for dilute solutions of non-reacting systems and for gases that are weakly soluble in liquid. The temperature dependence of Henry's constant for oxygen in water given by FOGG AND GERARD (1991) is as follows:

$$ln\left(\frac{P}{H_0}\right) = A + \frac{B}{T} + C\, ln\, T, \tag{43}$$

where H_0 denotes the dimensionless representation of Henry's law constant in partial oxygen pressure P at 1 atm. The coefficients A, B and C are listed in Table VI.

Table VI Coefficients A, B *and* C *used for calculating Henry's constant, Fogg and Gerard (1991)*

A	B	C	Temperature range
-171.2542	8391.24	23.24323	273-333 K
-139.485	6889.6	18.554	273-617 K

2.5.3 Empirical modelling of gas solubility in electrolytic solutions

The addition of salt to water changes its solvent properties. It can reduce or increase the solubility of gas. This phenomenon is commonly called the *salting in and out effect* and it is a result of molecular interactions between charged and neutral particles in a liquid solution LONG AND McDEVIT (1952), MASTERTON (1975). Increasing salt concentration, the gas solubility is nearly always found to decrease due to the salting-out effect of the ions. This effect, as derived from Henry's law constant, can be related in Setschenow linear SETSCHENOW (1889) salting out function CORTI ET AL. (1990), PITZER (1995), WEISENBERGER AND SCHUMPE (1996). At moderate high-salt concentrations, the effect of salt concentration, C_s, on the solubility, C_G, of a sparingly soluble gas as compared to that in pure water, $C_{G,0}$ was described by SETSCHENOV (1889) in the following form:

$$log\left(\frac{C_{G,0}}{C_G}\right) = KC_s \tag{44}$$

Parameter K (Setschenov´s constant) is specific to the gas as well as to the salt and shows a moderate temperature dependency RÖNNHOLM ET AL. (1999B) AND RÖNNHOLM (2001). The relation usually holds well up to salt concentration of about 2 kmol/m^3 and sometimes more than 5 kmol/m^3. At higher salt concentrations, the gas solubility tends to be underestimated WEISENBERGER AND SCHUMPE (1996). The equation can also be applied for mixed electrolyte solutions according to SCHUMPE (1993) as follows:

$$log\left(\frac{C_{G,0}}{C_G}\right) = log\left(\frac{H}{H_0}\right) = \sum_i (h_i + h_G)C_i\,, \tag{45}$$

where C_i denotes the concentration of ion i in the solution and h_i is a ion-specific parameter.

WEISENBERGER AND SCHUMPE (1996) extended the model of SCHUMPE (1993) to the temperature range 273-363 K by assuming h_G, (the gas-specific constant) as a linear function of the temperature:

$$h_G = h_{G,0} + h_T(T - 298.15) \quad (46),$$

where $h_{G,0} = 0$ [m^3/kmol], $h_T = -0.334*10^{-3}$ [m^3/kmol·K] and parameters h_i are as listed in appendix 1.

Only a few publications concerning measurements of the solubility of oxygen in aqueous sulphuric acid BOHR (1910), BRUHN ET AL (1967), CHRISTOFF (1906), GEFFCKEN (1904), HAYDUK (1991), KLYUEVA (1967) and TURCHINOV (1967) were found.

With respect to the direct leaching of zinc sulphide conditions, experimental values for the oxygen solubility cannot be found. However, based on information found, good approximations are available. In this work, the gas solubility values determined by the model of WEISENBERGER AND SCHUMPE (1996) and SCHUMPE (1993) were chosen as the most suitable. Examples of the calculated oxygen solubility values can be seen in Figure 10.

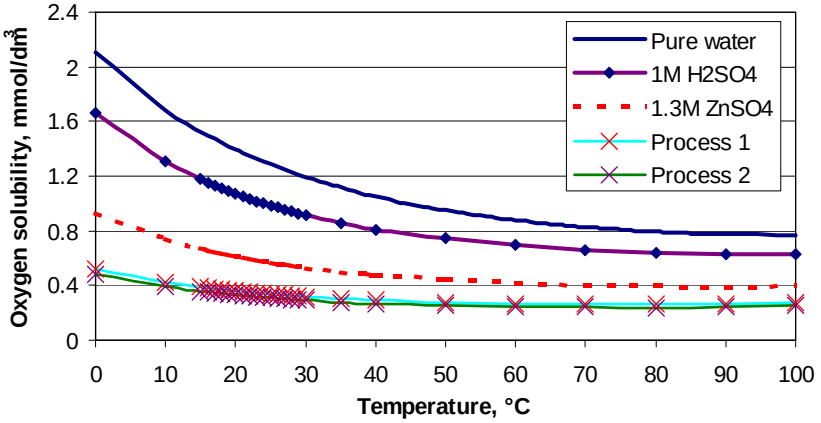

Figure 10 Calculated oxygen solubilities in different liquids as a function of temperature

The solubility of oxygen was calculated in water and in salt solutions containing 1 M H_2SO_4, 1.3 M $ZnSO_4$ and two complex process solutions containing different amounts of H_2SO_4, $ZnSO_4$ and $Fe_2(SO_4)_3$. Process solution 1 contained together 3 M sulphates and solution 2 contained 2.7 M sulphates. The solubilities were calculated with the WEISENBERGER AND SCHUMPE (1996) and SCHUMPE (1993) model presented and the values are listed in Appendix 1.

As can be seen from the calculated values, the solubility of oxygen in process solutions is significantly less than in pure water. However, the solubility of oxygen in process solution 1 and 2 were nearly the same. Increasing temperature (at a constant partial pressure) under 100 °C decreases the solubility. At higher temperatures, the solubility may pass through a minimum. At a partial pressure of 1.013 bar, the solubility of oxygen in pure water passes through a minimum at about 95 °C HAYDUK (1991) and RAUTIO (1996).

CHAPTER 3 EXPERIMENTAL PART

The main focus of the experimental part of this work is carried out with four experimental apparatus: *bubble swarm system, water model, mass transfer equipment and autoclave* designed and developed especially for this purpose. Experimental method and procedure are explained beginning of each Chapter. However, it should be noticed that analysers like for example HUT bubble size analyzer and oxygen analyzer were used in several experimental set-ups, but presented only once.

Also additional tests of density, surface tension and viscosity of different solutions at elevated temperatures were conducted to give more information, and which were used explaining the results of the main experiments. In these measurements the calibration was carried out comparing the experimental values for pure water to values found in literature.

3.1 DENSITY OF THE SOLUTION

The densities of the liquids were determined with an aerometer (Franz Widder GmbH types 1263-1268) in a 500 ml glass container. The temperature of the liquid was controlled within the range 20-90 °C using a circulated water bath and was measured to an accuracy of ±0.1 °C. The constant temperatures were assured by stirring the liquid. The density values where collected approximately between every 3 °C. Only gravity and buoyancy forces affected the aerometer while measuring. The accuracy of the experiment was considered to be the same as that of the aerometer, ±1 g/dm^3 ANTTONEN JA KASKIALA (2004). Figure 11 shows the density results for the distilled water; these follow closely the values reported by PERRY (1976).

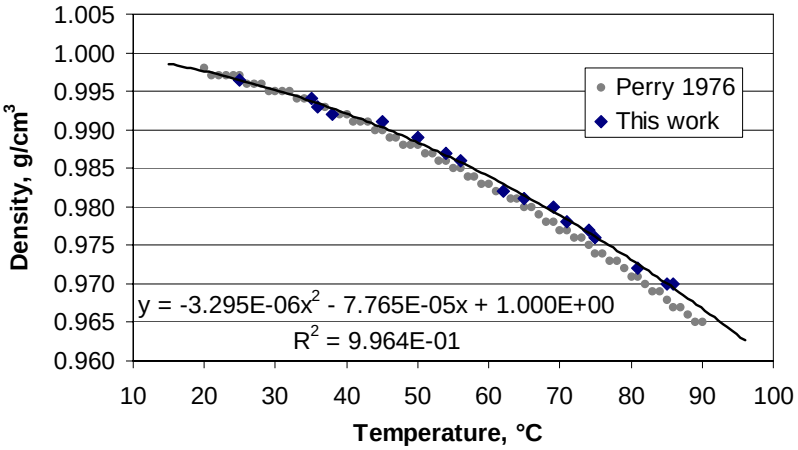

Figure 11 Measured and published (Perry, 1976) density values for pure water as a function of temperature (Fitted line follows the experimental values)

Densities of the process solutions 1 and 2 were significantly greater than for water, see Figure 12. The process solution 1 was from the early stages of the leaching and solution 2 from the later stages. Solid particles were filtered before the experiment.

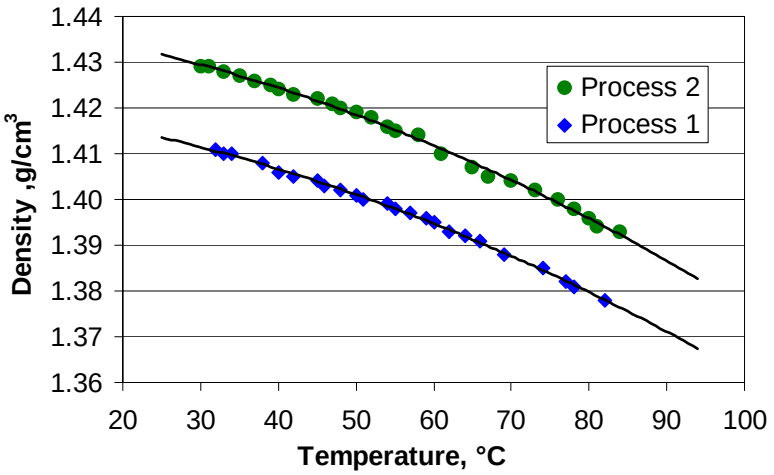

Figure 12 Measured density values and fitted line for process solutions 1 and 2 as a function of temperature

Other examined solutions, numbers 1 to 7, were prepared with distilled water and commercial reagents H_2SO_4 (96-98 vol-%), $ZnSO_4 \cdot 7H_2O$ and $Fe_2(SO_4)_3 \cdot 5H_20$ with impurities less than 0.5%. Density values calculated at different temperatures from the line fitted for experimental results are presented in Appendix 2.

3.2 SURFACE TENSION OF THE SOLUTION

Surface tension, together with other chemical and physical properties of gas and solution, affects the bubble sizes and the total area of the gas-liquid interaction. The phenomenon of surface tension is actually due to a layer of a few molecules (1-10 at most in thickness) SEPPÄLÄ (1973). A molecule of a liquid is subjected to forces due to its neighbours. When coming to the free surface of a liquid, the molecule moves to the surface against unbalanced forces so is not surrounded symmetrically by other molecules anymore. The direction of these forces acting on the molecules forming the surface layer is essentially normal to the free surface of the liquid. Thus molecules in the boundary layer possess additional energy because work has been done in bringing them to the surface. This additional energy may be regarded as surface energy BURDON (1949). The phenomena of surface and interfacial tension are readily explained in terms of these forces ABRAMZON (1993). The molecules that are located within the bulk of a liquid are, on average, subjected to equal forces of attraction in all directions, whereas those located at, for example, a liquid-air interface experience unbalanced attractive forces resulting in a net inward pull, see Figure 13.

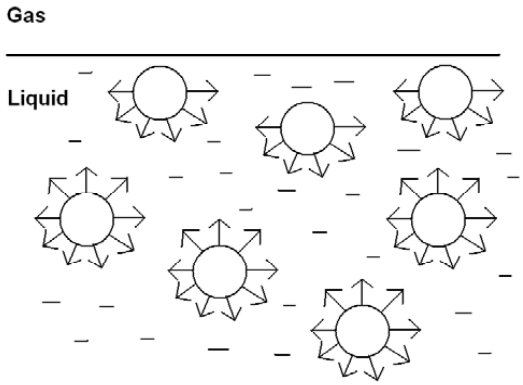

Figure 13 Attractive forces between molecules at the surface and in the interior of the liquid

Bubbles or droplets of liquids tend to be spherical, because a sphere is the shape with the smallest surface-to-volume ratio. Thermodynamically, the surface tension is defined as the surface free energy per unit area. In a dynamic sense, surface tension represents the work of energy required to create one unit of additional surface area at constant temperature IIDA AND GUTHRIE (1988).

The surface affects both Helmholtz *dF* and Gibbs *dG* energies. The link between these quantities and the surface area is the work needed to change the area by a given amount and the fact that d*F* and d*G* are equal (under different conditions) to the work *w* done in changing the energy of a system. At constant volume and temperature, the work of surface formation can be identified with the change in Helmholtz energy as follows:

$$dF = \sigma \cdot dA\,. \tag{47}$$

Because the Helmholtz energy decreases ($dF<0$) if the surface area decreases ($dA<0$), surfaces have a natural tendency to contract. The important conclusion is that the pressure on the concave side of an interface is always greater than the pressure on the convex side. The relation can be expressed by the Laplace equation as follows, see also Figure 14.

$$\boldsymbol{P}_{in} = \boldsymbol{P}_{out} + \frac{2\boldsymbol{\sigma}}{\boldsymbol{r}} \qquad (\mathrm{r} > 0) \tag{48}$$

so

$$\Delta \boldsymbol{P} = \frac{2\boldsymbol{\sigma}}{\boldsymbol{r}} \qquad (\mathrm{r} > 0) \tag{49}$$

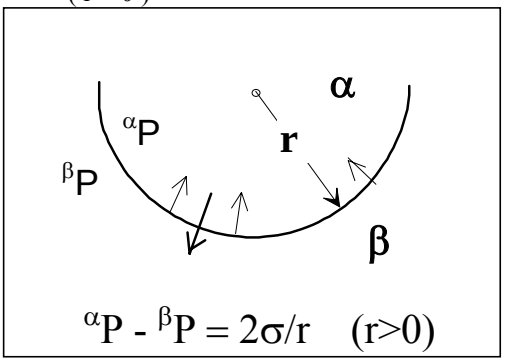

Figure 14 Pressure difference over the boundary layer

There are many methods for calculating the surface tension of the dilute aqueous solutions of a single electrolyte. Other than the empirical methods, there are theoretical models that involve a combination of thermodynamic equations with an adsorption model HORVATH (1985), LI ET AL. (1999), LI AND LU (2001), KASKIALA ET AL. (2003).

The surface and interfacial tension measurement methods can be classified as static, detachment and dynamic. Static methods usually offer a greater potential for accurate measurement than detachment methods, especially when surface-active agents are involved, but detachment methods tend to be more convenient to operate, especially at elevated temperatures. Analyzer KSV Sigma 70, based on the detachment method, was used in the experiments. It has a computer-controlled tensiometer and is valid for either Du Nouy rings or Wilhelmy plates, see Figure 15.

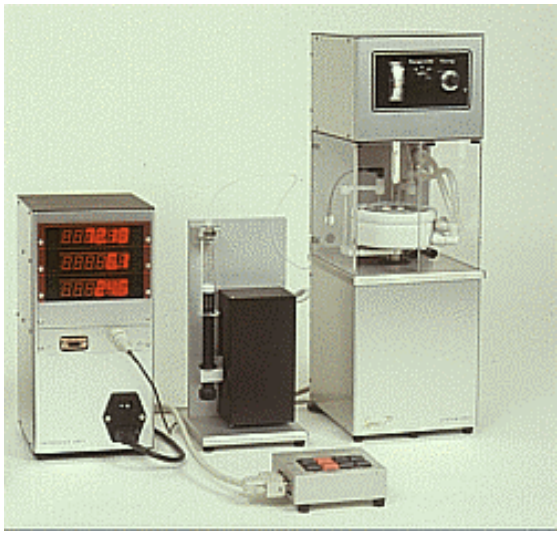

Figure 15 Surface tension equipment KSV Sigma 70

The ultra-sensitive tensiometer measures the difference between rest weight and the maximum weight of the platinum ring on the boundary surface, see Figure 16. Software calculates automatically the surface tensions. The experiments were carried out in a temperature range of 25 - 80 °C, using the water as a heat transfer fluid. The magnetic built-in stirrer of the tensiometer enables sample mixing during heating. The accuracy given by the manufacturer was ±0.5 mN/m at the calibration temperature of 20 °C. The standard deviation of the experiments ranged from 0.03 to 0.42 mN/m.

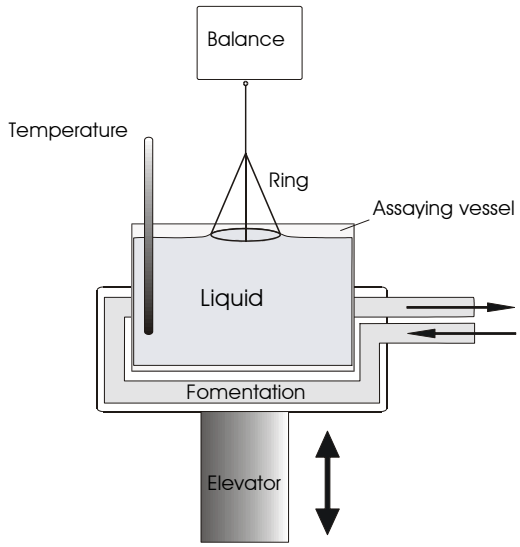

Figure 16 Schematic presentation of the ring method used for surface tension measurements

All the samples were prepared in STP conditions using distilled water and a sample volume of 100 ml. Other reagents used were H_2SO_4 (96-98 vol-%), $FeSO_4 \cdot 7H_2O$ and $ZnSO_4 \cdot 7H_2O$ with impurities less than 0.1%.

Figure 17 illustrates how the measured values for the surface tension of distilled water quite closely approach the reference data in Lange's Handbook of Chemistry (1973) and LAINE (1999). The values indicate the almost linear dependence of water surface tension on temperature.

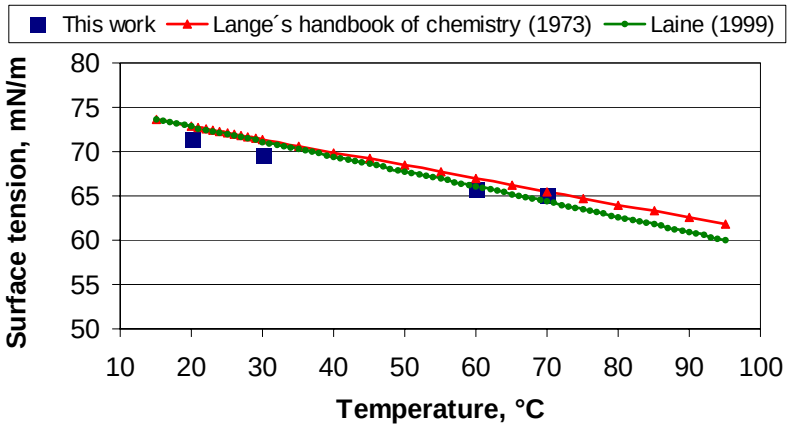

Figure 17 Experimental and reference data for surface tension of pure water as a function of temperature

If a surface-active agent is present at the interface, it modifies the surface tension ATKINS (1994). The tendency for surface-active molecules to accumulate into the interface favours an expansion of the interface; this must, therefore, be balanced against the tendency for the interface to contract under normal surface tension forces SHAW (1980).

Solutions consisted of 100 g/l zinc sulphate gave surface tension values greater than 25 or 50 g/l of zinc sulphate in 25 g/l sulphuric acid, as can be seen in Figure 18. Surface tension values with different zinc contents were, however, quite close to these at a temperature of 75 °C.

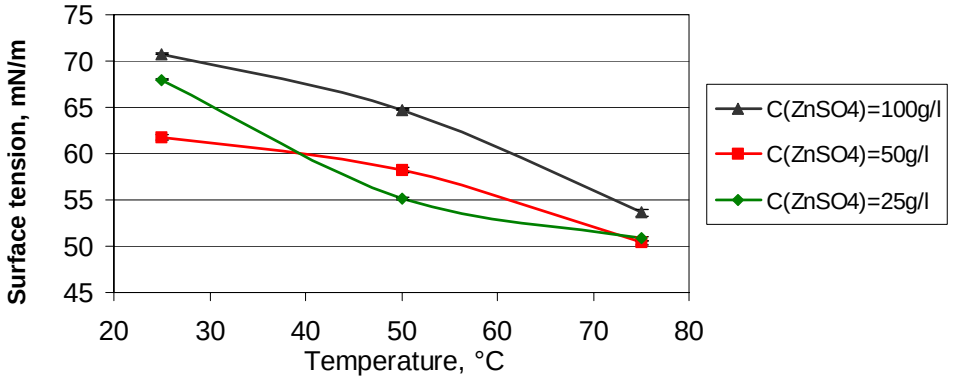

Figure 18 Surface tensions of 25 g/l sulphuric acid as a function of temperature with different zinc sulphate 25, 50 and 100 g/l concentrations

Figure 19 shows the surface tension values of an aqueous solution containing 25 g/l sulphuric acid with 25, 50 and 100 g/l of iron sulphate, respectively, at elevated temperatures. Increasing sulphuric acid, temperature and iron sulphate decreases the surface tension values. However, values with 50 and 100 g/l of iron sulphate were close to each other. OWUSU (1992) also found that the introduction of Fe^{3+}/Fe^{2+} ions (and acid) into the system did not have an influence on the interfacial tension values within reasonable accuracy limits.

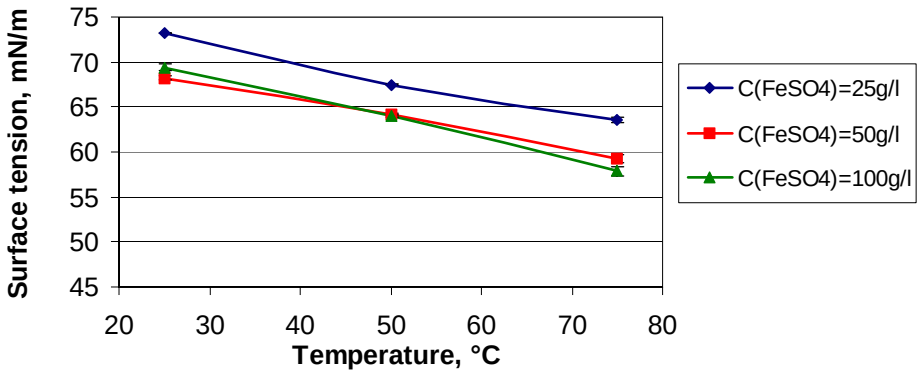

Figures 19 Surface tension of 25 g/l sulphuric acid with different iron concentrations

Increasing sulphuric acid in a solution containing 100 g/l zinc sulphate decreased the surface tension. Increasing the temperature also decreased the surface tension, as can be seen in Figure 20.

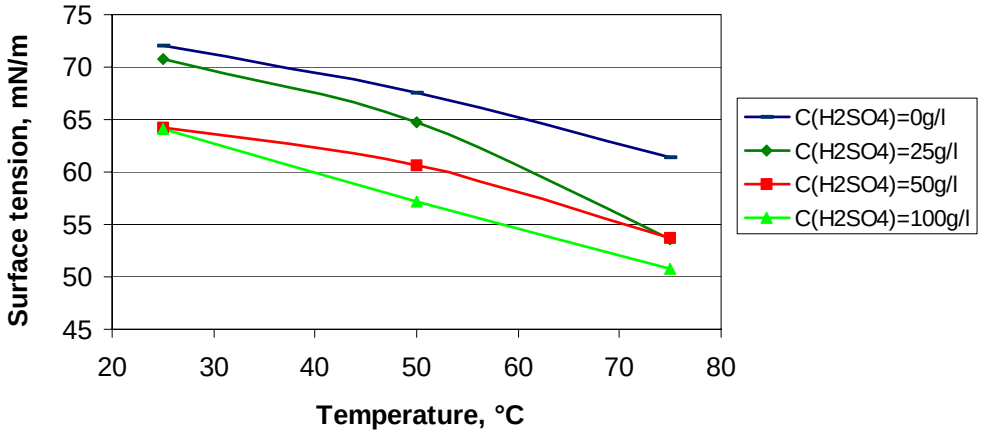

Figure 20 Surface tensions of 100 g/l of zinc sulphate with different sulphuric acid concentrations

Compared to water, surface tensions in real process solutions 1, 2 and 3 changed significantly above a temperature of 60 °C. Solution 1 had a local maximum surface tension value at 70 °C, and solutions 2 and 3 decreased when the temperature increased. At 80 °C, the surface tension values for process solutions 1, 2 and 3 were 40.4, 47.51 and 60.32 mN/m, respectively, see Figure 21. Process solutions used in surface tension

measurements were not used in other experiments of this work. However, the amount of sulphate concentration varied as well between 2.7-3 M as in process solutions listed in Appendix 2.

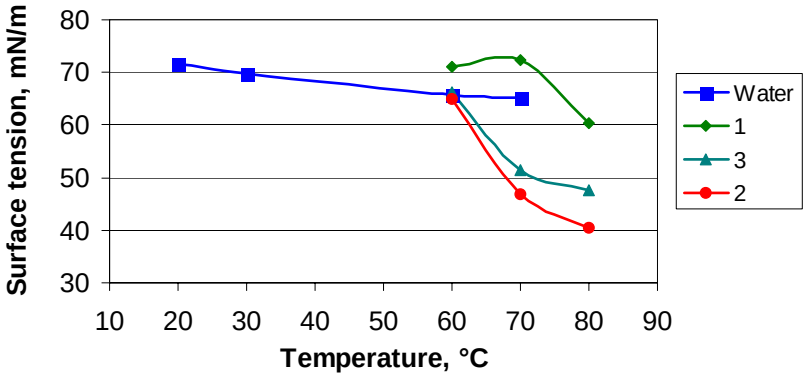

Figure 21 Surface tensions of three different zinc leaching process solutions

Closely related experiments where conducted by OWUSU (1992), who reported values of 54.0±1.0 mN/m at superatmospheric pressures in zinc leaching and in the absence of surfactants.

3.3 VISCOSITY OF THE SOLUTION

The viscosity of the solution has a significant effect on the bubble sizes and the mass transfer between gas and liquid, as stated earlier. Viscosities of aqueous solutions with two or three components are well researched and reported. However, for complex process solutions, viscosity values need to be examined separately. The viscosity measurements were carried out with a Schott Gerät AVS 400 capillary viscometer, which measures the flow rate and pressure in the capillary. Measurements were carried out with different sized capillaries, depending on the liquid examined. The capillary was submerged in an oil bath and measurements taken at elevated temperatures.

Experimental values for kinetic viscosity of water closely conforms to the values reported by LOBO (1989), see Figure 22. As can be seen, the viscosity increases with the sulphuric acid content and decreases with increasing temperature in the range examined.

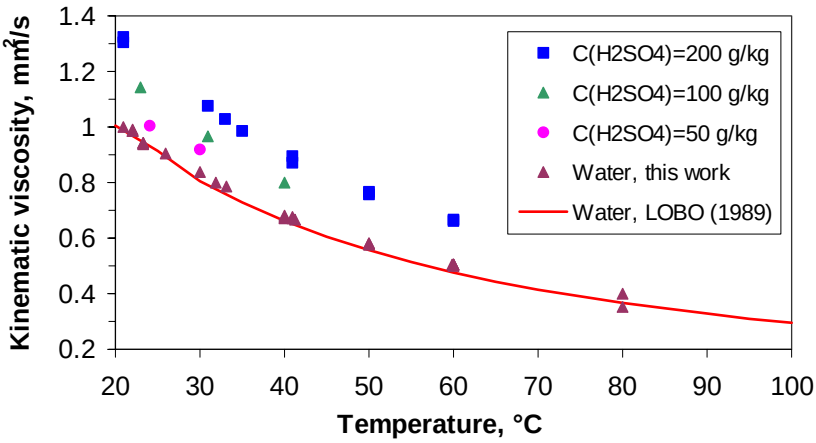

Figure 22 Kinetic viscosities of water and dilute sulphuric acid as a function of temperature

Reasonable viscosity values for process solutions 1 and 2 were gained only up to temperature of 40 °C, see Figure 23. At higher temperatures, the measurement technique was disrupted by an unwanted boiling effect.

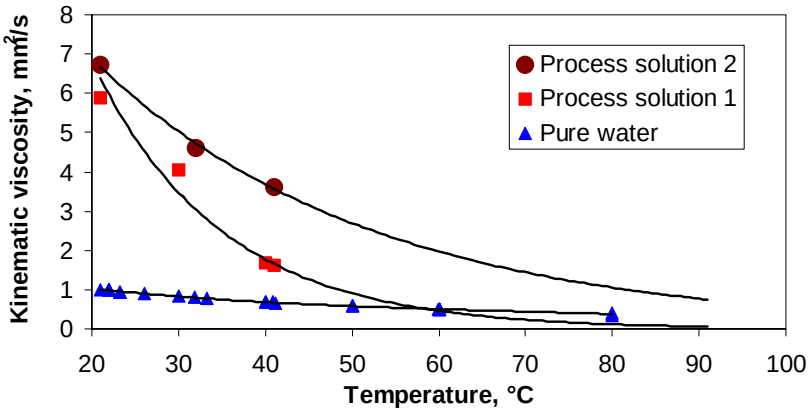

Figure 23 Kinematic viscosity of water and process solutions 1 and 2 with fitted line

The experiments indicate a strong decrease of the kinetic viscosity of process solutions as a function of temperature, as well as greater viscosity values in comparison to water. Measured viscosity results are considered reliable for solutions of one or two components, since results approach the values reported in the literature, but, for real process solutions, only the strong decrease of the kinetic viscosity with temperature is considered informative. Experimental values are listed in Appendix 4.

3.4 BUBBLE SWARM SYSTEM

The effect of liquid properties on bubble size was analysed in an especially designed and built laboratory set-up with a square 0.6-litre square glass decanter on top of a magnetic agitator with a heater (Kika® Werke RCT basic), see Figure 24.

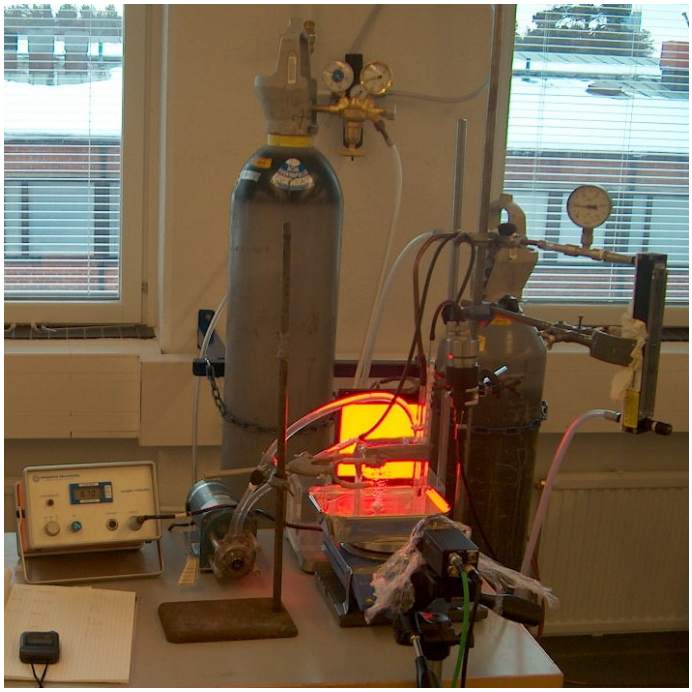

Figure 24 Picture of the bubble swarm system set-up

The aim of the experiments with a bubble swarm system was to study the effect of temperature and liquid properties on bubble size and oxygen dissolution with different gas flow rates. The bubbles size was analysed with an HUT Bubble Size Analyser developed by GRAU AND HEISKANEN (2002). Each experiment consisted from 5000 to 20 000 bubbles and was taken as an average of three tests. For each bubble the maximum and minimum Feret diameters F_{max} and F_{min} are determined by detecting the bubble at a 22 number of angles. The bubble volume equivalent diameter d_e is calculated as $d_e = \sqrt{F_{min} F_{max}^2}$. Results are presented as a sauter mean diameter (D_{32}), which is based on the volume-to-surface mean of the bubbles STOCKHAM AND FOCHTMAN (1977) and calculated from the volume equivalent diameter as $D_{32} = \frac{\sum_{i=1}^{n} d_e^3}{\sum_{i=1}^{n} d_e^2}$

Oxygen gas was blown into liquid through a sparger Duran® with a porosity of 40-100 μm. The gas flow rate was controlled and measured with a rotameter and needle valve, see Figure 25.

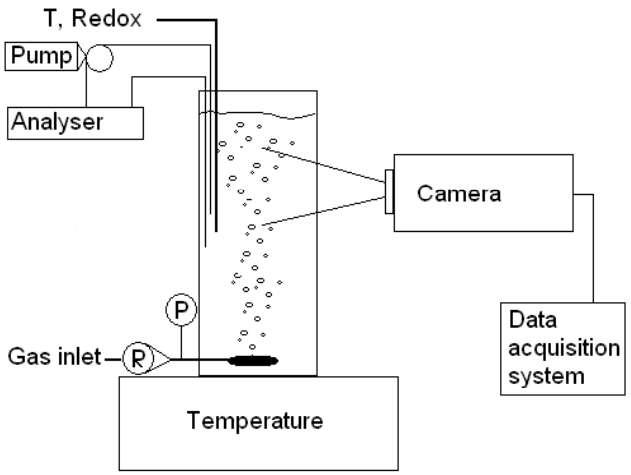

Figure 25 Schematic picture of bubble swarm system

3.4.1 Temperature effect

Increasing the gas flow rate increases the bubble diameter, as pointed out earlier by O'CONNOR ET AL. (1990) and JAMIALAHMADI ET AL. (2001). As the temperature increases the bubble size decreases; this is due to the lowering of the surface tension and viscosity, as stated earlier by LIN ET AL. (1998), O'CONNOR ET AL. (1990), JAMIALAHMADI ET AL. (2001) and KOMAROV AND SANO (1998). With the gas flow rate 0.04 l/min, the bubble size had a minimum close to 50 °C which then increased, probably due to the incomplete gas expansion before the liquid phase at temperatures above 50 °C, as can be seen in Figure 26. With a lower gas flow rate of 0.03 l/min, the gas expanded completely before the liquid phase and the bubble size only decreased with temperature. Results of the experimental values of this chapter are listed in Appendix 5.

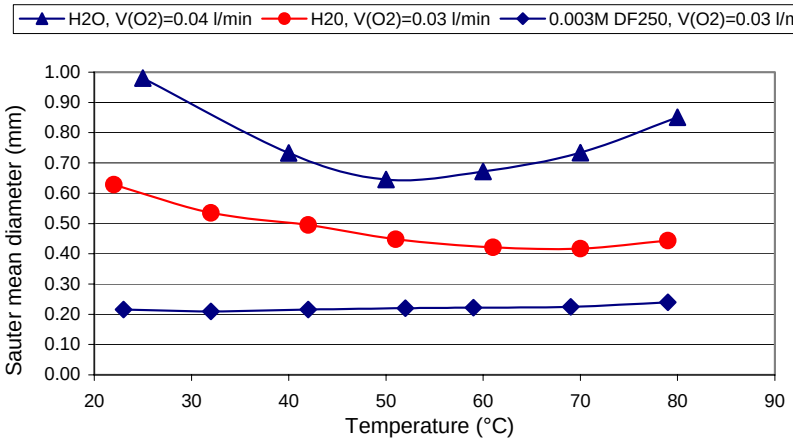

Figure 26 Sauter mean diameter of bubble population in water and 0.003M DowFroth 250A with gas flow rates 0.03 and 0.04 l/min

3.4.2 Liquid properties effect

The effect of surface tension of liquid on bubble size was determined with water containing frother DowFrother 250A, chemical formula $CH_3(OC_3H_6)_4OH$. When surface tension decreased from 72 to 50 mN/m (pure water and 0.003 M DF250A) at 25 °C, the bubble diameter decreased 66% from 0.63 mm to 0.22 mm with a gas flow rate of 0.03 l/min, as can also be seen in Figure 26. At temperature 80 °C, the same decrease under similar conditions was 46%, from 0.44 mm to 0.24 mm. Surface tension values at 25 °C were collected from KASKIALA ET AL (2003) and LASKOWSKI (2004). The experiments indicate that bubble size reaches minimum with low surface tension; since even the surface tension, viscosity and density of the liquid decreases with temperature, the diameter stays almost the same, 0.20-0.24 mm within a temperature range of 23-80 °C. As for water, with the same gas flow rates, the diameter decreased from 0.62 mm to 0.43 mm with the same temperature change. The composition of the liquids used in the experiments for determining the affect of surface tension and density on the sauter mean-diameter at 80 °C is listed in Table VII.

Table VII Composition of liquids 1-7 examined with bubble swarm system at 80 °C

Liquid	Water	H_2SO_4	$FeSO_4$	$CuSO_4$	$ZnSO_4$	DF250	Process	Surface tension*	Density**	Sauter mean
	Distilled	30g/l	30g/	2.4g/l	250 g/l	0.003M	solution	mN/m	g/m^3	mm
1	x							64	973	0.44
2	x	x						62	990	0.42
3	x	x	x					63	1020	0.24
4	x	x	x	x				63	1021	0.21
5	x	x	x	x	x			51	1250	0.25
6	x					x		42	973	0.24
7							x	45	1380	0.25

* Approximated from experimental results, see chapter 3.2
** Approximated from experimental results, see chapter 3.1

JAMIALAHMADI ET AL. (2001) stated that the surface tension and viscous forces are two major contributing forces influencing the bubble size during its formation. At very low gas flow rates, the bubble diameter is controlled entirely by surface tension and buoyancy forces and viscous forces can be ignored, see also Figure 27.

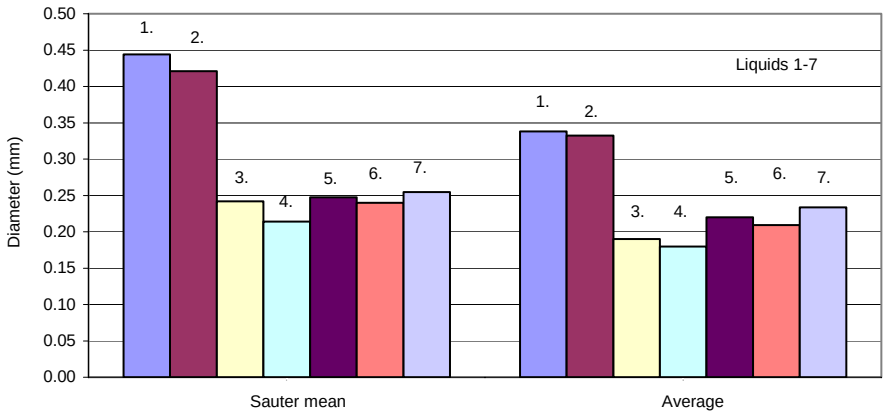

Figure 27 Sauter and average bubble size in liquids 1-7 at 80 °C

Decreasing the surface tension from liquid 1 to 6 decreased the bubble diameters. Also, the increasing of liquid density decreased the bubble diameter in the order 1, 2 and 3, respectively. However, the effect of density on bubble size was not straightforward, since in following liquids 3-7 the bubble size maintained almost the same even though the densities varied. At low liquid surface tensions, the effect of density was ignored, see liquids 1, 6 and 7. When sulphates were added to the solution, the bubble diameter decreased significantly, see liquids 2 and 3. The effect of sulphates is discussed as bubble coalescence in the following section.

3.4.3 Bubble coalescence

According to LESSARD AND ZIEMISKI (1971), the valence combination of the salts 3-1 and 2-2 begin to prevent coalescence at ambient temperature in the concentration range 0.030-0.036 M, 2-1 and 1-2 in the range 0.056-0.060 M, and 1-1 in the range 0.16-0.23 M. YANG ET AL (2001) stated that the higher temperature may promote coalescence of small bubbles and CRAIG ET AL. (1993) noticed coalescence decreased with temperature approximately in the range 20-50 °C. According to experiments conducted at 80 °C with pure water and 30 g/l H_2SO_4, the bubble size distributions were almost the same, see Figure 28. This indicates that sulphuric acid does not have an effect on the coalescence, as stated by CRAIG ET AL. (1993) and WEISSENBORN (1995). However, process solution (liquid 7) with a high salt concentration and 0.003 M DF250 (liquid 6) with low surface tension most probably prevented the coalescence and therefore caused the narrow and similar distribution of bubbles, as can be seen in Figure 28. Liquid 6 had a concentration much greater than critical coalescence concentration = 3.3×10^{-5} mol/l, which is considered to be the limit for 0% coalescence even with a frother addition, according to LASKOWSKI (2004). TSANG ET AL. (2004) found more salt was needed to prevent coalescence of smaller bubbles.

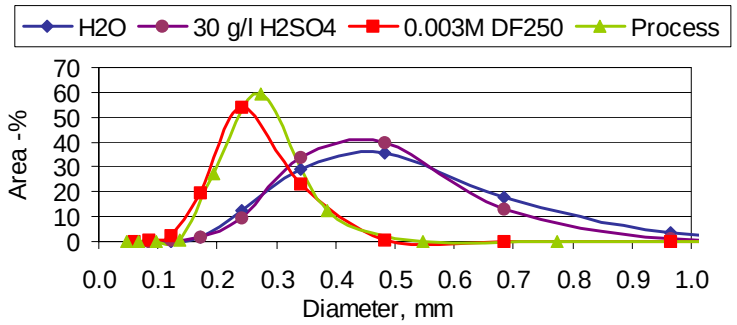

Figure 28 Total gas and liquid (H_2O, 30 g/l H_2SO_4, 0.003 M DF250 and process solution) interface as a function of bubble size

For real process solution, the non-coalescence of bubbles is most likely to be observed due to high salt concentration, which would also result in the bubble formation, breakage and in the turbulent motion (viscous forces) being the dominating factor in bubble size distribution. Values are listed in Appendix 5. Section 3.5.1 further discusses bubble coalescence.

3.4.4 Oxygen dissolution

Except that the vessel was changed to a closed 1-litre decanter, the same laboratory scale set-up was also used for analysing the oxygen dissolution in liquids. The measurements were carried out using the dynamic method of analysing the oxygen concentration changes. This method has been widely used in air-water systems HIRAOKA ET AL (2001); LINEK (1987); ZHU ET AL (2001). Dissolved oxygen in the liquid was initially removed with injected nitrogen (99.9999%) gas. The nitrogen gas was changed to oxygen at a specified gas flow rate, and the increase in the oxygen concentration of the liquid was measured with an Orbisphere Model 26071 oxygen analyser with membrane 2958A. The analyser consists of an electronic circuit with dissolved oxygen as a part of it. Oxygen undergoes a reaction at the cathode, enabling a measurable electric current to flow, which is then proportional to the amount of oxygen in the sample. VAN'T RIET (1979) stated that an error of less than 6% for k_La values when response time τ is much smaller than $1/k_La$, which applies in this work. A response time of 6 seconds was measured, the same as that given by the manufacturer. In the experiments, the liquid sample was withdrawn and circulated through the sensing membrane back to decanter. The required liquid flow for the sensor was adjusted using a tube pump (Masterflex® model 7518-60). The liquid flow caused by the pump and gas flow was noticed to maintain a homogeneous concentration of oxygen in the continuous phase.

Temperature has a significant effect on the oxygen solubility. For water below 100 °C, an increase in temperature at constant partial pressure usually decreases the solubility. The same was observed experimentally, as shown in Figure 29. In this case, the oxygen flow rate of 1.5 l/min was chosen as the most suitable.

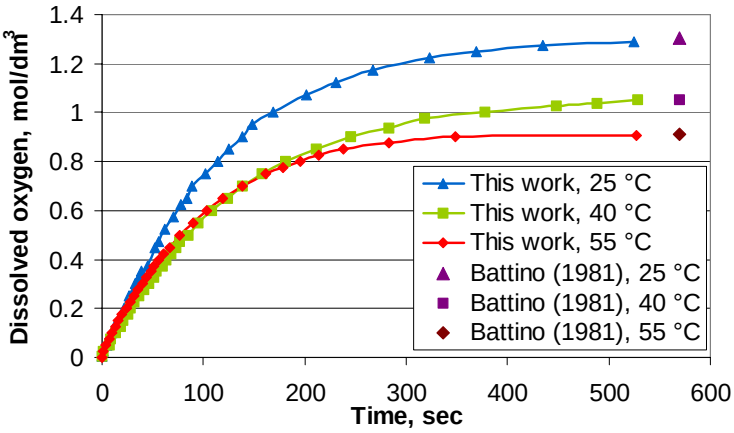

Figure 29 Oxygen dissolution in 1 M sulphuric acid as a function of time at different temperatures (Oxygen pressure of 1 bar and gas flow rate 1.5 l/min)

The presence of salts or electrolytes in the water increases the "salting-out effect" and the solubility decreases. The lower solubility of oxygen due to this effect can also be seen as a lower equilibrium value. However, oxygen dissolved in a similar manner into pure water and 1 Molar sulphuric acid at 40 °C and 1 bar, as can be seen in Figure 30.

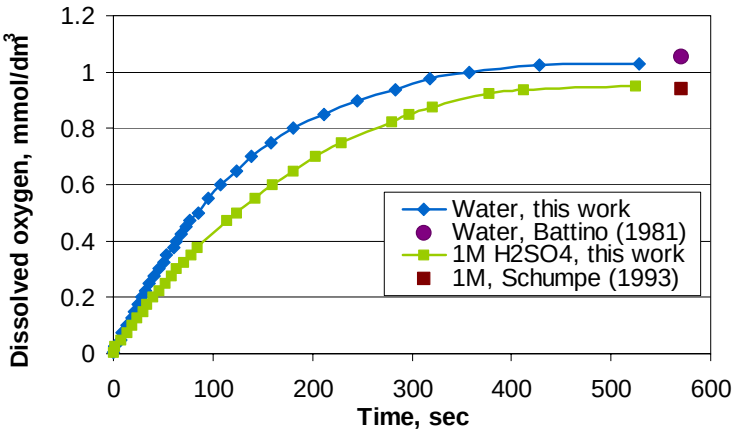

Figure 30 Oxygen dissolution in pure water and 1 M H_2SO_4 at temperature 40 °C and oxygen pressure of 1 bar

Oxygen solubility decreased approximately by 8-11% when the sulphuric acid concentration was increased to 1 M. The mass transfer coefficient k_La values were determined using the model for the liquid phase:

$$\frac{dC}{dt} = k_L a(C_\infty - C), \tag{50}$$

where C is the concentration of dissolved oxygen at time t and C_∞ the equilibrium value in the liquid. The mass transfer coefficient k_La value is obtained from the straight line derived from Equation 51, after which integration takes the form:

$$ln(C_\infty - C) = -k_L at + ln(C_\infty - C_0). \tag{51}$$

An example of the linearization (51) of the transfer coefficient k_La vs. time can be seen in Figure 31, in which the value of the k_La is the slope 0.0093. The correlation of the k_La values were determined by the least square method.

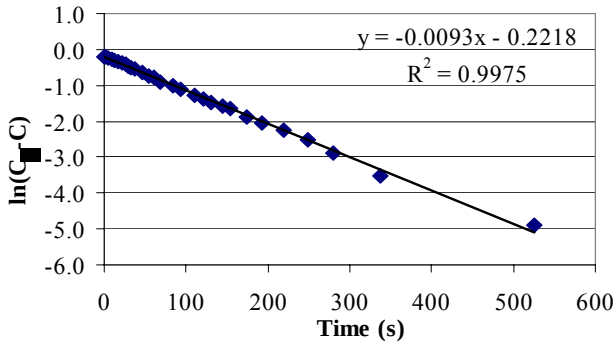

Figure 31 Determining the mass-transfer coefficient k_La from the slope of the fitted trend line

All the mass transfer coefficients k_La and R^2 values of the experiments are shown in Table VIII. How the mass transfer coefficient values increased with temperature, gas flow rate and acid concentration can be seen from the results.

Table VIII Experimental values of k_La and the correlation coefficient R^2

Temperature (°C)	Gas flow (l/min)	Acid concentration (mol/l)	Mass transfer coeff. (1/s)	R^2
25	1.5	1	0.0071	0.973
40	1.5	1	0.0085	0.978
55	1.5	1	0.0093	0.998
40	**0.75**	0	0.0042	0.998
40	**1.5**	0	0.0077	0.983
40	**2.25**	0	0.0141	0.976
40	1.5	**0**	0.0078	0.993
40	1.5	**1**	0.0085	0.978

Experimental values for the mass transfer coefficient k_La ranged between 0.0042-0.0141 (s^{-1}) with the lowest R^2 value 0.973. Consistent with the findings of HIRAOKA ET AL. (2001) and ZHU AND WU (2002), the volumetric mass transfer increased with liquid temperature. As expected, increasing the gas flow rate improved the mass transfer. According to the experiment findings, the mass transfer was enhanced slightly by the addition of the sulphuric acid, which is probably due to the longer residence time of the gas bubble in liquid.

3.5 WATER MODEL OF THE REACTOR

The pilot water model of the atmospheric leaching reactor TAKALA ET AL. (2000) was built and used to describe the flow conditions and the gas-liquid interactions in the process. In a downdraft-type reactor, the gas is injected at the bottom towards the impeller, which is placed below the centre tube. The impeller disperses the injected gas and causes a downdraft flow in the centre tube. Mixing and buoyancy forces together causes circulation of the solution in the reactor, see Figure 32.

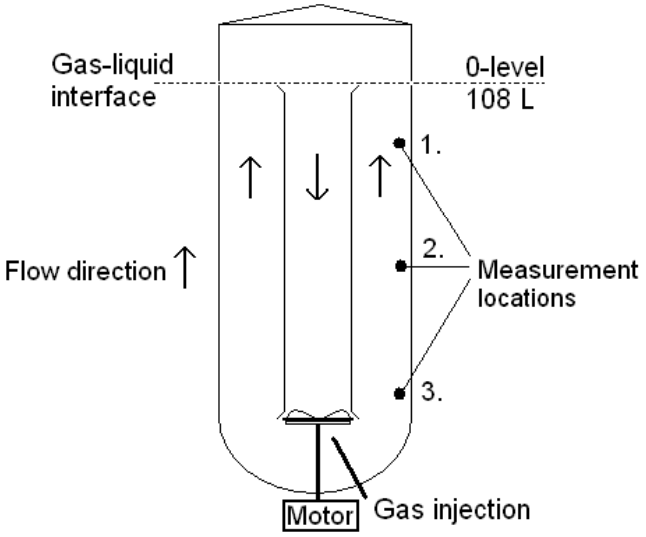

Figure 32 Schematic picture of the atmospheric leaching reactor´s water model

Liquid volume in the water model is 108 litres when filled up to the so-called 0-level. The rotational mixing speed of the impeller was measured and controlled with a frequency controller by ABB (ACS800) connected to the motor. The gas flow rate was measured and controlled with a rotameter and a needle valve. The gas pressure and temperature was measured before the reactor and before the rotameter. Used gas volumes are considered to be at ambient temperature. In order to avoid refraction errors during photographic measurements, the water model was surrounded with a square tank filled with water, as shown in Figure 33.

Figure 33 Pictures of the water model

The water model was used for studying gas-liquid interactions such as gas dispersion properties and mass transfer under different operating conditions, shown in Table IX. The results of the experiments presented in this chapter are tabulated in Appendix 6.

Table IX Gas-liquid interactions studied with different parameters

	Mixing speed RPM	Gas flow [l/min]	$ZnSO_4$ [M]	NaCl [M]	Soap [ml]	Liquid [cm]	Measurement Location
Bubble coalescence	600	2.5	0…0.2	0…0.4	0	0	1
Bubble size	354…981	0…45	0…0.2	0…0.4	0	0	1
Gas hold-up	354…981	0…45	0…0.2	0	0	0, 2, 4	Surface
Surface areation	354…981	0…45	0	0	5	0, 2, 4	Surface
Power consumption	354…981	0…45	0	0	0	0	-
Volumetric mass transfer	354, 600, 981	0…5	0	0	0	0	1,2,3

3.5.1 Bubble coalescence

The process solution contains great amounts of impurities and salts in the solution, which are known to have an important effect on the sizes and the coalescence of the bubbles. Bubble size was measured in the water model using the HUT Bubble Size Analyser developed by GRAU AND HEISKANEN (2002) and presented earlier in Chapter 3.4. The samples were taken from measurement place 1 where the bubble coalescence and break-up rates were assumed to reach a balance. The effect of hydrostatic pressure was ignored. The rotational mixing speed was set to 600 RPM and gas flow rate to 2.5 l/min. The number of bubbles analyzed ranged from 5000 to 20 000 bubbles in each test; results shown are the average of three different experiments.

LESSARD AND ZIEMINSKI (1971) defined transition concentration as the electrolyte concentration at which 50% coalescence occurs, on a scale where 100% coalescence is for water and 0% coalescence is the concentration where no further change in coalescence is measured with increasing electrolyte concentration. The critical coalescence concentration CCC values determined as LASKOWSKI (2004) suggested in the pilot water model can be seen in Figure 34.

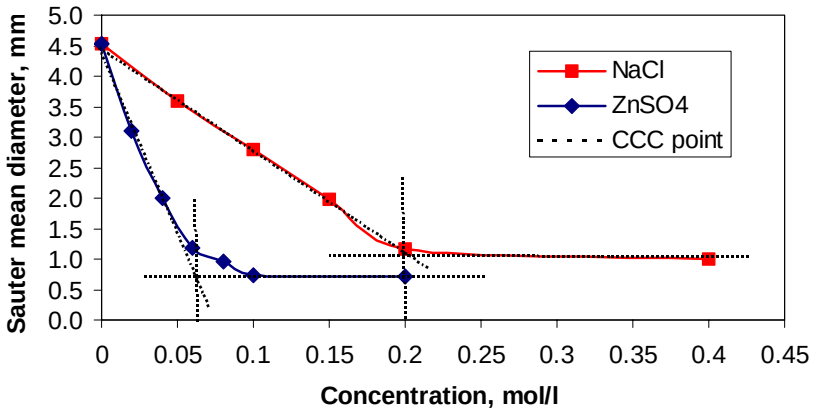

Figure 34 Sauter mean diameter of bubbles in aqueous solution as a function of NaCl and $ZnSO_4$ concentration with 600 RPM and 2.5 l/min

The CCC values determined were slightly higher than the transition concentration reported earlier, see Table X. It can be noted that values were determined in different flow conditions; this affected the results.

Table X Transition concentrations reported and critical coalescence concentrations (CCC) determined

	Transition concentration			CCC
	Lessard and Zieminski (1971)	Zahradnik et al. (1995)	Craig et al. (1993)	This work
Salt	[mol/l]	[mol/l]	[mol/l]	[mol/l]
NaCl	0.175	0.145	0.078	0.2
$ZnSO_4$	0.03-0.036	-	-	0.06
$MgSO_4$	0.032	0.036	0.02	-
H_2SO_4	0.056-0.060	-	No effect	No effect

At concentrations less than CCC, the bubble size is assumed to be controlled by the break-up and coalescence. In concentrations exceeding the CCC values, such as the real process solution, the non-coalescence of bubbles occurs and the bubble size is controlled by the breakage in the impeller region. In a non-coalescing medium, the size distribution of bubbles coming out from the impeller zone is expected to be preserved in other regions of the reactor, as was stated by PARTHASARATHY AND AHMED (1994). Closer investigations of coalescence, such as those of MARRUCCI (1969), TSANG ET AL. (2004), CRAIG ET AL. (1993), CRAIG (2004) AND WEISSENBORN AND PUGH (1996) are beyond the scope of this work.

3.5.2 Mixing effect on bubble size

Gas bubble size varied significantly in different liquids (pure water, 0.2 M NaCl and 0.1 M $ZnSO_4$), with different mixing speeds and gas flow rates, as can be seen in Figure 35.

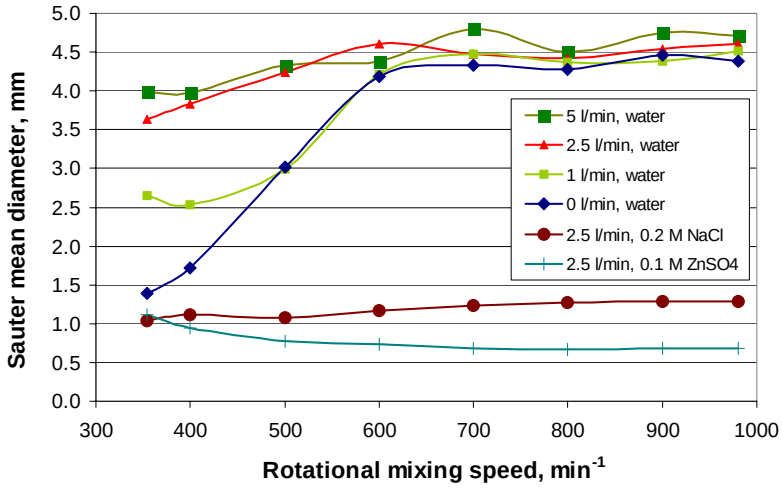

Figure 35 Sauter mean bubble diameter as a function of rotational mixing speed in water, 0.2 M NaCl and 0.1 M $ZnSO_4$ solutions at different gas flow rates

GREAVES AND KOBBACY (1981) stated that as the impeller speed increases, the eddies residing at the surface grow in intensity; this was noticed in the water model as well. Mixing created a vortex, which grew with the increase in the mixing speed, causing more gas to drawn into the liquid from the surface, as can be seen in Figure 36.

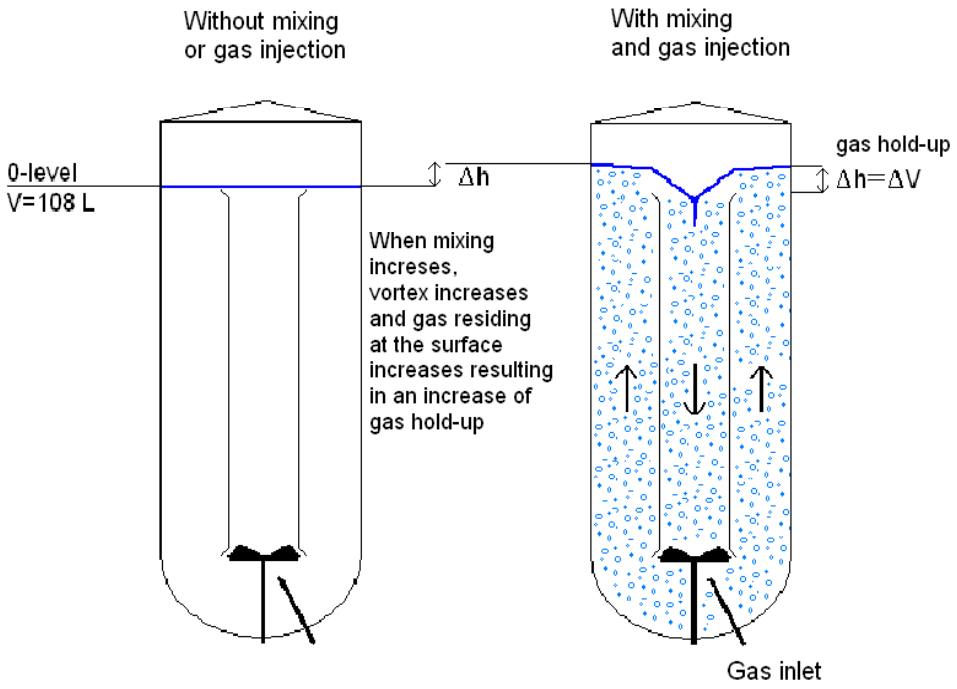

Figure 36 Schematic pictures of the vortex and total gas hold-up created in water model

With water, the increase in the gas content was followed by a rapid increase in the bubble size due to the coalescence behaviour. Especially at speeds <600 RPM, the vortex behaviour grew and an increase in gas content was notable. At rotational mixing speeds >600 RPM, the bubble size moderately increased with gas flow in water and the coalescence of bubbles apparently reached 100%. With non-coalescing solutions 0.2 M NaCl and 0.1 M $ZnSO_4$, the bubble size remained almost constant over the mixing speed range examined.

3.5.3 Gas flow effect on bubble size

Bubble size in the 0.1 M $ZnSO_4$ solution remained almost constant at different gas flow rates. Only with small gas flow rates were slight variations noticed, as can be seen in Figure 37.

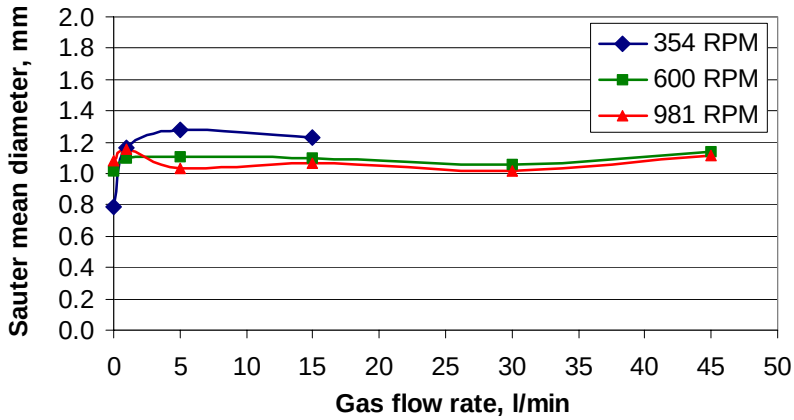

Figure 37 Sauter mean bubble diameter as a function of gas flow rate at rotational mixing speeds 354, 600 and 981 RPM

3.5.4 Gas hold-up

The overall gas hold-up in the solution was defined as follows:

$$\text{Gas hold-up } \% = \frac{V_{Gas}}{V_{Liquid} + V_{Gas}} \cdot 100, \tag{52}$$

where V_{liquid} and V_{Gas} were calculated by measuring the liquid surface heights, as illustrated in Figure 36. The liquid surface declined towards the centre due to flow conditions when operating. The height of the liquid surface was determined as the average from the reactor wall to the centre tube circle, ignoring the centre tube itself. This was considered to represent the overall gas hold-up with sufficient accuracy, even though the results contain slight inaccuracies relating to the problematic vortex.

Experiments indicated the bubble size decreased as the concentration of the zinc sulphate was increased. Simultaneously, the overall gas hold-up showed the same type of behaviour and increased up to the CCC ≈ 0.06 M point and flattened out afterwards, as can be seen in Figure 38. The growing effect of gas hold-up is mostly due to the longer residence time of the gas bubble, since the rising velocity of the bubble decreases with

diameter CLIFT ET AL. (1978). The very small effect of electrolyte concentration on gas hold-up after transition concentration was noticed by ZAHRADNIK ET AL. (1995).

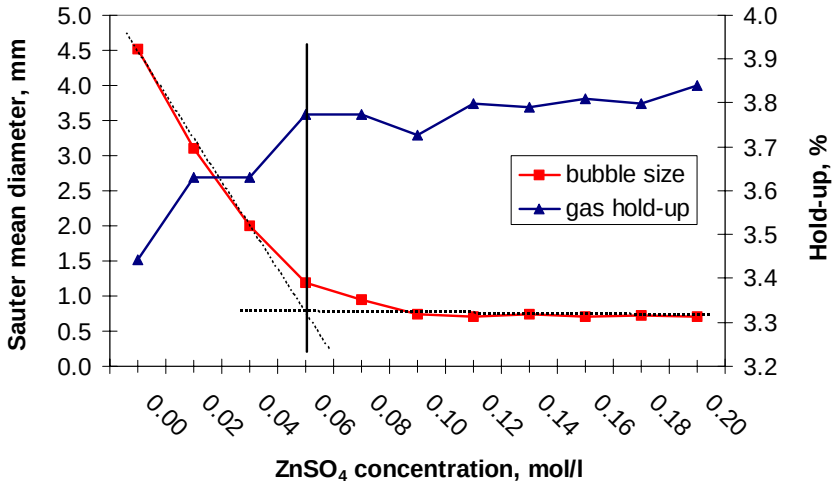

Figure 38 Sauter mean bubble diameter and gas hold-up as a function of zinc sulphate concentration (Gas flow rate 2.5 l/min and 600 RPM)

The gas hold-up was measured in a non-coalescence solution (0.1 M $ZnSO_4$) and was noticed to increase linearly as a function of rotational mixing speed, see Figures 39 and 40.

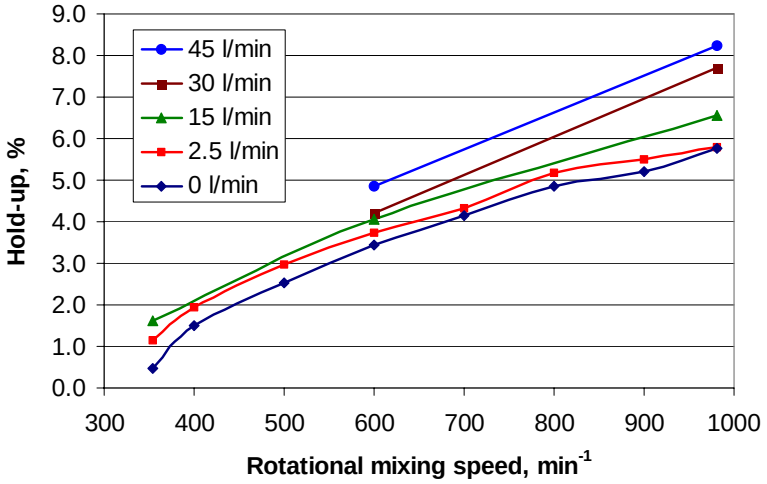

Figure 39 Gas hold-up in 0.1 M $ZnSO_4$ solution as a function of rotational mixing speed at different gas flow rates

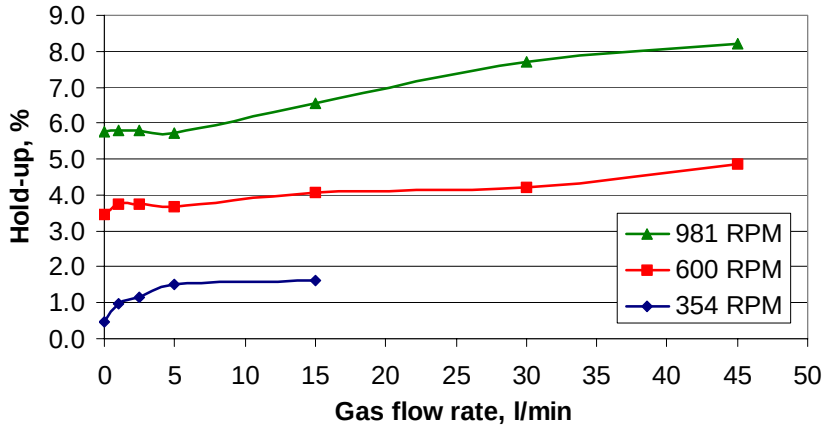

Figure 40 Gas hold-up in 0.1 M $ZnSO_4$ solution as a function of gas flow rate at rotational mixing speeds 354, 600 and 981 RPM

The previous tests were carried out with a liquid volume of 108 L (surface at 0-level). Increasing the liquid volume (height +2 and +4 cm) had no important effect on the gas hold-up, as can be seen in Figure 41.

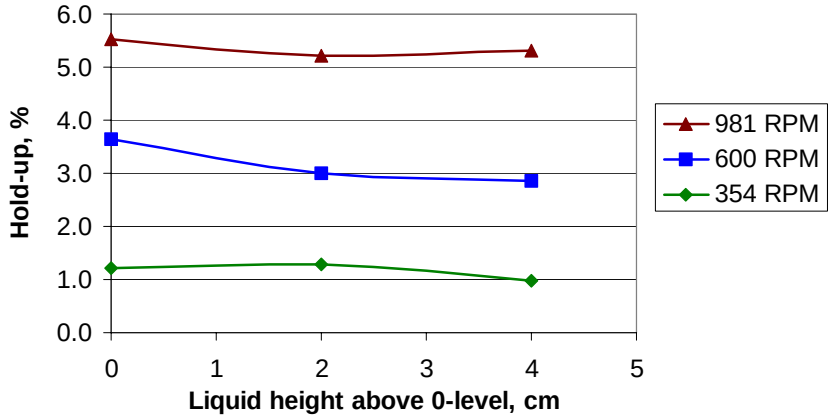

Figure 41 Gas hold-up as a function of water height above 0-level at rotational mixing speeds 354, 600 and 981. Gas flow rate 5 l/min

3.5.5 Surface aeration

Earlier, it was noticed that the gas appeared in the liquid even without injection. Therefore, when no gas was injected, all the gas entering, leaving and circulating in the reactor was originally from the open gas-liquid surface. The portion (not gas rate) of the gas entering from the surface was determined by measuring the concentration of the dissolved oxygen in the liquid. The injected gas was changed to pure nitrogen (99.999%).

Therefore, all the oxygen in the liquid originated from only the atmosphere through the surface. Without nitrogen injection, the oxygen concentration in the water reached an equilibrium $C_{O2,eq}$ according to Henry's law. If nitrogen gas was injected, the oxygen concentration in liquid eventually reached a "balance" C_{O2} of gases (air from the surface and injected nitrogen). When 100% of the gas was originally from the surface, the relation $C_{O2}/C_{O2\ eq.} = 1$, and when the relation $C_{O2}/C_{O2,eq.} \approx 0$, all the gas was injected nitrogen. The concentrations were assumed to demonstrate the relation between gas flow rate from the surface and that injected with the following relation:

$$\frac{C_{O_2}}{C_{O_2,eq}} \approx \frac{\dot{V}_{Surface}}{\dot{V}_{Injected}}. \tag{53}$$

The kinetic and pressure effect on oxygen concentration was ignored. The rate of gas entering from the surface decreased rapidly as the injected gas flow rate was increased, as illustrated in Figure 42. NIENOW AND CHAPMAN (1979) also observed surface aeration to decrease with an increase in the gas flow rate and even at low mixing rates.

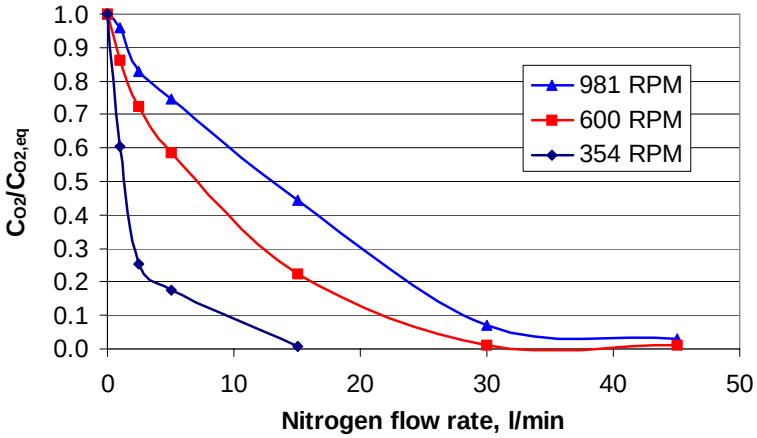

Figure 42 Relative oxygen concentration change as a function of nitrogen flow rate at mixing speeds 354, 600 and 981 RPM and at 0-level

An increase in surface aeration was observed when the mixing speed was increased; this was due to a greater downdraft in the centre tube and a stronger liquid flow towards the centre of the tube.

The liquid volume and addition of surface active agents was found to have an effect on the surface aeration. The reduction in surface aeration as a function of rotational mixing speed with different liquid heights can be seen in Figure 43.

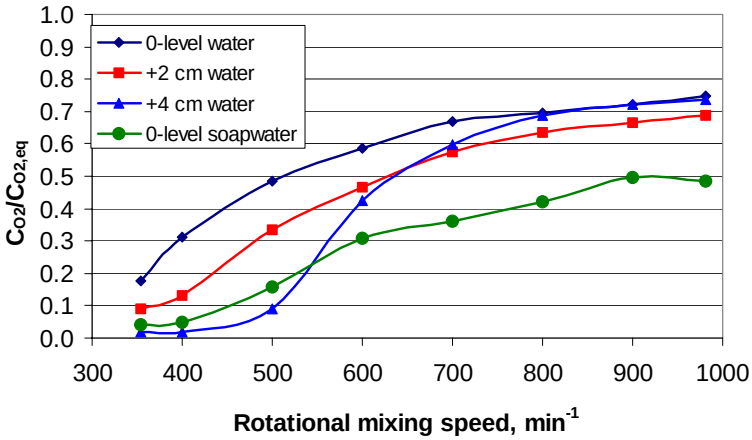

Figure 43 Relative oxygen concentration change in water with different heights and in soap water as a function of rotational mixing speed (Nitrogen flow rate of 5 l/min)

As can be seen in Figure 43, using soap water instead of pure water reduced the surface aeration significantly. In the experiment, a total of 5 ml of soap was added to the liquid for the purpose of creating conditions of non-coalescence.

Surface aeration was related to the vortex on the gas-liquid surface. Increasing the liquid height (+2 and +4 cm) decreased the vortex and therefore also the amount of gas entraining into liquid, see schematic picture of the vortex behaviour in Figure 44.

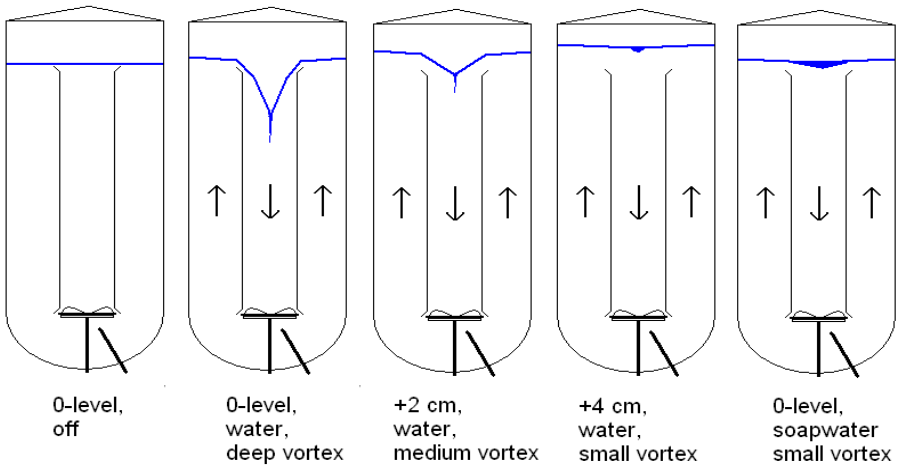

Figure 44 Schematic picture of changes at the gas-liquid surface at different water heights (0-level, +2 and +4 cm) and for soap water

Another interesting observation was made when the soap-water volume was changed from 0-level to +4 cm. Increasing the liquid volume increased the foaming of the process. With a small amount of liquid, the flow on the surface was strong towards the downdraft in the centre tube and carried the foam back to the circulation of the reactor. When liquid volume was increased, the surface flow became smaller and foam was able to accumulate on the surface. Increasing the liquid even more, the level of the foam bath started to rise.

3.5.6 Power consumption

The power consumption P [W] was estimated from the rotational mixing speed RPM and torque τ of the motor with following equation:

$$P = \tau \cdot \mathrm{RPM} \cdot \frac{2 \cdot \pi}{60}. \tag{54}$$

With increasing mixing speed the power consumption increased as expected, see Figure 45. The liquid used in the experiment was 0.1 M zinc sulphate.

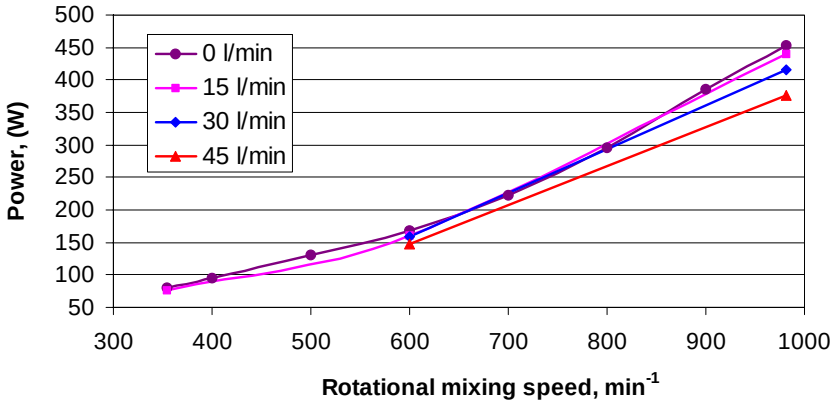

Figure 45 Power consumption as a function of rotational mixing speed at different gas flow rates

An increase in the gas flow rate, on the other hand, decreases the power consumption, as can be seen from the relative power consumption drop P_g/P_0 shown in Figure 46.

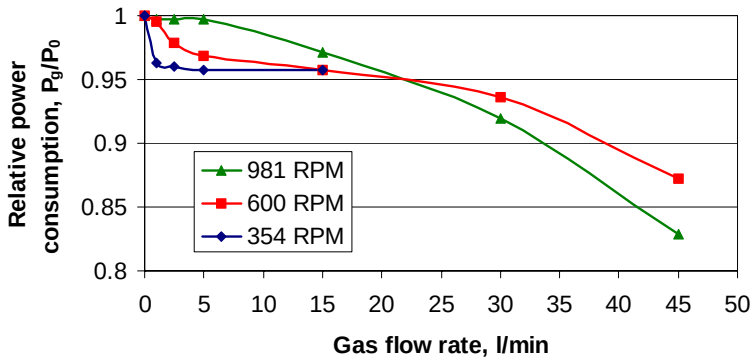

Figure 46 Relative power consumption P_g/P_0 as a function of gas flow rate with different rotation mixing speeds

With mixing speeds of 354 and 600 RPM, the relative power consumption decreased more than at 981 RPM; this was due to gas entering from the vortex and increasing the gas contents. For the same reason, the power consumption decreased more as a relative value at small gas flow rates <5 min/l.

3.5.7 Volumetric mass transfer coefficient k_La

The effect of the gas flow rate on the mass transfer coefficient k_La at different impeller speeds and measurement locations 1 and 3 can be seen in Figure 47. The mass transfer coefficient values were measured with dynamic pressure method and calculated as presented in Chapter 3.4.4.

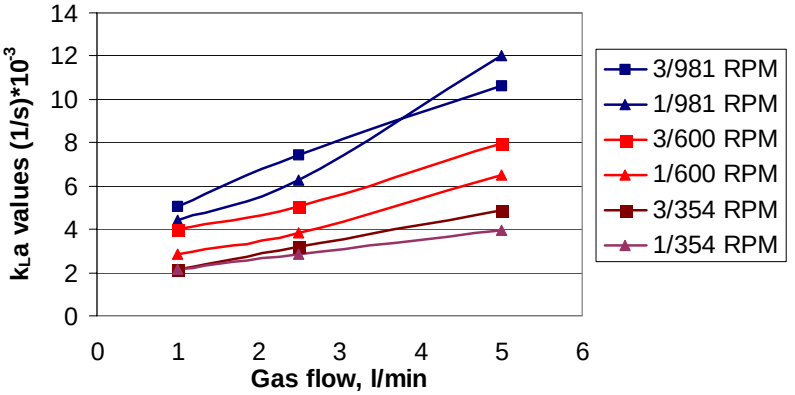

Figure 47 Mass transfer coefficient k_La *[*s^{-1}*]*$\times10^{-3}$ *in measurement location 1 and 3 as a function of gas flow rate with mixing speeds 354, 600 and 981 RPM*

The volumetric mass transfer values represent the average of three experiments and were carried out with tap water and oxygen gas (99.999%). The volumetric mass transfer coefficient measured at location 2 with a gas flow rate of 2.5 l/min and 600 RPM gave an average value of $(4.57\pm0.06)\times10^{-3}$ [s^{-1}]. Increasing the gas flow rate and mixing speed of the impeller increased the gas mass transfer due to a greater gas hold-up and gas-liquid contact area. The measured values ranged between $(2.17\text{-}12.00)\times10^{-3}$ [s^{-1}]. The mass transfer was more efficient at measurement place 3 than 1, due to a shorter distance to the impeller, where the flow conditions were more favourable for mass transfer.

3.6 GAS-LIQUID MASS TRANSFER EQUIPMENT

The following experimental set-up was designed for determining the mass transfer coefficient $K \approx k_L$ (m/s) values between gas and liquid phases. The gas-liquid interface examined was created with an inverted and immersed "glass-cup" with a diameter of 0.055 m, Figures 48 and 49.

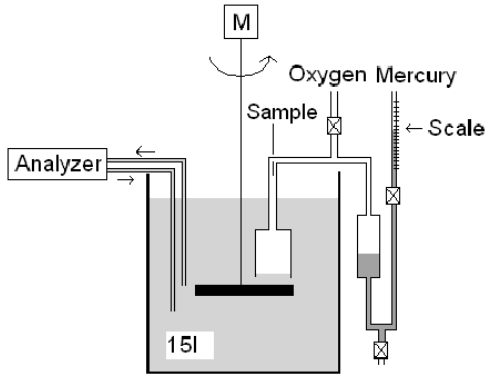

Figure 48 Schematic picture of the experimental arrangements

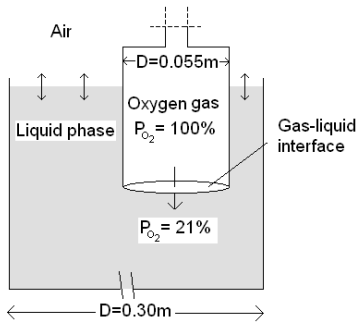

Figure 49 Schematic picture of the experimental arrangements

The interface between pure oxygen gas and test liquid was controlled with a mercury regulator. The volume of oxygen that dissolved from the gas phase was determined by measuring the mercury when the initial level of the interface was adjusted at the end of the experiment. The driving force for the gas mass transfer was the oxygen concentration differences. The liquid was in contact with pure oxygen in the test section and with air at other gas-liquid interfaces. The ratio between these two interfaces was 1:30, which was large enough to keep the liquid phase in equilibrium with the air. The oxygen content accumulating into distilled water was <1% larger than in equilibrium after three hours of the experiment, and therefore could be ignored. Oxygen concentration was measured with an oxygen analyser (Orbisphere Model 26071) in experiments carried out with pure water.

In the experiments, the mass transfer of gas entering the liquid is determined by measuring the amount of gas entering into the liquid through a certain area A in time t. Then the mass transfer coefficient can be written as follows:

$$k_l = \frac{D}{\delta} = \frac{\Delta n}{tA(C^* - C)}. \tag{55}$$

Solubility values used in the calculations were presented in Section 2.4. The reproducibility of the k_L determination was carried out with distilled water at 60 RPM; the result was 19.24±0.63 [m/s] with a 95.0% confidence level. According to reproducibility experiments, the error of the gas-liquid mass transfer equipment is considered to be less than 5% throughout the experimental program. Values of the experiments carried out in Section 3.6 are listed in Appendix 7.

3.6.1 Gas phase concentration

Gas mass transfer occurs in both directions from the interface. The addition of nitrogen and mostly vapour pressure decreased oxygen content by 9% in one-hour and 12% in three-hours, see Figure 50. Gas samples taken were analysed using the high-accuracy Gas Chromatograph HP 5880A. The driving force for the oxygen mass transfer therefore changes during the experiment and needs to be taken into consideration. According to gas-phase measurements, the oxygen contents of 95% in the one-hour experiment and 93% in the three-hour were used in mass transfer coefficient calculations.

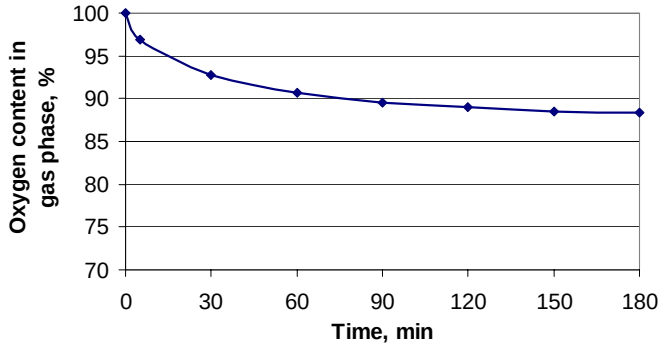

Figure 50 Oxygen content in gas phase as a function of time (water with 45 RPM)

3.6.2 Mass transfer coefficient k_L values between oxygen and water

Increasing the mixing intensity increased the mass transfer coefficient k_L. Values of oxygen mass transfer into distilled water ranged between (13.8-19.16)×10^{-5} [m/s], see Figure 51 CALDERBANK AND MOO-YOUNG (1961) determined the same coefficient value to be 13.5×10^{-5} [m/s]. K_L values increased with rotational mixing speed due to enchanting the surface removal and turbulence at the interface. The liquid phase was

stirred with a four-90° blade impeller (r = 0.06 m, h = 0.02 m) with 0.02 m from the cup. Propellers were set to cross the whole gas-liquid interface examined. The mixing speeds 30, 45 and 60 RPM were chosen to cover liquid flow conditions from a moderate flow of 30 RPM (without vertical impact or waving effect on the interface) to a rigorous flow of 60 RPM, which was assumed to simulate similar flow conditions to those of a gas bubble in a free rise.

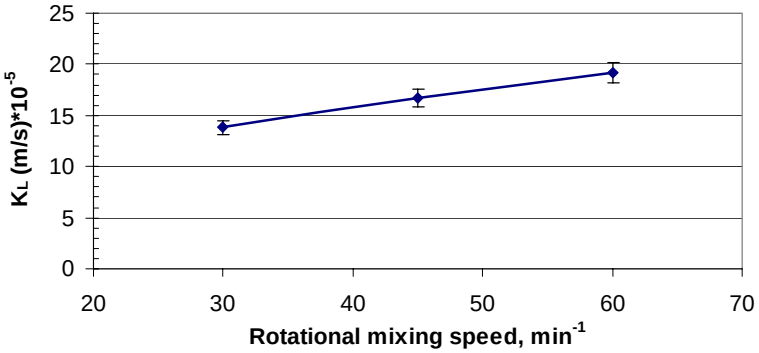

Figure 51 Mass transfer coefficient k_L between oxygen and water as a function of rotational mixing speed

3.6.3 Pressure effect on k_L values

Hydrostatic pressure mostly affects the gas phase and gas side mass transfer k_G , and therefore plays a minor role in increasing the total mass transfer coefficient, since $k_L << k_{G,,}$ as stated earlier in Section 2.3. Increasing the hydrostatic pressure from 200 to 800 Pa did not affect the mass transfer coefficient, see Figure 52. The same effect has also been reported by TERAMOTO ET AL. (1974), who carried out experiments with a pressure range of 2-100 atm.

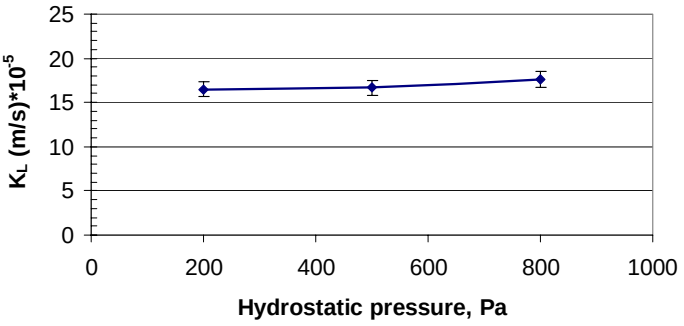

Figure 52 Mass transfer coefficient k_L between oxygen and water as a function of hydrostatic pressure with 45 RPM

3.6.4 Mixing and electrolytes effect on k_L values

K_L values increased with rotational mixing speed due to the enchanting of the surface removal and turbulence at the interface, see Figure 53.

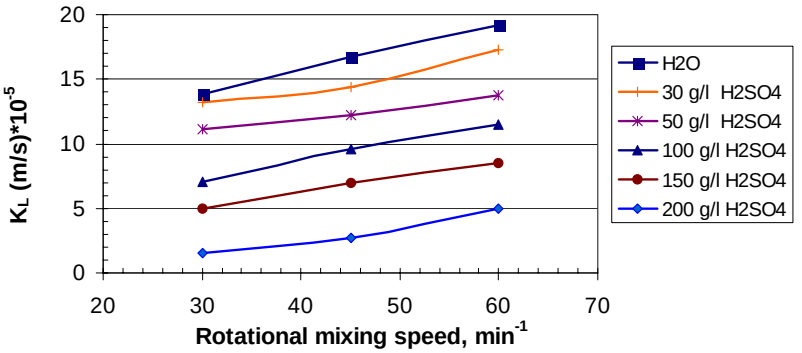

Figure 53 Mass transfer coefficient k_L between oxygen and different liquids as a function of rotational mixing speed

Increasing electrolyte concentration decreased the mass transfer coefficient, as can be seen in Figures 53 and 54. Results indicate the same trend as correlations (33) and (34) for k_L values, which decrease when diffusivity of the gas decreases and when viscosity of the liquid increases. According to the equations, an increase of liquid density should enchant the mass transfer coefficient. Experiments indicated the effect of the density on k_L to be smaller than diffusivity and viscosity, since the total k_L value decreased despite the density increasing.

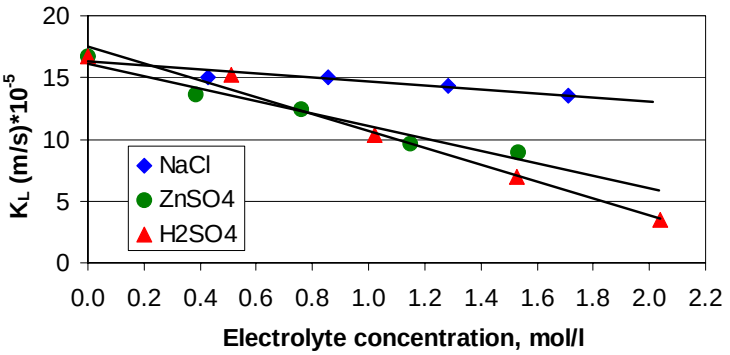

Figure 54 Mass transfer coefficient k_L *between oxygen and aqueous solutions containing electrolytes with 45 RPM*

Mass transfer coefficient k_L decreased more rapidly when zinc sulphate and sulphuric acid was increased than when sodium chloride was increased.

3.6.5 Mass transfer coefficient k_L between oxygen and process solution

The mass transfer coefficient k_L values between oxygen and process solutions were much lower than for water, see Figure 55. The k_L values varied between $(4.72\text{-}11.32)\times10^{-5}$ for process solution 1 and $(1.50\text{-}3.78)\times10^{-5}$ [m/s] for process solution 2.

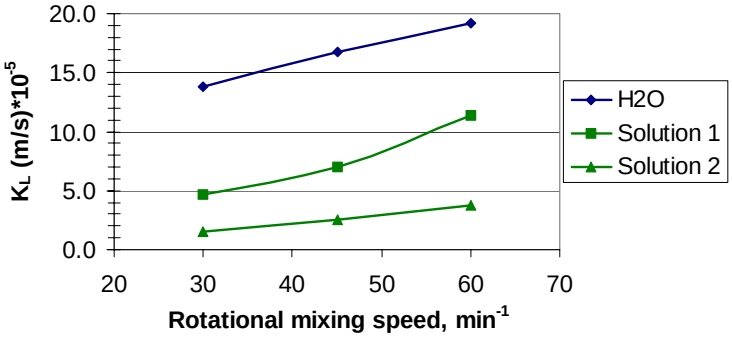

Figure 55 Mass transfer coefficient k_L between oxygen and process solutions 1 and 2 as a function of rotational mixing speed

Process solution 2 contained more zinc sulphates than solution 1, which was sufficient to lower the mass transfer value.

3.7 MODIFIED HIGH TEMPERATURE AND PRESSURE AUTOCLAVE

The leaching experiments at higher temperatures and pressures were carried out in a specially designed and built autoclave with a total reactor volume of 30.162 litres. The purpose of the autoclave experiments was to determine the oxygen consumption rate through a known flat gas-liquid interface at temperatures and pressures corresponding to actual process conditions. The reactor was placed in a temperature-controlled oil bath, see Figure 56.

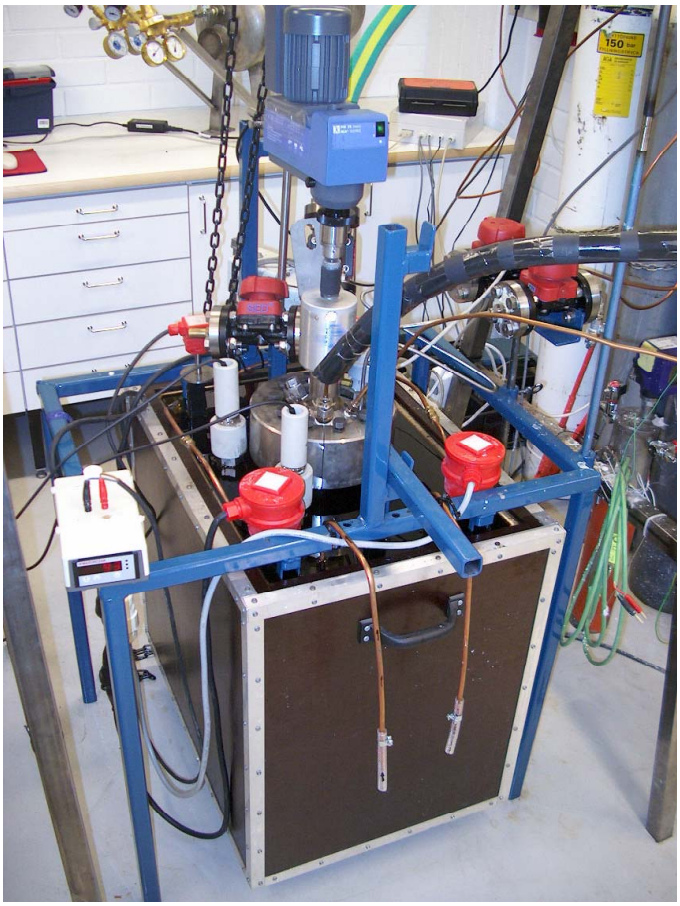

Figure 56 Picture of the modified autoclave

A centrally located axis equipped with 45° six-bladed stirrers with a diameter of 0.133 m in the liquid phase and 0.08 m in the gas phase was employed to mix both the gas and liquid phases. The mixing was chosen to keep the liquid and gas phase well mixed without breaking the gas-liquid interface. Six symmetrically placed bafflets measuring 2×30×320 mm on the wall of the reactor were used to increase the effectiveness of the mixing and

avoid the formation of vortexes. Total gas pressure in the reactor was controlled by feeding the oxygen (99.999%) into the gas phase above the solution. Oxygen was introduced to the reactor from a separate container with a volume of 29.5 litres. Initially, the container was pressurised to P_{O2} = 10 bars; the ideal gas law was assumed to apply. The pressure inside the reactor was kept at 1 or 3 bars. A schematic picture of the autoclave can be seen in Figure 57.

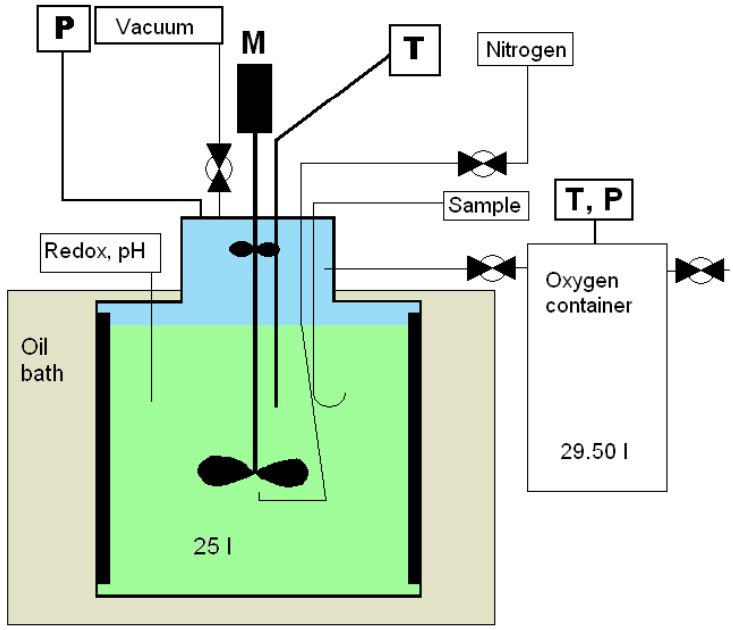

Figure 57 Schematic picture of the modified autoclave. Gas phase is shown in blue, solution in green.

The temperature of the solution was measured with an SEM 104/P Pt-100 thermometer with an accuracy of ±0.2% and the pressure with a Wika Transmitter UT-10 pressure gauge with an accuracy of ±0.15%; both were connected to the Windaq data acquisition system. Redox potential and pH were measured with a Jumo standard electrode with an active platinum element, while an Ag/AgCl conductive system was used to take redox and pH measurements; both were connected to dTRANS Rd01 transmitters.

3.7.1 Experimental procedure

The overall leaching reaction was composed of the following main stages: 1. oxygen dissolution, 2. oxidation of the iron (Fe^{2+}) and 3. zinc dissolution by three-valent iron (Fe^{3+}) as can be seen in Figure 58.

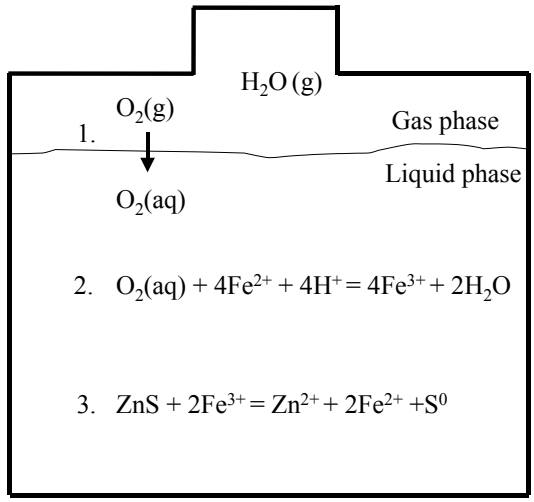

Figure 58 Main stages 1, 2 and 3 in the autoclave experiments

In this work, the oxygen consumption rate refers to stages 1 and 2. The oxygen consumption rate through the flat gas-liquid interface (d = 0.32 m) was determined by measuring the oxygen pressure drop in the container; values were therefore given in units of mmol/(m^2s).

With only a few exceptions involving process solutions, the experiments were carried out batchwise with the following procedure.

- The aqueous mixture of H_2SO_4 and $ZnSO_4 \cdot 7H_2O$ was preheated to 90 °C in a reactor immersed in an oil bath.
- After 10-12 h of preheating and stirring, other chosen reagents – lignosulphonate, non-foaming reagent entchäumer 7800, $FeSO_4 \cdot 7H_2O$, $CuSO_4 \cdot 5H_2O$, ZnS concentrate, octhene and ethanol – were added to the solution.
- After closing the reactor, the air was removed by applying 5 minutes of suction with 0.4 bars underpressure.
- The experiment was started by the introduction of a constant oxygen pressure 1±0.015 bar into the reactor.

- All the required values – temperature and pressure of reactor and container, redox potential and liquid samples – were collected.

- The first 6 hours of the experiment comprised the stabilising stage (mostly temperature and vapour pressure).

- At 72 hours, the oxygen pressure was increased to 3 bars and the experiment was continued for the following 7-10 days.

The oxygen consumption rate was determined as an average value at time range when consumption remained fairly constant.

Experiments were carried out with different solutions and one with O_2-SO_2 gas mixture, all are listed in Table XI. The temperature of the experiments was held at 90 °C, mixing speeds were 200 or 250 RPM and pressures 1 or 3 bars. The ZnS concentrate used contained approximately 50% Zn, 10% Fe and 30% S. Data from the experiments are listed in Appendix 9.

Table XI Composition of the solutions and gas studied

Substance	Standard solution	Variable amount	Units	Other information
H_2O	18.8		l	Distilled
H_2SO_4	50		g/l	96-97%
Zn^{2+}	100	0 and 60	g/l	$ZnSO_4´7H_2O$
Fe^{2+}	10		g/l	$FeSO_4´7H_2O$
Cu^{2+}	1		g/l	$CuSO_4´5H_2O$
Lignosulphonate	4.58		g	commercial
Entchäumer 7800	0.5		ml	commercial
ZnS concentrate	20	100	g/l	see text
Octhene		1.5 and 3	vol-%	>99%
Ethanol		1.5 and 3	vol-%	>99.5%
SO_2		2	vol-%	±2%

Total solution volume 25 litres (STP)

In addition, two different process solutions were examined at temperatures ranging from 50 to 90 °C, mixing speeds ranging from 200 to 250 RPM and pressures from 1 to 3 bars.

3.7.2 Gas phase in the reactor

The composition of the gas phase played an important role in the experiments; it was therefore studied separately by comparing the calculated and measured results to reported values.

When the total pressure in the reactor was kept at $P_{tot} \approx 3$ bars, the partial pressure for oxygen and water was calculated using the HSC programme to be $P_{O2}/P_{tot} \approx 0.77$ and

$P_{H2O}/P_{tot} \approx 0.23$ in equilibrium and giving $P_{H2O} = 0.23 \times 3$ bars ≈ 0.69 bars in the reactor, see figures in Appendix 8.

Values reported by KESKINEN (1989) for vapour pressures in equilibrium were 0.7017 bars at 90 °C, 0.312 bars at 70 °C and 0.1235 bars at 50 °C.

The vapour pressure was also experimentally measured for the standard solution. The reactor was initially pressurised to $P_{tot} \approx 3$ bars ($P_{tot} \approx P_{O2} + P_{H2O}$) with oxygen feeding. In the closed reactor, the oxygen was consumed according to stages 1 and 2 and eventually left only vapour pressure $P_{H2O} \approx P_{tot} = 0.766$ bars ($P_{H2O}/P_{3bars} \approx 0.26$) in the gas phase, as can be seen in Figure 59

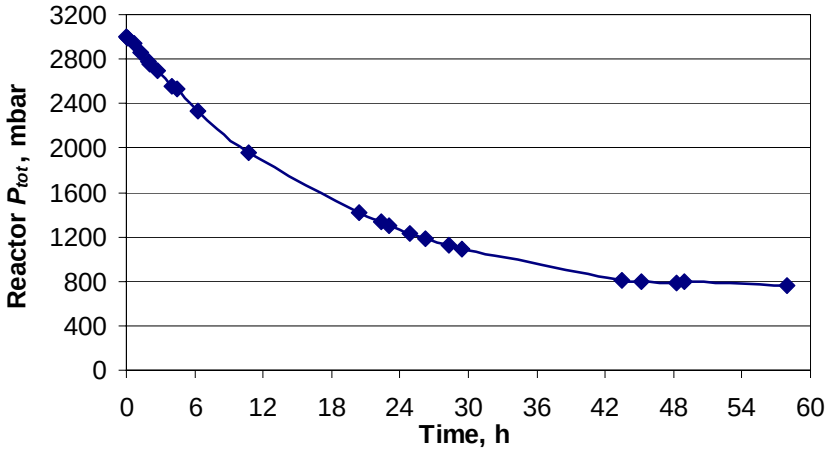

Figure 59 Total pressure in the reactor as a function of time

With respect to the differences between calculated and measured situations (equilibrium vs. dynamic state, water vs. solution), the vapour pressure values P_{H2O}/P_{tot} were almost the same, 0.23 and 0.26. Both results indicate P_{O2} to be different from 100% and to be more or less replaced by the vapour pressure.

3.7.3 Effect of octhene, ethanol and sulphur dioxide on oxygen consumption rate

Attempts to improve the dissolution rate were carried out with 1.5 vol-% and 3 vol-% of octhene (water insoluble) or ethanol (water soluble) in the standard solution. Since oxygen has better solubility in octhene and ethanol the small addition was expected to increase also the oxygen consumption rate. Also, one experiment was carried out in a standard solution but with a gas mixture of 98 vol-% O_2 and 2 vol-% SO_2, which is found by ADAMS AND MATTHEW (1981), NAMI (1988), FERRON (2000) and ZHANG (2000) to improve the oxidizing of iron(II). Experiments were divided and conducted using two different mixing speeds: 200 and 250 RPM. Oxygen consumption rate, redox potential and sample analysis results were from the same experiment, but are presented separately.

3.7.3.1 Oxygen consumption rate

The oxygen consumption rate in the reactor was measured by recording the absolute pressure drop in the container. As the oxygen was consumed in the leaching reaction, the pressure in the container decreased. The first 72 hours of the experiment were conducted in at 1 bar pressure in the reactor. At 72 hours, the reactor pressure was increased to 3 bars, which caused a pressure drop in the container, as can be seen in Figure 60.

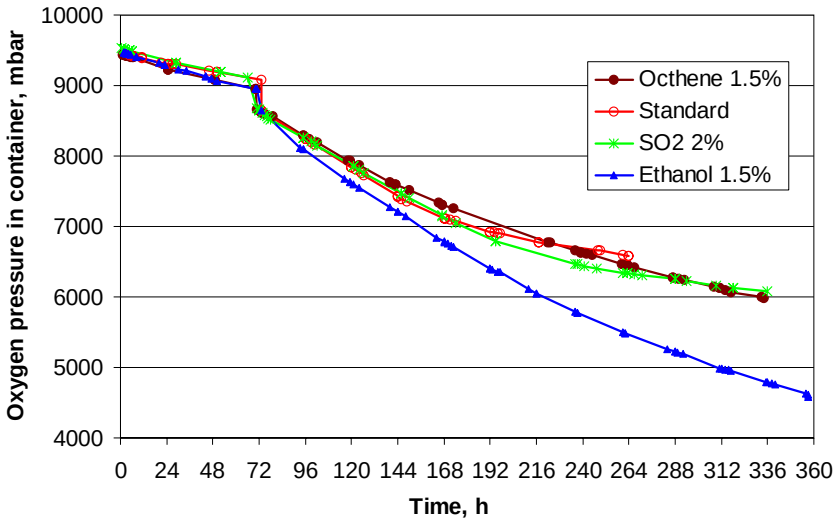

Figure 60 Oxygen pressure in the container as a function of time with different solutions. Rotational mixing speed 200 RPM, 90 °C and 1 bar <72 h and 3 bars > 72 h.

With a mixing speed of 200 RPM, the oxygen consumption rate slightly increased with the solution containing 1.5 vol-% ethanol compared to other experiments (standard, 1.5 vol-% octhene and 2 vol-% SO_2 gas).

With a mixing speed of 250 RPM, the oxygen consumption rates were, until 144 hours, almost the same with all the solutions, as can be seen in Figure 61.

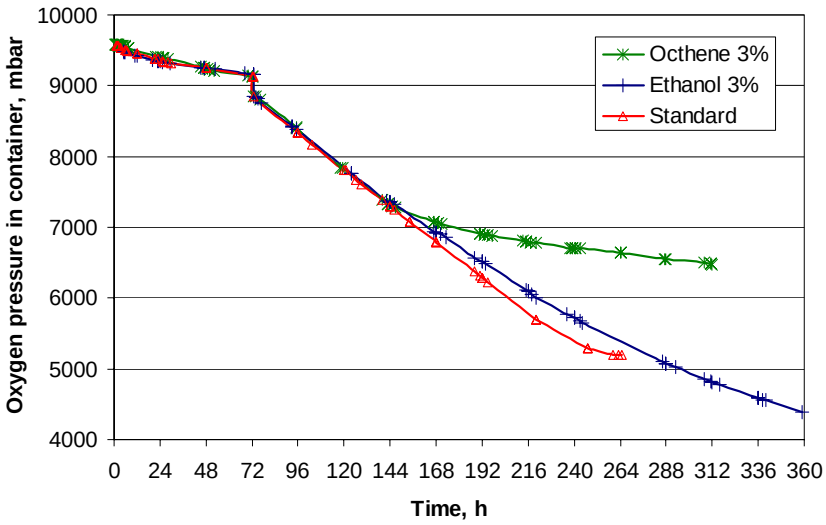

Figure 61 Oxygen pressure in the container as a function of time with different liquids. Rotational mixing speed of 250 RPM

The addition of 1.5 or 3 vol-% ethanol to the solution favoured oxygen consumption proceeding further during the experiment (concerning oxygen consumption), which indicates ethanol interferes with stage 3.

Experiments indicate stages 1 and 2 occur. Also, stage 3 showed a rate-controlling effect since the oxygen consumption rates were noticed to have decreased. The effect of stage 3 became noticeable after 144 hours of the experiment, see Figures 60 and 61. Oxygen consumption rates in different solutions were calculated as an average of the 96 and 144 hours of the experiments. This was considered reasonable as the consumption rates remained fairly constant throughout the time range, without temperature and pressure effects, and yet stage 3 retained a minor role. Calculated values varied between 0.061-0.091 mmol/(m^2s) and are tabulated in Table XII. With mixing speeds of 250 RPM, the values were greater due to more efficient surface renewal at the gas-liquid surface.

Table XII Determined average oxygen consumption rate values between 96-144 h

	200 RPM				250 RPM		
Oxygen consumption rate	Standard	Ethanol 1.5%	Octhene 1.5%	SO2 2%	Standard	Ethanol 3%	Octhene 3%
mmol/(m^2s)	0.070	0.073	0.061	0.065	0.089	0.086	0.091

3.7.3.2 Redox potential

The coupled reduction and oxidation processes that take place simultaneously are called *redox reactions* and can be measured in the form of voltage (potential). Oxidation and reduction reactions are considered to represent stages 2 and 3 in this work. Therefore, measured redox potentials of the solution illustrated the balance between stages 2 and 3

during the experiments. All the iron was introduced into solution as Fe^{2+} and as the redox potential increased stage 2 occurred faster than stage 3, as shown in Figure 62.

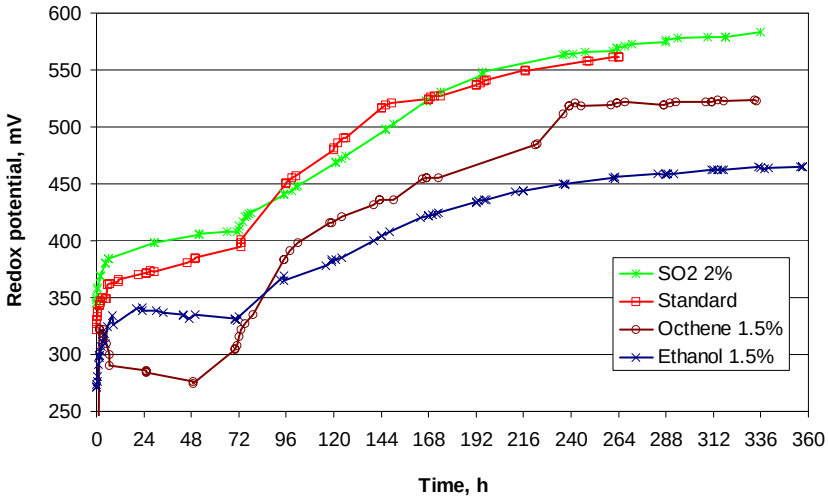

Figure 62 Measured redox potentials as a function of time with different liquids. Rotational mixing speed of 200 RPM

Experiments gave the highest redox potential values with the standard solution and with a gas mixture of 2 vol-% SO_2. With 1.5 vol-% octhene and ethanol in the solution, the redox potential values were low throughout the experiment, which indicates either stage 2 occurred slower or stage 3 faster when compared to the standard solution.

In the experiment with 3 vol-% of octhene in the solution the oxidation rate improved, see Figure 63.

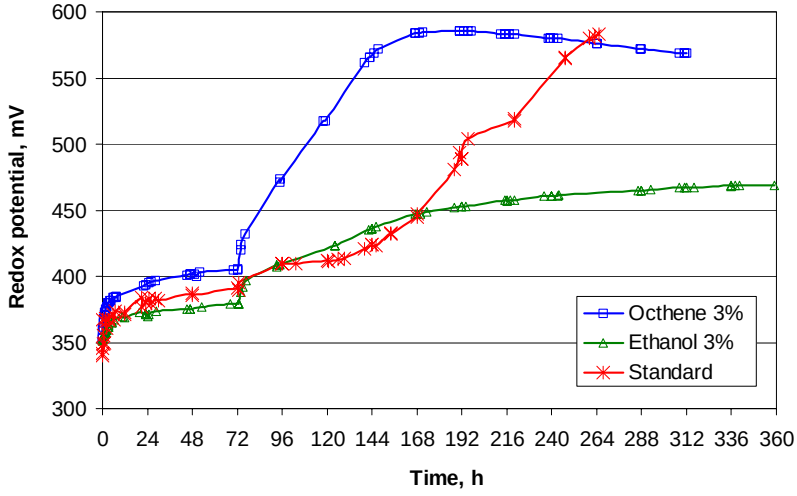

Figure 63 Measured redox potentials as a function of time with different liquids. Rotational mixing speed of 250 RPM

The redox potential increasing rate slowed down or even stopped during each experiment, which indicated the kinetics of stage 3 decreased. This was probably due to a combination of the reacting surface area of the particle decreasing, and the reaction product layer on the surface growing, according to the shrinking-core model presented in Section 2.3.2.

With both mixing speeds, the addition of ethanol gave low redox potential values, which indicated ethanol reduced the kinetics of stage 2 or accelerated the kinetics of stage 3. However, taking into consideration the oxygen consumption rates, which were almost the same in all experiments, the ethanol is assumed to accelerate the kinetics of stage 3.

3.7.3.3 Dissolution of concentrate

The kinetics of stage 3 was studied taking liquid samples (from 15 to 20) during the experiments. Solid contents were weighted after filtering and dissolved zinc and iron contents were analysed with an atomic absorption analyser at the Analysing Centre of HUT. The recovery and dissolution of the concentrate was not the main focus of the experiments; more detailed investigations of solid-liquid reactions were beyond the scope of this work. Mixing efficiency was considered to be sufficient to keep the liquid phase well mixed and the samples representative of the liquid.

The decrease of the solid concentration (g/l) and increase of dissolved Zn^{2+} concentration (g/l) as a function of time in the standard solution experiment can be seen in Figure 64.

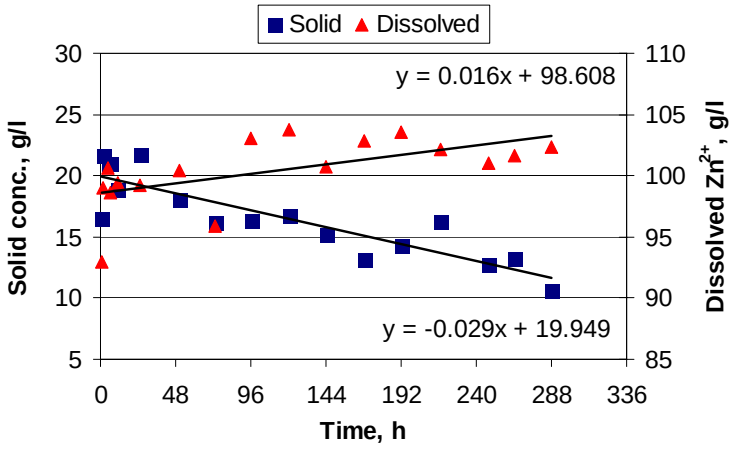

Figure 64 Measured contents of solid undissolved concentrate and dissolved zinc concentrations in standard solution as a function of time

Straight lines were fitted into experimental values and from these lines the average concentration changing rates were calculated. Values for dissolved iron concentrations were analysed and determined with the same procedure. All the average values of concentration change rate determined during the different experiments are listed in Table XII.

Table XII Solid particles dissolution and zinc and iron concentration rates determined in different experiments

		200 RPM				250 RPM		
Average rates		Standard	Ethanol 1.5%	Octhene 1.5%	SO2 2%	Standard	Ethanol 3%	Octhene 3%
Solid dissolution	(mg/h)	29	17	46	30	25	27	39
Dissolved Zn^{2+}	(mg/h)	16	19	16	29	39	24	22
Dissolved iron	(mg/h)	2	3	2	2	6	5	0

It was noticed that a small amount of the dissolved zinc or iron was filtered, together with solid particles, which caused measured dissolved zinc amounts to become smaller and solid amounts larger than the real ones. However, the determined average values were considered sufficient for the purpose to indicate the leaching and to allow stage 3 to occur.

3.7.4 Effect of dissolved Zn^{2+} on oxygen consumption rate

The amount of zinc sulphate affects significantly the solubility of oxygen as stated earlier. The process solution contained high contents of dissolved sulphates; the effect of this on the oxygen consumption rate was studied with different concentrations. Decreasing the dissolved Zn^{2+} content from 100 g/l to 0 g/l in the solution increased the oxygen consumption rate significantly; this could be seen as a pressure drop in the container, see Figure 65.

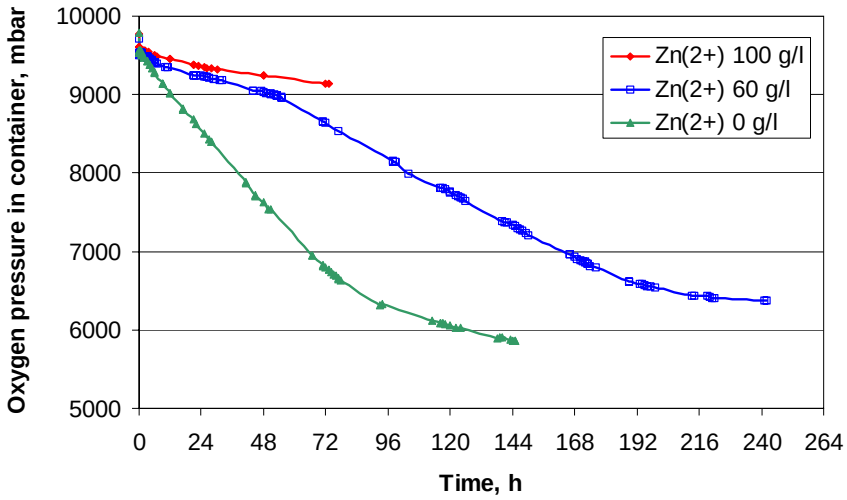

Figure 65 Oxygen pressure in container as a function of time for different solutions. Rotational mixing speed of 250 RPM.

Pressure in the reactor was kept at 1 bar with a mixing speed of 250 RPM. The slight change in the oxygen consumption rate at approximately 48 hours with 60 g/l Zn^{2+} was due to a human error; the wrong mixing speed was corrected from 200 to 250 RPM. However, the oxygen consumption rates after 48 hours are comparable to others. Average oxygen

consumption rates were calculated between 50 and 72 hours of the experiment, and are tabulated in Table XIII. The experiment was carried out with 3 bars and 100 g/l Zn^{2+} was the standard solution presented earlier in Section 3.7.1.1 and in Table XII.

Table XIII Determined average oxygen consumption rate values with different solutions at 1 or 3 bars and 250 RPM

	3 Bar	1 Bar		
Average oxygen consumption rate	Zn^{2+} 100 g/l	Zn^{2+} 100 g/l	Zn^{2+} 60 g/l	Zn^{2+} 0 g/l
mmol/(m^2s)	0.089	0.022	0.036	0.157

Decreasing the pressure from 3 bars to 1 bar decreased the oxygen consumption rate from 0.089 to 0.022 mmol/(m^2s) and decreasing the Zn^{2+} concentration from 100 g/l to 0 g/l increased the oxygen consumption rate from 0.022 to 0.157 mmol/(m^2s).

Redox potential of solutions increased as a function of time, as can be seen in Figure 66.

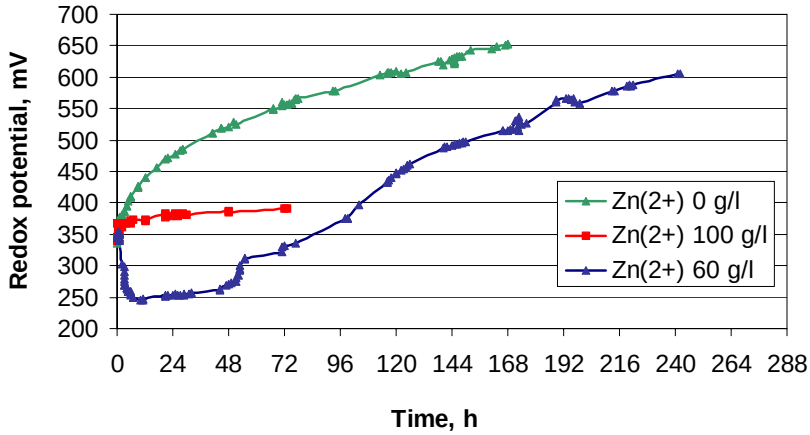

Figure 66 Redox potential as a function of time for solutions with 0, 60 and 100 g/l zinc sulphate. Rotational mixing speed of 250 RPM.

Decreasing of redox potential before <48 hours with 60 g/l Zn^{2+} was due to the mixing speed error mentioned above. Therefore, the results should be taken into consideration only after 48 hours of the experiment. The increase in redox potential in each experiment indicated oxygen consumption occurred through stages 1 and 2. 100 g/l of dissolved Zn^{2+} in the solution gave low redox potential values, which indicated the oxidation (stage 2) in the experiment was only slightly faster than reduction (stage 3).

3.7.5 Effect of solid particles on oxygen consumption rate

The effect of the oxygen consumption rate was studied by comparing the standard solution containing 20 g/l of concentrate to a solution containing 100 g/l of concentrate. That increasing the amount of concentrate in the solution increased the oxygen consumption rate could be seen as a pressure drop in the container, see in Figure 67.

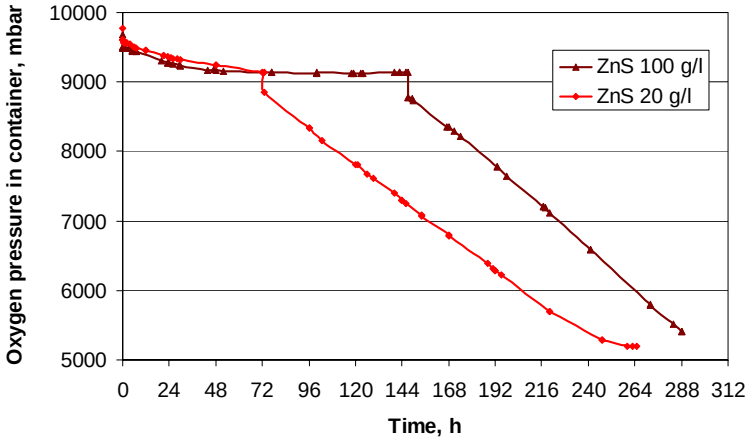

Figure 67 Oxygen pressure in container as a function of time for solutions containing 20 and 100 g/l of concentrate. Rotational mixing speed of 200 RPM.

The rapid pressure drops at 72 hours and 144 hours were due to pressure changes from 1 to 3 bars in the reactor. The experiment with ZnS content of 100 g/l was kept at a pressure of 1 bar for a longer time only to see the effect of oxygen consumption rate to almost cease, which was considered not to affect the determination of the consumption rates. Average oxygen consumption rates were calculated for 20 g/l of concentrate between 96 and 144 hours and for 100 g/l of concentrate between 168 and 216. Calculated average values were 0.100 mmol/(m^2s) for 100 g/l and 0.089 mmol/(m^2s) for 20 g/l of concentrate. The interesting flattening of the oxygen consumption rate with 100 g/l of concentrate at 1 bar pressure was probably due to contamination from the concentrate or reaction products gathering on the gas-liquid surface. The effect of contamination on the calculated oxygen consumption rate was not studied more closely.

When the solution contained 100 g/l of concentrate, the redox potential values were low throughout the experiment, as can be seen in Figure 68.

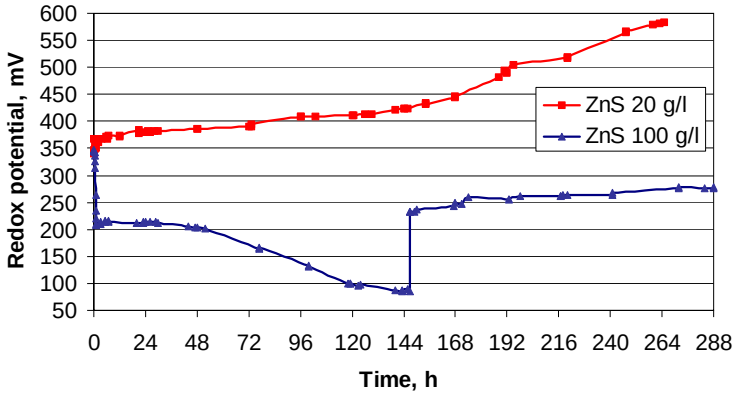

Figure 68 Redox potential as a function of time for solutions with 20 and 100 g/l of concentrate. Rotational mixing speed of 250 RPM

The experiments indicated iron oxidation (stage 2) was slow compared to reduction (stage 3). With oxygen pressure of 1 bar (<144 hours) in the reactor, the redox potential even decreased. The experiments suggested that, with a high content (100 g/l) of concentrate in the solution, the availability of oxygen through stages 2 and 3 became rate controlling.

3.7.6 Oxygen consumption rate and redox potential in process solutions

The oxygen consumption rate in process solution 1 and 2 was studied at different temperatures, pressures and mixing speeds. Process solutions were taken from the Boliden Kokkola Oy leaching process. A small amount of "fresh" concentrate was added to process solutions (10 g/l) in order for stage 3 to occur in the experiments. Increasing the temperature from 50 to 90 °C increased only slightly the oxygen consumption rate in the process solution even though the properties of the liquid (lower surface tension and viscosity) were more favourable for the mass transfer to occur. However, at the same time, oxygen solubility in the liquid phase and oxygen partial pressure in the gas phase decreased, having a negative effect on stage 1. Increasing oxygen pressure from 1 to 3 bars and stirring speed from 200 to 250 RPM had a more significant affect on the oxygen consumption rate than increasing the temperature, as could be seen in the pressure drop rate, see Figure 69.

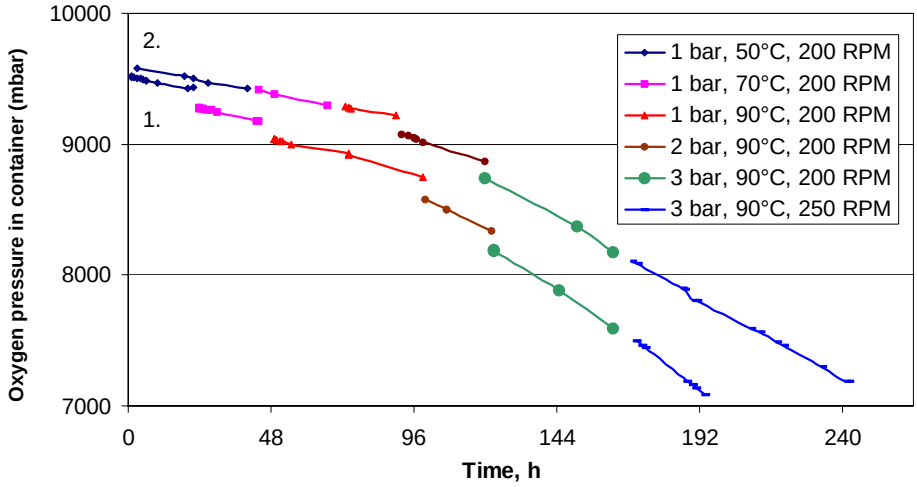

Figure 69 Oxygen pressure in container with process solution 1 and 2. Temperature at 50 °C, 70 °C or 90 °C, pressure at 1, 2 or 3 bars and mixing speed of 200 or 250 RPM

The average oxygen consumption rates were calculated between given times. After changing the parametes, approximately 6 hours was allowed for the temperature and pressure to stabilise. Calculated average oxygen consumption rates are listed in Table XIV.

Table XIV Determined average oxygen consumption rate values at different temperatures, pressures and mixing speeds for process solutions 1 and 2

			Solution 1	Solution 2
Pressure	**Temp.**	**RPM**	**Oxygen consumption rate**	
bar	°C	min^{-1}	$mmol/m^2s$	$mmol/m^2s$
1	50	200	0.018	0.018
1	70	200	0.021	0.018
1	90	200	0.022	0.017
2	90	200	0.045	0.031
3	90	200	0.060	0.049
3	90	250	0.075	0.070

The process solution 2 sample was taken from the later stages of the leaching and contained more dissolved sulphates in the solution, which most probably caused the smaller oxygen consumption rate values compared to solution 1.

Measured redox potential values of process solution 2 slightly increased throughout the experiment, whereas process solution 1 values decreased until 96 hours and increased thereafter, see Figure 70.

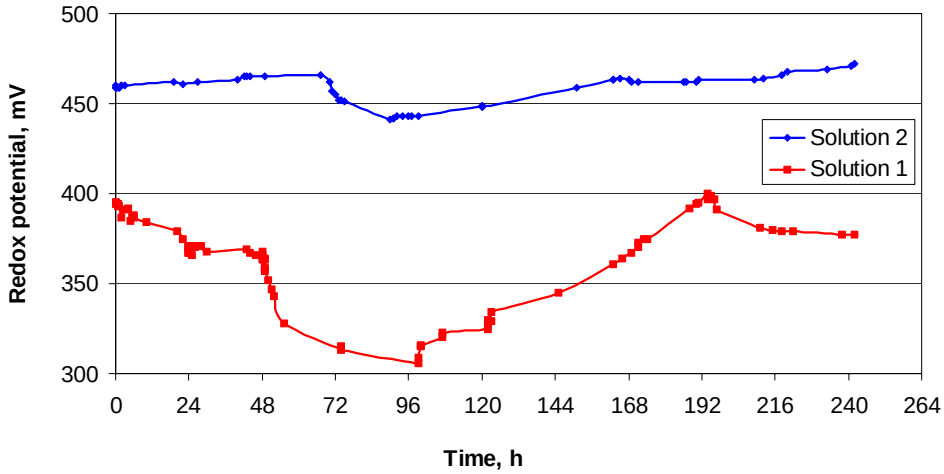

Figure 70 Redox potential values of process solutions 1 and 2 as a function of time

Oxidation and reduction reaction kinetics in process solutions changed according to conditions. At high temperatures and low pressures the oxidation (stage 2) was slower than reduction (stage 3). Increasing the pressure enchanted the kinetics of stage 2 to become slightly faster than reduction.

Even though the leaching experiments with process solutions were carried out as in the same test, the results can be considered succesful. The results were logical and comparable to other experiments presented. For example, under the same conditions, and when process solutions had more sulphates in the solution, the experiment with 100 g/l of concentrate (the composition closest to that of the process solution) gave an oxygen consumption rate value of 0.100 mmol/(m^2s), while process solutions gave 0.07-0.75 mmol/(m^2s).

CHAPTER 4 DISCUSSION

The dissolution of sulphidic zinc concentrate in aqueous sulphuric acid with oxidizing dissolved oxygen present is highly temperature dependent. Above 80 °C, the reaction rate increases significantly. According to ARAUCO AND DOYLE (1986), BOBECK AND SU (1985), LOCHMANN AND PEDLIK (1995), HALAVAARA (1996), AALTONEN (2002) the dissolution is assumed to follow the shrinking-core model and to be controlled first by the chemical reaction and later by the zinc diffusion through the elementary sulphur layer.

Oxygen is injected and dispersed into the process where it acts as an oxidizer, with iron couple Fe^{3+}/Fe^{2+} as an important intermediate. The ferrous iron oxidation rate is found to be first order with respect to oxygen and to be limited by the chemical reaction. Therefore, the availability of oxygen for reactions has an important effect on the kinetics of the whole process. The lack of poorly soluble oxygen in the solution is emphasized during the early stages of dissolution and when operating in atmospheric pressures.

The gas-liquid mass transfer in zinc leaching solution was studied with four new items of experimental apparatus *bubble swarm system, water model, mass transfer equipment and autoclave* designed and developed especially for this purpose. Also additional tests were carried out to give supporting information of process solutions and the effect of temperature on density, surface tension and viscosity.

4.1 GAS DISPERSION

The results gained with the *bubble swarm system* and *water model* revealed that the non-coalescence effect on the occurrence of bubbles is controlled by formation and breakage in the region close to the impeller, as are bubble sizes.

Experiments with the *water model* indicated the gas hold-up increased linearly with mixing speed range examined. With the gas flow rates examined, the overall hold-up remained almost constant. Increasing the gas flow rate, however, decreased the power consumption, due to the lower density and viscosity of the solution easing the mixing.

Water model experiments indicated that the surface aeration and foaming in the leaching process could be controlled with the liquid volume and gas flow rate chosen. When having more than the optimum amount of liquid, the foaming increases, while when having less than the optimum amount, the surface aeration increases. Surface aeration can be ignored when there is sufficient gas injection together with the required minimum mixing speed for proper dispersion.

4.2 VOLUMETRIC MASS TRANSFER COEFFICIENT

The volumetric mass transfer measurements conducted with the dynamic pressure method (A) in the *water model* revealed the oxygen mass transfer rate to increase with mixing speed and gas flow rate as expected. Volumetric mass transfer values ranged between (2.17-12.00)×10^{-3} s^{-1}, with higher values closer to the impeller. The value measured by **method A** was 7.9×10^{-3} s^{-1}, with a gas flow rate of 5 l/min and 600 RPM at measuring place 3. The same volumetric mass transfer coefficient determined by **method B** from the experimental results gained by using the *mass transfer equipment* and *water model* gave values of 10×10^{-3} s^{-1}, see Table XV.

Table XV Volumetric mass transfer coefficient determined by two methods A and B. Mixing speed of 600 RPM and gas flow rate of 5 l/min

Method B						**Method A**
Mass transfer equip.	Mass transfer equip.	Water model	Water model			Water model
Measured	Measured	Measured	Measured	Calculated		Measured
Mixing	Mass transfer coef.	Gas hold-up	Bubble size	a=6ε/D	K_La	K_La
RPM [1/min]	K_L, [m/s]	ε, [%]	D, [m]	[m^2/m^3]	[1/s]	[1/s]
60	0.0001924	3.8	0.00439	52	0.0100	0.0079
45	0.0001670	3.8	0.00439	52	0.0087	0.0079
30	0.0001381	3.8	0.00439	52	0.0072	0.0079

The volumetric mass transfer coefficient values gained with method A and method B were close the same. The results are considered satisfactory when taking into consideration the assumption that flow conditions in the *mass transfer equipment* were considered to resemble almost stable gas-liquid interface with 30 RPM and then bubble in free rise with 60 RPM.

4.3 MASS TRANSFER COEFFICIENT

According to experiments with the *mass transfer equipment,* the mass transfer coefficient $k_{L,}$ between oxygen and pure water varied between (13.81-19.24)×10^{-5} m/s, depending mainly on the flow conditions at the gas-liquid interface. The flow conditions were controlled by mixing. The lowest rotational mixing speed of 30 RPM slightly stirred the liquid, whereas the highest – 60 RPM – was assumed to resemble the bubble in free-rise conditions. The values closely conformed to the earlier results by CALDERBANK AND MOO-YOUNG (1961), who determined the same value to be 13.5×10^{-5} m/s. The results indicated the mass transfer coefficient to be affected only slightly by the hydrostatic pressure. Increasing sulphuric acid, zinc sulphate or sodium chloride content, on the other hand, decreased the mass transfer coefficient values notably, sulphuric acid and zinc sulphate having a stronger effect than sodium chloride. Mass transfer values between oxygen and process solutions ranged between (1.5-11.32)×10^{-5} m/s, depending on the used mixing speed of 30 RPM to 60 RPM.

4.4 OXYGEN CONSUMPTION RATE

Modified high temperature and pressure *autoclave* was used to determine the oxygen consumption rates mmol/(m^2s) in different solutions prepared to correspond to a real process solution. The *oxygen consumption rate* was considered to represent stages of oxygen dissolution and reaction with Fe^{2+}. Increasing zinc concentrate ZnS content from 20 to 100 g/l increased the oxygen consumption rate approximately 13%. Calculated values were 0.089 mmol/(m^2s) for 20 g/l and 0.100 mmol/(m^2s) for 100 g/l of concentrate. With a higher content of concentrate in the solution, the reduction of iron occurred faster than oxidation and the redox potential of the solution remained low throughout the experiment.

Oxygen consumption rates increased significantly when oxygen pressure was increased or the content of dissolved Zn^{2+} was decreased. Relative oxygen consumption rate values (N/N_{100}) compared to 100 g/l zinc sulphate with 3 bars pressure can be seen in Figure 71.

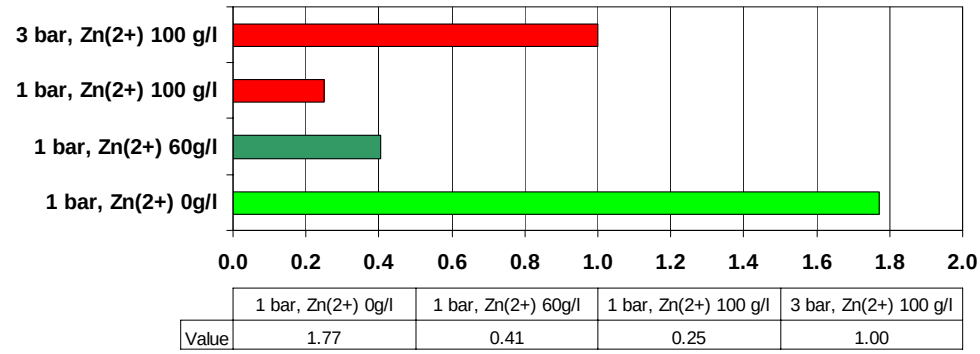

	1 bar, Zn(2+) 0g/l	1 bar, Zn(2+) 60g/l	1 bar, Zn(2+) 100 g/l	3 bar, Zn(2+) 100 g/l
Value	1.77	0.41	0.25	1.00

Figure 71 Relative oxygen consumption rate values into different solution containing 0, 60 and 100 g/l of Zn^{2+} at 1 and 3 bars

Attempts to improve the oxygen consumption rate were carried out with additions of octhene and ethanol in the standard solution. Also a gas mixture of O_2-SO_2 was tested. Results indicated the oxygen consumption rate remained almost the same, as can be seen in the relative value (N/N_{stand}) in Figure 72.

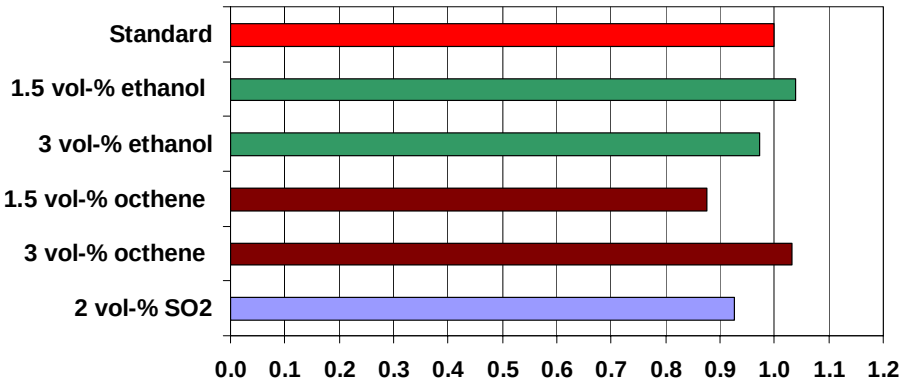

	2 vol-% SO2	3 vol-% octhene	1.5 vol-% octhene	3 vol-% ethanol	1.5 vol-% ethanol	Standard
Value	0.93	1.03	0.88	0.97	1.04	1.00

Figure 72 Oxygen consumption rate values with different solution and with mixed gas relative to standard solution

Only the experiment with 3 vol-% of octhene and 1.5 vol-% of ethanol in the solution to some extent increased the oxygen consumption rate, whereas others decreased it.

The oxygen consumption rate was tested with real process solutions. The increasing of the consumption rate with increasing pressure was noticed for process solutions as well, see Figure 73.

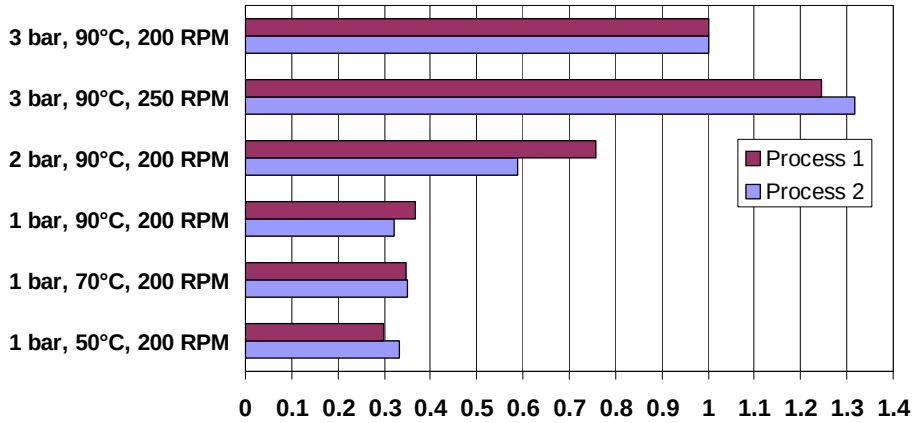

Figure 73 Relative oxygen consumption rate values for process solutions 1 and 2 at elevated temperatures, pressures and mixing speeds

Increasing rotational stirring speed significantly increased the oxygen consumption rate, but temperature did not have a similar effect. The oxygen consumption rate in the process solution varied from 0.018 to 0.075 mmol/(m^2s). Process solution 1 was from the earlier stages of the leaching and, due to a different composition of the solution, the measured values are slightly different, however, the same trends were evident.

4.5 ESTIMATION OF PROCESS PARAMETERS ON GAS-LIQUID MASS TRANSFER

This work summarizes state-of-the-art knowledge concerning gas-liquid mass transfer mechanisms, presents new experimental results and combines them with existing theories.

In practice, the processes chosen define the frames for the operating conditions; the attempts to improve the process were not always applicable. The effects of operating parameters are usually well known, even some profound changes made might stay open. For example, increasing the operating temperature primarily changes the properties of both gas and liquid phases, which secondarily affect the flow pattern, thickness and total contact area of the gas-liquid interface, the gas hold-up and the diffusivity and solubility of gases. As an outcome of this work, the following careful estimations as to how changing the main operating parameters affect the oxygen mass transfer in the zinc leaching process are presented in Table XVI. The estimations are based on information found in the literature and in the experimental results presented. Arrows indicate the direction of the change and numbers indicate references. Green arrows refer to the outcome of this work. The straight line demonstrates (close to) zero effect.

Effect of temperature, pressure, particle concentration, mixing and zinc sulphate concentration relate to autoclave experiments and gas injection to pilot water model experiments, which should be taken in to consideration. The effects are presented as a percentage change. Increasing dissolved zinc concentration had a negative effect –40 % on oxygen mass transfer, while increasing temperature did not have an important effect 0 % on it, increasing particle (concentrate) concentration slightly increased +13 % it, and increasing gas injection or total oxygen pressure increased +100 % it; increasing mixing increased it +25 %.

Table XVI Process parameters affecting oxygen mass transfer in zinc leaching. Arrows (↑↓) show the direction of change and green arrows refer to this work. References are numbered and listed on the next page

MASS TRANSFER $\left[\frac{mmol}{m^2 s}\right]$ N -		$K_L a$									ΔC $\left[\frac{mmol}{dm^3}\right]$	Approximated total effect
		$K_L = \frac{D}{\delta}$ [m/s]		Σ	a [m²/m³]			Σ				
Parameter	Liquid property	D [m²/s]	δ [m]		A [m²]	ε [%]						
Temperature 70→90 °C	Density				↓ 13	↓ 2		↑ 3			↓ 19	0%
	Surface tension	↑ 1, 10, 18 20, 21	not found	↑ 1, 18, 20	↑ 2,5,7	↑ 2	↑ 2, 14	↓ 3,4,5				
	Viscosity				↑ 2,5,7	↑ 2						
Pressure 1→2 bar	Density	not found	not found	↑ 12, 20	↑ 2, 13	↑ 2		↑ 11			↑ 19, 20	+100%
	Surface tension											
	Viscosity			▬ 6								
Zn^{2+} 60→100 g/l	Density	not found	not found	↑ 8	↑ 5			↑ 21			↓ 19	-40%
	Surface tension	↓	▬		not found	▬	↓ 16					
	Viscosity		↓		not found							
Particles 20→100 g/l	Small	not found	↓ 3	↓ 3	↑ 3,9	↑ 3,14	↑ 9	↑ 17			not found	+13%
	Coarse		↑ 3		↑ 3, 9	↓ 3	↓ 9	↓ 3				
Mixing 200→250 RPM	Turbulence	not found	↓ 1, 20	↑ 1, 20	↑ 1, 20	↑ 1, 20	↑ 1, 20	↑ 1			not found	+25%
Gas injection 1→5 l/min		not found	not found	not found	↑ 10	↑ 1		↑ 1, 3			not found	+100%

References of Table XIX.

0. This work
1. CALBERBANK AND MOO-YOUNG (1961)
2. LIN ET AL. (1998)
3. YANG ET AL. (2001)
4. HIRAOKA ET AL .(2001)
5. O'CONNOR ET AL. (1990)
6. TERAMOTO ET AL. (1974)
7. JAMIALAHMADI ET AL. (2001)
8. KASTANEK ET AL. (1993)
9. SADA ET AL. (1986) AND (1987)
10. ZHU AND WU (2002)
11. LETZEL ET AL. (1999)
12. YOSHIDA AND ARAKAWA (1968)
13. SCHÄFER ET AL. (2002)
14. ZOU ET AL. (1988)
15. DE SWART ET AL. (1996)
16. WILKINSON ET AL. (1994)
17. RAUTIO (1996)
18. DANCKWERTS (1951)
19. WEISSENBORN AND PUGH (1996)
20. TEKIE ET AL. (1997)
21. RUTHIYA ET AL. (2003)

4.6 RELIABILITY OF THE EXPERIMENTS

Density, surface tension and viscosity of the liquids were determined in order to support the main objectives of this work. The correlations of the liquid properties were sufficient to describe the effect of temperature, which was the information needed in other parts of the studies.

The HUT Bubble Size Analyser used in the bubble-size analysing experiments of this work was designed for the purpose by GRAU AND HEISKANEN (2002). Each experiment consisted 500 pictures and the total number of bubbles detected varied from 5000-20000, which was considered to be appropriate amount for representative bubble population.

In the bubble size experiments with *bubble swarm system*, the biggest error was noticed to happen by the temperature variation of the liquid (<3 °C). From the experiments of temperature effect on bubble size (Chapter 3.4.1) the liquid temperature change of 3 °C was calculated to cause maximum error of 5% to bubble sizes determined.

The dynamic pressure method used in volumetric mass transfer experiments was reported in VAN´T RIET, (1979) to have a maximum error of ± 6%. In reproducibility test in this work, the dynamic pressure method with oxygen analyzer Orbisphere Model 26071 gave values inside 3% at average measurement location with average gas injection and mixing speed (Chapter 3.5.7).

The most probably source of error in the *gas hold-up* measurements was due to a vortex on the surface. Measurement of the average liquid height did not take into account the amount of gas in the centre tube, which caused the biggest inaccuracy in hold-up measurements. The total error of hold-up values is, however, considered to be less than 10%, which was the same as the maximum vortex volume per total liquid volume.

The accuracy of the *mass transfer equipment* was determined using a reproducibility test, which indicated the results to have a maximum error of less than 5% throughout the experimental measurements. Results also match the results of the other researchers, CALDERBANK AND MOO-YOUNG (1961).

The results from modified *autoclave* equipment were studied in terms of values relative to the others in order to minimize errors. Results concerning the oxygen consumption rate in the process solution should be used with careful attention due to complex composition of the process solutions.

CHAPTER 5 CONCLUSIONS

Gas-liquid mass transfer was experimentally studied with the aim of gaining new knowledge of the atmospheric leaching process of sulphidic zinc concentrate. Four new items of experimental apparatus – *the water model, bubble swarm system, mass transfer equipment* and *autoclave* – were designed and developed for this purpose. The experiments focused on volumetric mass transfer, gas and liquid flow patterns, gas dispersion and bubble size, effects of liquid properties and temperature on bubble size, mass transfer coefficients k_L and oxygen consumption rates in different leaching solutions.

Based on the results of the current study, the following conclusions can be drawn:

♦ It was found that too much liquid in the process increases the foaming, while too little increases the surface aeration. Furthermore, increasing the gas flow rate decreases foaming. Therefore, it seems to be possible to control the foaming and the surface aeration by adjusting the liquid volume and gas flow rate in the process.

♦ As was expected, gas hold-up increases with mixing speed, while increasing the gas flow rate decreases the power consumption.

♦ In the experiments with process liquids, the bubbles formed during the gas injection were not found to coalesce. On the contrary, the breakage of bubbles took place in the region close to the impeller. This suggests that bubble size and, consequently, the total gas-liquid interface area can be controlled by means of the gas dispersion mechanism.

♦ The gas-liquid mass transfer parameters determined with oxygen were found to vary

- with volumetric mass transfer k_La between $(2.17\text{-}12.00)\times10^{-3}$ s^{-1} into pure water, and
- with mass transfer k_L between $(13.81\text{-}19.24)\times10^{-5}$ m/s into pure water, and
- between $(1.5\text{-}11.32)\times10^{-5}$ m/s with process solutions.

♦ The mass transfer coefficient k_L was only slightly affected by the hydrostatic pressure, whereas increasing electrolyte content notably decreased the values. Sulphuric acid and zinc sulphate additions have a stronger effect than sodium chloride. Both mass transfer parameters determined were also strongly dependent on the mixing intensity.

♦ In the leaching experiments, the oxygen consumption rate in the process solution varied from 0.018 to 0.075 mmol/(m^2s). Oxygen consumption rate was found to

- increase significantly with increasing oxygen pressure from 1 to 2 bars,
- increase considerably with increasing mixing speed from 200 to 250 RPM,
- increase slightly with increasing concentrate concentration from 20 to 100 g/l,
- not be affected by increasing temperature from 70 to 90 °C, and
- decrease considerably with increasing dissolved Zn^{2+} concentration from 60 to 100 g/l.

As an outcome of this research project, the following tentatively suggested implications for the process might be considered when considering improvements of the oxidizing stage:

♦ Using a lower operating temperature of around 80-85 °C instead of close to 100 °C would most likely increase the amount of oxygen available for reactions. However, lower temperature decrease the reaction rates at the same time, and therefore, the optimum conditions should be examined more closely before applied.

♦ The addition of a small amount – from 2 to 5% - of sulphur dioxide, which increases the rate of oxidation, could be separated from the roaster gas stream and used directly instead of producing sulphuric acid from it.

To establish the overall behaviour of oxygen mass transfer in the atmospheric zinc leaching process, further experimental studies are required. The following topics are suggested for further research:

♦ Characterisation of fluid flows on both side of the gas-liquid interface.

♦ Flow behaviours of process solution with gas injection in the pilot water model.

♦ Experimental determination of gas solubilities in process solutions at elevated temperatures.

References

Aaltonen, M., 2002, The electrochemical dissolution of sphalerite, Master´s Thesis. Helsinki University of Technology, Espoo, Pp. 70.

Abramzon, A.A., 1993, Surface tension of salt solution, *Russ. J. of App. Chem.*, Vol 66, No. 6, Part 2, 1139-1145.

Adams, R. W., Matthew, I.G., 1981, Leaching of Metal Sulphide Concentrates at atmospheric Pressure Using SO_2/O_2 Mixtures. *Proc. Australs. Inst. Min. Metall*. No. 280, December. Pp. 41-53.

Akita, K., Yoshida, F., 1974, Bubble size, interfacial area, and liquid phase mass transfer coefficient in bubble columns, *Ind. Eng Chem., Process Des. Dev*. 13, No. 4. 84-91.

Anttonen, K., Kaskiala, T., 2004, Experimental determination of process solution densities, (in Finnish), Helsinki University of Technology, Report TKK-MK-154. Pp. 22.

Arauco, H., Doyle, F.M., 1986, Hydrolysis and precipitation of iron during first stage pressure leaching of zinc sulphide concentrates, Edited by Bautista, R.G. et al SME-AIME, *Hydrometallurgical reactor design and kinetics,* Pp. 187-208.

Aromaa, J., 1990, Hydrometallurgian perusteet – teoriaa ja prosessi-esimerkkejä, TKK-V-KORR-9, Espoo, Pp. 134.

Atkins, P.W., 1994, *Physical Chemistry*. Oxford. University Press. 5th edition.

Au-Yeung, S. C. F., Bolton, G. L. 1986. Iron control in processes developed at Sherritt Gordon Mines. *Iron control in hydrometallurgy*, Edited by Dutrizac, J.E. and Monhemius A.J., Eds, Ellis Horwood, Chichester, England, Pp. 131-151.

Awakura, Y., 1986, Oxidation of Fe(II) in HCl and H_2SO_4 solutions with dissolved molecular oxygen in the presence and absence of a cupric catalyst. *Iron control in hydrometallurgy*, Edited by Dutrizac, J.E. and Monhemius A.J., Eds, Ellis Horwood, Chichester, England, Pp. 203-222.

Balaz, P., Ebert, I., 1991, Oxidative leaching of mechanically activated sphalerite. *Hydrometallurgy*, 27. Pp. 141-150.

Battino, R., 1981, Oxygen and ozone, *IUPAC Solubility Data Series*, Vol. 7, Pergamon Press, Oxford. NY.

Bever, M. B. 1986. Encyclopedia of materials science and engineering. Vol. 3. Pergamon Press. 844 s. ISBN 0-08-022158-0.

Bjorling, G., 1973. Leaching of mineral sulphide by selective oxidation at normal pressure, *International symposium on hydrometallurgy*, Evans E. J. I., New York, AIME, Pp. 701-717.

Bobeck, G., Su, H., 1985, The kinetics of dissolution of sphalerite in ferric chloride solution, *Metall. Trans.*, 16 B, Pp. 413-424.

Bockris, J. O´M., Khan, S.U.M., 1993, *Surface Electrochemistry* – A molecular level approach, Plenum Press, Pp. 750-753.

Bohr, C., 1910, *Z. Phys. Chem. German,* 71, Pp. 47-50.

Bruhn, G., Gerlach, J., Pawlek, F., 1967, *Z. Anorg. Allgem. Chem. German*, 337, Pp. 68-79.

Buban, K.R., Collins, M. J., Masters, I. M., Trytten, L. C., 2000, Comparison of direct pressure leaching with atmospheric leaching of zinc concentrates, *Lead-Zinc 2000*, Proceedings of the Lead-Zinc 2000 Symposium, TMS Fall Extraction & Process Metallurgy Meeting, Pittsburgh, U.S.A., October 22-25, Edited by Dutrizac et al., Minerals, Metals and Materials Society, Pp. 727-738.

Burdon, R.S., 1949, Surface tension and the spreading of the liquids, Cambridge.

Calderbank, P.H., Moo-Young, M.B., 1961, The continuous phase heat and mass-transfer properties of dispersions, *Chem. Eng. Sci.,*Vol 16, Pp. 39-54.

Chen, C.-C., 2002, Applied Thermodynamics for Process Modeling, *AIChE J.*, Vol. 48, No 2, Pp. 194-200.

Cheng, C.Y., Clarkson, C. J., Manlapig, E. V. 1994. The leaching of zinc sulphide concentrate in sulphate-chloride solutions with ferric ions. The AusIMM Proceedings 2, Pp. 57-62.

Chmielewski, T; Charewicz, W. A. 1984. The oxidation of Fe(II) in aqueous sulphuric acid under oxygen pressure, *Hydrometallurgy*, Vol. 12. s. 21-30.

Christoff, A., 1906, *Z. Phys. Chem.*, 55, Pp. 622-34.

Clegg, S.L., Brimblecombe, P., 1990, Solubility of volatile electrolytes in multicomponent solutions with atmospheric applications, *Chemical modeling of aqueous systems II*, ACS Symp. Ser, ISSN: 0097-6156. Pp. 59-73.

Clift, R., Grace, J.R., Weber, M.E., 1978, *Bubbles, Drops and Particles*, Academic Press, Inc. UK. Pp. 26.

Corriou, J.P., Gely, R., Viers, P., 1988. Thermodynamic and kinetic study of the pressure leaching of zinc sulphide in aqueous sulphuric acid, *Hydrometallurgy*, 21, Pp.85-102.

Corti, H., Krenzer, M., Pablo, J., Prausnitz J., 1990, Effect of a dissolved gas on the solubility of an electrolyte in aqueous solution, *Ind. Eng. Chem. Res.,* 29, 1043-1050.

Craig, V.J., Ninham, B.W., Pashley, R.M., 1993, The effect of electrolytes on bubble coalescence in water, *J. Phys. Chem*., 97, Pp. 10192-10197.

Craig, V.S.J., 2004, Bubble coalescence and specific-ion effects, *Current Opinion in Colloid & Interface Science*, 9, Pp. 178-184.

Crundwell, F.K., 1987, Kinetics and Mechanism of the oxidative dissolution of a zinc sulphide concentrate in ferric sulphate solutions, *Hydrometallurgy*, 19, Pp. 227-242.

Cussler, E.L., 1997, *Diffusion, Mass transfer in fluid systems,* 2nd ed., Cambridge University Press, UK.

Danckwerts, P.W., 1951, Significance of liquid-film coefficients in gas absorption, *Ind. Eng. Chem.,* 43, Pp. 1460-1467.

Danckwerts, P.W., 1967, *Gas-liquid reactions*, McGraw-Hill, Chemical Engineering Series.

De Swart, J.W.A., Van Vliet, R.E., Krishna, R., 1996, Size, structure and dynamics of "large" bubbles in a two-dimensional slurry bubble column, *Chem. Eng. Sci.,* Vol. 51, No 20, Pp. 4619-4629.

Debye, P., and E. Hückel. 1923. Zur Theorie der Elektrolyte. I. *Gefrierpunktserniedrigung und verwandte Erscheinungen.* 24, 185–206.

Dreisinger, D.B., Peters, E., 1987, The mathematical modelling of the zinc pressure leach. The Metallurgical Society Inc. Mathematical Modelling of Materials Processing Operations, Palm Springs, CA, USA.

Dreisinger, D.B., 1989, The oxidation of ferrous sulphate by molecular oxygen under zinc pressure-leach conditions. *Hydrometallurgy*, 22, Pp. 101-119.

Dreisinger D.B., Peters, E., Talaba, M., DeGraaf, K.B., Owusu G., Swiniarski R., 1990, The kinetics of the Sherritt Gordon zinc pressure leach process, *Lead-Zinc ´90* Symp., California, Pp. 313-333.

Eriksson, G., Hack, K., 1990, Chemsage - a computer program for the calculation of complex chemical equilibria, *Metal. Trans. B*, **21B**, Pp. 1013.

Evans, G., 1907, Red oxide of iron, zinc sulphate, and sulphuric acid, *Patent,* Great Britain 0711338 19071212.

Evans, G., 1909, Manufacture of zinc sulphate and ferric oxide, *Patent,* US 914649 19090309.

Ferron, C. J., 2000. Atmospheric leaching of zinc sulphide concentrates using regenerated ferric sulphate solutions, *Lead-Zinc 2000*, Proceedings of the Lead-Zinc 2000 Symposium, TMS Fall Extraction & Process Metallurgy Meeting, Pittsburgh, U.S.A., October 22-25, Edited by Dutrizac et al., Minerals, Metals and Materials Society, Pp. 711-726.

Fogg, P. G. T., Gerard, W., 1991, Solubility of gases in liquids, Chishester, UK.

Forward, F. A., Veltman, H., 1959, Direct leaching of zinc-sulfide concentrates by Sheritt Gordon, *J. Metals*, Vol 12, Pp. 836-840.

Fowler, T. A. and Crundwell, F. K., 1999. Leaching of zinc sulfide by Thiobacillus ferrooxidans: bacterial oxidation of the sulfur product layer increases the rate of zinc sulfide dissolution at high concentrations of ferrous ions, *App. Environ. Microbiol.*, Vol, 65, No 12, Pp. 5285-5292.

Fugleberg, S., 1998, Continuous improvement at the Kokkola zinc plant, *Zinc and lead processing*, Edited by J.E. Gonzales et al. The metallurgical society of CIM.

Fugleberg S., 1999, Finnish expert report on best available techniques in zinc production, Finnish Environment Institute, ISSN:1238-7321. Pp. 46.

Fugleberg, S., Järvinen A., 2002. Method for leaching zinc concentrate in atmospheric conditions. Outokumpu OYJ. *Patent*, US 6340450, Publ. 22.1.2002.

Fukuma, M., Muroyama, K., Yasunishi, A., 1987, Specific gas-liquid interfacial area and liquid-phase mass transfer coefficient is a slurry bubble column, *J. Chem. Eng. Jpn*, Vol. 20, No. 3, Pp. 321-324.

Geffcken, G., Z. 1904, *Phys. Chem. German*, 49, Pp. 257-302.

Grau, R. A., Heiskanen, K., 2002, Visual technique for measuring bubble size in flotation machines, *Min. Eng.*, 15, Pp. 507-513.

Greaves, M., Kobbacy, K.A.H., 1981, Surface aeration in agitated vessels, *Fluid Mixing, IchemE Symposium Series,* No. 64, Pp. H1-J1.

Halavaara, P., 1996, Factors affecting on the dissolution rate of zinc sulphide, Master's thesis, (in Finnish), Lappeenranta University of Technology, Department of Chemical Technology.

Harnby, N., Edwards, M.F., Nienow, A.W., 1997, *Mixing in the process industries*, Butterworth-Heinemann, Oxford, UK.

Harvey, T.J., Yen, W.T., 1998, The influence of chalcopyrite, galena and pyrite on the selective extraction of zinc from base metal sulphide concentrates, *Min. Eng.* Vol. 11, No 1, Pp. 1-21.

Hayduk, W., 1991, Final report concerning the solubility of oxygen in sulphuric acid-zinc pressure leaching solutions. University of Ottawa, Ontario. Canada.

Higbie, R., 1935, The rate of absorption of a pure gas into a still liquid during short periods of exposure, *Trans. Am. Inst. Chem. Eng*., 35, Pp. 36-60.

Hiraoka, S., Kato, Y., Tada, Y., Kai, S., Inoue, N., Ukai, Y., 2001. Power Consumption and Gas-Liquid Mass Transfer Volumetric Coefficient in a Mechanically Agitated Vessel with Wire-Gauze Impeller, *J. Chem. Eng. Jpn,* Vol. 34, No. 5, Pp. 600-605.

HSC Chemistry for Windows, Ver. 5.1, Outokumpu Research Oy, Pori, Finland.

Holmes, P.R., 2000, The kinetics of the oxidation of pyrite by ferric ions and dissolved oxygen: an electrochemical study, *Geochim. Cosmochim. Acta*, Vol. 64, No. 2, Pp. 263-274.

Horvath, A. L., 1985, *Handbook of Aqueous Electrolyte Solutions: Physical Properties, Estimation and Correlation Methods*, Ellis Horwood, Chichester, England.

Iida, T., Guthrie R.I.L., 1988, *The physical properties of liquid metals*, Clarendon Press, Oxford, UK. Pp. 109-144.

Iwai, M., Majima, H., Awakura, Y., 1982, Oxidation of Fe(II) in sulphuric acid solutions with dissolved molecular oxygen, *Metall. Trans. B*, Vol. 13B, Pp. 311-318.

IZA, International Zinc Association, 2004, Zinc guide.

Jamialahmadi, M., Zehtaban, M. R., Muller-Steinhagen, H., Sarrafi, A., Smith, J.M., 2001, Study of bubble formation under constant flow conditions, *Trans IchemE,* Vol. 79, Part A, Pp. 523-532.

Kammel, R., Pawlek, F., Simon, M., Xi-Ming, L., 1987, Oxidising leaching of sphalerite under atmospheric pressure, *Metall., 41*, 2, Pp. 158-161.

Kantanen, H., 1996, Sinkkirikasteiden liukenemisnopeuksien vertailu, Raportti 96111-ORC-T, Outokumpu Research Oy, Pori, Finland, Pp. 13.

Kaskiala, T., 2001A, Atmospheric direct leaching of sphalerite, Part I- oxygen solubility, Helsinki University of Technology Publications in Materials Science and Metallurgy, TKK-MK-124, Espoo.

Kaskiala, T. 2001B, Atmospheric direct leaching of sphalerite, Part II- reaction kinetics, Helsinki University of Technology Publications in Materials Science and Metallurgy, TKK-MK-125, Espoo, Finland.

Kaskiala, T., 2002, Determination of oxygen solubility in aqueous sulphuric acid media, *Min. Eng.,* Vol. 15, Pp. 853-857.

Kaskiala, T., Salminen J., 2002, Thermochemical modelling and oxygen solubility measurements in acidic zinc leaching solution, Proceedings, 15th International Congress of Chemical and Process Engineering, Prague, Czech Republic.

Kaskiala, T., Aspola, L., Oksanen J., Salminen, J., 2003, Atmospheric direct leaching of sphalerite - Part III- Surface tension, Helsinki University of Technology Publications in Materials Science and Metallurgy, TKK-MK-142, Espoo, Finland.

Kastanek, F., Zahradnik, J., Kratochvil, J., Vermak, J., 1993, Chemical reactors for gas-liquid systems, Ellis Horwood series in Chemical Engineering. Pp. 406.

Keskinen, K.I., 1989, Kemian laitetekniikan taulukoita ja piirroksia, Otatieto 845, University Press, Finland.

Kirk-Othmer 1998, Encyclopedia of Chemical Technology, John Wiley & Sons, New York, 4th ed., Vol. 25, Pp. 790.

Klyueva. A.V., 1967, *Trans. Ural. Politekh. Inst*., Russ., No. 155, Pp. 39-44.

Knuutila, K., 1985, Effect of semiconducting properties of mineralsulphides on electrochemical dissolution, (in Finnish), Helsinki University of Technology, TKK-V-C44, Espoo, Finland.

Komarov, S.V., Sano, M., 1998, Bubble behavior and heat transfer in preheated gas injection into liquid bath, *ISIJ International*, Vol. 38, No. 10, Pp. 1047.

Koukkari, P., Penttilä, K., Hack, K., Petersen, S., 2000, ChemSheet – an efficient worksheet tool for thermodynamic process simulation, *Microstructures, Mechanical properties and process-computer simulation and modelling*, edited by Brechet Y., Euromat99 Vol 3, Wiley-VCH.

Laine, J., 1999, Nesteiden ainearvoja prosessilaskentaa varten, Tampere, Finland, Pp. 93.

Lange's handbook of chemistry, 1973, Dean, J.A., Editor, 11ed. McGraw-Hill Book Co, Inc. New York.

Laskowski, J.S., 2004, Testing flotation frothers, SME Annual Meeting, 23-25 Feb., Denver, Colorado, USA.

Lekhal, A., Chauhari, R. V., Wilhelm, A. M., Delmas, H., 1997, Gas-liquid mass transfer in gas-liquid-liquid dispersions, *Chem. Eng. Sci.,* Vol 52, No. 21/22, Pp. 4069-4077.

Lessard, R. R., Zieminski, S. A., 1971, Bubble coalescence and gas transfer in aqueous electrolytic solutions, *Ind. Eng. Chem. Fundam.,* Vol. 10, No. 2, Pp. 260-269.

Letzel, H.M., Schouten, J.C., Krishna, R., Van Den Bleek, C.M., 1999, Gas hold-up and mass transfer in bubble column reactors operated at elevated pressure, *Chem. Eng. Sci.,* Vol. 54, Pp. 2237-2246.

Li, Z-B., Li, Y.-G., and Lu, J.-F., 1999, Surface Tension Model for Concentrated Electrolyte Aqueous Solutions by the Pitzer Equation, *Ind. Eng. Chem. Res*., 38, Pp. 1133-1139.

Li, Z., Lu B., 2001, Surface tension of aqueous electrolyte solutions at high concentrations – representation and prediction, *Chem. Eng. Sci*. 56, Pp. 2879-2888.

Linek, V., 1987, Critical Review and Experimental Verification of the Correct Use of the Dynamic Method for the Determination of Oxygen Transfer in Aerated Agitated Vessels to Water, Electrolyte Solutions and Viscous Liquids, *Chem. Eng. J.*, 34, Pp. 11-34.

Lin, T.-J., Tsuchiya, K., Fan, L.-S., 1998, Bubble flow characteristics in bubble columns at elevated pressure and temperature, *AIChE J.*, Vol. 44, No 3, Pp 545-560.

Lobo, V.M.M., 1989, Physical Sciences Data 41: Handbook Of Electrolyte Solutions, 2 volumes part A & B, Elsevier, New York.

Lochmann, J., Pedlík, M., 1995, Kinetics of dissolution of sphalerite in ferric sulfate solution, *Hydrometallurgy,* Vol. 37, Pp. 89-96.

Long, F. A. and McDevit, W. F., 1952, Activity coefficients of nonelectrolyte solutes in aqueous salt solutions, *Chem. Rev.,* **51,** 119-169.

Lotens, J.P., Wesker, E., 1987, The behaviour of sulphur in the oxidative leaching of sulphidic minerals, *Hyrdometallurgy*, 18. Pp. 39-54.

Lu, L., Xie, H., 1998, The leaching of zinc sulphide concentrates with synergistic catalysts, Proceedings, 3rd International Conference on Hydrometallurgy, Kunming, China, Pp. 246-249.

Marrucci, G., 1969, A theory of coalescence, *Chem. Eng. Sci.*, Vol. 24, Pp. 975-985.

Masterton, W., 1975, Salting coefficients for gases in seawater from scaled-particle theory, *J. Sol. Chem.,* Vol. 4, No. 6, 523-534

Mathews, C.T., Robins, R.G., 1972, The oxidation of aqueous ferrous sulphate solutions by molecular oxygen, *Proc. Aust. Inst. Min. Met*., Pp. 242.

Merchuk, J.C., 1983, Basic Models for Mass Transfer: Modular Instruction Series, module B4.4, *AIChEMI Modular Instruction, Series B,* Pp. 33-38.

Moo-Young, M., Blanch, H.W., (1987) Design of biohemical reactors, Mass transfer criteria for simple and complex systems. Pp. 746-753,

Nami, F., 1988, The kinetics of zinc sulphide leaching by oxygen, sulphur dioxide and ferrous sulphtate, *Dissertation*, Colombia University, Pp. 225.

Narita, E., 1983, Solubility of oxygen in aqueous electrolyte solutions, *Hydrometallurgy, 10.* Pp. 21-37.

Neou-Syngouna, P., 1990, A kinetic study of the ferric chloride leaching of an iron activated bulk sulphide concentrate, *Hydrometallurgy,* Vol. 23, Pp. 203-219.

Nienow, A.W., Chapman, C.M., 1979, Gas recirculation rate through impeller cavities and surface aeration in sparged agitated vessels, *Chem. Eng. J.*, Vol. 17, Pp. 111-118.

Nienow, A. W. 1996, Gas-liquid mixing studies: A comparison of Rushton turbines with some modern impellers. *Trans IchemE*, Vol. 74, Part A. Pp. 417-423.

Nyberg J., Characterisation and control of the zinc roasting process, *Dissertation,* University of Oulu, Finland, Pp 116.

O'Connor, C. T., Randall, E. W., Goodall, C.M., 1990, Measurement of the effect of physical and chemical variables on bubble size, *Int. J. Min. Process.*, 28, Pp. 139-149.

Owusu, G., Dreisinger, D.B., Peters, E., (1995), Effect of surfactants on zinc and iron dissolution rates during oxidative leaching of sphalerite when ferric sulphate is absent, *Hydrometallurgy,* 38, Pp. 315-324.

Owusu, G., 1992, Surface tension and contact angle due to lignin sulphonates in the system: liquid sulphur, aqueous zinc sulphate and zinc sulphide, *Can. J. Chem. Eng.*, Vol. 79, Pp. 173-180.

Pal, U., 2001, Emerging technologies for metal production. *The minerals, metals and materials society*, *JOM*. Vol. 53, No. 10, Pp. 25.

Palencia Perez, I., 1990, Leaching of a copper-zinc bulk sulphide concentrate using an ferric sulphate dilute solution in a semicontinuous system. Kinetics of dissolution of zinc, *Hydrometallurgy,* Vol 23, Pp. 191-202.

Palencia Perez, I., Dutrizac, J.E., 1991, The effect of the iron content of sphalerite on its rate of dissolution in ferric sulphate and ferric chloride media, *Hydrometallurgy,* 26, Pp. 211-232.

Parker, E. G. 1981. Oxidative pressure leaching of zinc concentrates, *CIM Bulletin*, 74(829), Pp. 145-150.

Parker, E. G., Romanchuk, S., 1980, Pilot plant demonstration of zinc sulphide pressure leaching, *Lead-Zinc-Tin '80*, Proc. World Symp. Metall. Environ. Control, Publisher, Metall. Soc., AIME, Warrendale, PA, Pp. 407-25.

Parthasarathy, R., Ahmed, N., 1994, Sauter mean and maximum bubble diameters in aerated stirred vessels, *Trans IChemE*, Vol. 72, Part A, Pp. 565-572.

Pedersen, T., 2001, Oxygen Absorption into Moving Water and Tenside Solutions, *Water Res.* Vol. 34, No. 9, Pp. 2569-2581.

Pesonen, P., 2000, Sulfidimineraalien liukenemisen sähkökemiallinen diagnosointi-metodiikka, Licenciate´s thesis, Helsinki University of Technology, Espoo, Finland, Pp. 87.

Pitzer, K., S., 1973, Thermodynamics of electrolytes. 1. Theoretical basis and general equations, *J. Phys. Chem,* Vol. **77,** No 2, 268-277.

Pitzer, K., S., 1995, *Thermodynamics*, 3rd ed., McGraw-Hill, New York, USA.

Pohjola, Kaisa, 1997, The redox potential of iron in high pressure aqueous solutions. Master's thesis, (in Finnish), Helsinki University of Technology, Finland.

Pourbaix, M., 1966, Atlas of Electrochemical Equilibria in Aqueous Solutions, Pergamon Press, New York, USA.

Rastas, J., 1986, Mathematical model of zinc calcines leaching process, (in Finnish), Metallurgisten prosessien kinetiikasta, Report TKK-V-C63, Otaniemi, Helsinki university of technology, Finland, Pp.69-110.
Rautio, M., 1996, Hapen liukoisuus ja pelkistymistekniikka sekoitusreaktoriolosuhteissa, *Master´s thesis*, Helsinki University of Technology, Finland.

Roine, A., 1999, HSC-Software ver. 4.1, 88025-ORC-T, Outokumpu Research Centre, Pori, Finland.

Ruthiya, K.C., Van Der Schaaf, J., Kuster, B.FM., Schouten, J.C., 2003, Mechanism of physical and reaction enhancement of mass transfer in a gas inducing stirred reactor, *Chem. Eng. J.,* 96, Pp, 55-69.

Rytioja, Aija, 1997, The direct leaching of zinc sulphide -developing a method for testing the solubility of zinc concentrates, Master's thesis, (in Finnish), University of Oulu, Finland, Pp. 79.

Rönnholm, M. R., Wärnå, J., Salmi, T., Turunen, I., Luoma, M., 1999A, Kinetics of oxidation of ferrous sulphate with molecular oxygen, *Chem. Eng. Sci*., Vol. 54, Pp. 4223-4232.

Rönnholm, M. R., Wärnå, J., Salmi, T., Turunen, I., Luoma, M., 1999B, Oxidation Kinetics of Ferrous Sulfate over Active Carbon, *Ind. Eng. Chem. Res*., Vol. 38, Pp. 2607-2614.

Rönnholm, M. R., 2001, Kinetics and Reactor Design for Oxidation of Ferrous Sulfate with Molecular Oxygen in Sulfuric Acid Milieu Using an Active Carbon Catalyst, *Dissertation*, Åbo Akademi, Turku, Finland.

Sada, E., Kumazawa, H., Lee, L.H., Iguchi, T., 1986, *Ing. Eng Chem. Process Des. Dev.,* Vol. 25, No. 2, Pp. 472-476.

Sada, E., Kumazawa, H., Lee, L.H., Narukawa, H., 1987, *Ind. Eng. Chem. Res.,* Vol. 26, No. 1, Pp. 112-116.

Salminen, J., 1998, Some industrial applications of thermodynamics and kinetics with $NaOH-H_2O_2-H_2O-O_2$- system, Licentiate's thesis, Helsinki University of Technology, Finland.

Salminen, J., Koukkari, P., Jäkärä, J., Paren, A., 2000, Thermochemical experiments and modelling of the PO bleaching stage, *J. Pulp Pap. Sci.*, Vol. 26, 441.

Salminen, J., Kaskiala, T., 2003, Oxygen Solubility in Industrial Process Development, *Ind. Eng. Chem. Res.,* Vol 42, Pp. 1827-1831.

Schumpe, A., 1993, The estimation of gas solubilities in salt solutions, *Chem. Eng. Sci*., 48, 153-158.

Schäfer, R., Merten, C., Eigenberger, G., 2002, Bubble size distribution in a bubble column reactor under industrial conditions, *Experimental Thermal and Fluid Science* 26, Pp. 595-604.

Seppälä, K., 1973, Tutkimus peitoskuonien pintajännityksestä, Master's thesis (in Finnish), Helsinki University of Technology, Finland, Pp. 45.

Setschenow, A., 1889, Über die Konstitution der Salzlösungen auf Grund ihres Verhaltens zu Kohlensäure, *Z. Phys. Chem.,* IV, 117-125.

Shaw, D. J., 1980, *Introduction to colloid and surface chemistry*, Butterworths, 3rd ed., London, UK, Pp. 60-61

Sippola, H., 1992, Solubility of ferrous sulphate in sulphuric acid – a thermodynamic model, Licentiate thesis, Helsinki University of Technology, Espoo, Finlandia.

Stockham, J.D., Fochtman, E.G., 1977, Particle Size Analysis. *Ann Arbor Science*, Michigan. USA.

Takala, H., 1999, Leaching of zinc concentrates at Outokumpu Kokkola plant, *Erzmetall,* 52, No. 1, Pp. 37-42.

Takala, H., Oinonen, Y., Höglund, K., 2000, Equipment for the leaching of solid matter from sludge, *Patent FI*, US 6,793,816 B1, 109456B.

Teixeira, L. A., 1986, Precipitation of jarosite from manganese sulphate solutions, *Iron control in hydrometallurgy*, Edited by Dutrizac, J.E. and Monhemius A.J., Eds, Ellis Horwood, Chichester, England, Pp. 431-453.

Tekie, Z., Li, J., Morsi, B.I., 1997, Mass transfer parameters of O_2 and N_2 in Cyclohexane under elevated pressures and temperatures: A statistical approach*, Ind. Eng. Chem. Res*., Vol. 36, Pp. 3879-3888.

Teramoto, M., Tai, S., Nishii, K., Teranishi, H., 1974, Effects of Pressure on Liquid-Phase Mass Transfer Coefficients, *Chem. Eng. J*., Vol. 8, Pp. 223-226.

Toor, H.L., Marchello, J.M., 1958, Film-penetration model for mass transfer and heat transfer, *A.I.Ch.E. J.,* 4, Pp. 97-101.

Troman's. D., 1998a, Temperature and pressure dependent solubility of oxygen in water: a thermodynamic analysis, *Hydrometallurgy* Vol. 48, Pp. 327-342.

Troman's, D., 1998b, Oxygen solubility modeling in inorganic solutions: Concentration, Temperature and Pressure effects, *Hydrometallurgy,* Vol. 50, Pp. 279-296.

Troman's, D., 2000A, Oxygen modeling in ammoniacal leaching solutions: leaching of sulphide concentrates, *Min. Eng.*, Vol. 13, No. 5, Pp. 487-515.

Troman's. D., 2000B, Modeling oxygen solubility in water and electrolyte solutions, *Ind. Eng. Chem. Res*., Vol. 39, Pp. 805-812.

Tsang, Y.H., Koh, Y-H., Koch, D.L., 2004, Bubble-size dependence of the critical electrolyte concentration for inhibition of coalescence, *J. Colloid Interface Sci.*, 275, Pp. 290-297.

Turchinov. V.V., 1967, Nauch. Tr. Irkutsh. Gas., *Nauch.-Issled. Inst. Redk. Tsvet. Metal.*, Russian. 16, Pp. 293-9.

Uusipaavalniemi, E., Karlman, S.-G., Takala, H., 1996, Handling of Iron at the Zinc Plant in Kokkola, Iron Control and Disposal, *Canadian Institute of Mining, Metallurgy and Petroleum*, Ottawa, Canada, Canada. Pp. 101-115.

Van´t Riet, K., 1979, Review of measuring methods and results in nonviscous gas-liquid mass transfer in stirred vessels*, Ind. Eng. Chem. Process Des. Dev*., Vol. 18, No. 3, Pp. 357-364.

Verbaan, B., Mullinger, B., 1980, The leaching of sphalerite in acidic ferric sulphate media in the absence of elemental sulphur, *NIM Report*, No. 2038, Rangburg. South Africa.

Verbaan, B., Crundwell, F. K., 1986, An electrochemical model for the leaching of a sphalerite concentrate, *Hydrometallurgy*, 16, Pp. 345-359.

Vracar, R.Z., 1997, Kinetics of Fe(II) ions by gaseous oxygen at high temperatures in an autoclave, *Hydrometallurgy* 44, Pp. 113-124.

Walter, J.F., Blanch H.W., 1986, Bubble break-up in gas-liquid bioreactors: break-up in turbulent flows, *Chem. Eng. J.*, Vol. 32, B7-B17.

Weisenberger, S., Schumpe, A., 1996, Estimation of gas solubilities in salt solutions at temperatures from 273 K to 363 K, *AIChE J.*, Vol 42, No. 1, Pp. 298-300.

Weinberg, M., 1981, Surface tension effects in gas bubble dissolution and growth, *Chem. Eng. Sc.* Vol. 36, Pp. 137-141.

Weissenborn, P.K., 1995, Surface Tension and Bubble Coalescence Phenomena of Aqueous Solutions of Electrolytes, *Langmuir*, 11, Pp. 1422-1426.

Weissenborn, P.K., Pugh, R.J., 1996, Surface tension of aqueous solutions of electrolytes: relationship with ion hydration, oxygen solubility, and bubble coalescence, *J. Colloid Interface sci.,* 184, Pp. 550-563.

Whitman, W.G., 1923, Preliminary experimental confirmation of the two-film theory of gas absorption, *Chem. Metall. Eng*., 29, 251, Pp. 146-149

Wilkinson, P.M., Haringa, H., Van Dierendonck, L.L., 1994, Mass transfer and bubble size in bubble column under pressure, *Chem. Eng. Sci.*, Vol. 49, No. 9, Pp. 1417-1427.

Williams, J.R., Brandley, H.W., 1911, Extracting zinc and copper from ores. *US Patent* 1006330 19111017.

Xuezhong, C., Land, L., (1998), Oxidative pressure acid leaching of zinc sulfide concentrate. *Proceedings of 3rd international conference on hydrometallurgy*, China, Pp. 241-245.

Yang, W., Wang, J., Jin, Y. 2001, Gas-Liquid Mass Transfer in a slurry Bubble Column Reactor under High Temperature and High Pressure, *Chinese J. Chem. Eng.,* Vol. 9, No. 3, Pp. 253-257.

Yoshida, F., 1988, Bubble Column Research in Japan, *Chem. Eng. Tech*., 11, Pp. 205-212.

Yoshida, F., Arakawa, S., 1968, Pressure dependence of liquid phase mass transfer coefficients, *Am. Inst. Chem. Eng. J.*, Vol. 14, Nro. 6, Pp. 962-963.

Yung, C.-N., 1989, A Numerical Study of Parameters Affecting Gas Bubble Dissolution, *J. Colloid Interface Sc.*, Vol. 127, No 2, Pp. 442-452.

Zahradnik, J., Fialova, M., Kastanek, F., Green, K.D., Thomas, N.H., 1995, The effect of electrolytes on bubble coalescence and gas hold-up in bubble column, *Chem. Eng. Res. Des.*, No. 73, A3, Pp. 341-346.

Zhang, W., 2000, Iron(II) oxidation by SO_2/O_2 in acidic media: Part I, Kinetics and mechanism, *Hydrometallurgy,* 55, Pp. 229-245.

Zhi-Bao, Li., 2001, Surface tension of aqueous electrolyte solutions at high concentrations – representation and prediction, *Chem. Eng. Sci.,* 56, Pp. 2879-2888.

Zhu, Y., Bandopadhayay, P. C., Wu, J., 2001. Measurement of Gas-Liquid Mass Transfer in an Agitated Vessel – A Comparison between Different Impellers. *J. Chem. Eng. Jpn.,* Vol. 34, No. 5, Pp. 579-584.

Zhu Y., Wu, J., 2002, Gas-to-liquid mass transfer in hot sparged system, Proceedings, 9th APCChE 2002 and Chemeca 2002, 29 September – 3 October, Christchurch, New Zealand.

Zou, R., Jiang, X., Li, B., Zu, Y., Zhang, L., 1988, Studies on gas hold-up in a bubble column operated at elevated temperatures, *Ind. Eng. Chem. Res.,* Vol. 27, Pp. 1910-1916.

Appendix 1

Gas solubility parameters of the model by WEISENBERGER AND SCHUMPE (1996).

hi		hj		hg,0		$hx10^3$	
Cation	m^3/kmol	Anion	m^3/kmol	Gas	m^3/kmol	m^3/kmolK	Temp. K
h^+	=0	OH^-	0.0839	H_2	-0.0218	-0.299	273-353
Li^+	0.0754	HS^-	0.0851	He	-0.0353	+0.464	278-353
Na^+	0.1143	F^-	0.0920	Ne	-0.0080	-0.913	288-303
K^+	0.0922	Cl^-	0.0318	Ar	+0.0057	-0.485	273-353
Rb^+	0.0839	Br^-	0.0269	Kr	-0.0071	n.a.	298
Cs^+	0.0759	I^-	0.0039	Xe	+0.0133	-0.329	273-318
$NH4^+$	0.0556	NO_2^-	0.0795	Rn	+0.0447	-0.138	273-301
Mg^{2+}	0.1694	NO_3^-	0.0128	N_2	-0.0010	-0.605	273-345
Ca^{2+}	0.1762	ClO_3^-	0.1348	O_2	=0	-0.334	273-353
Sr^{2+}	0.1881	BrO_3^-	0.1116	NO	+0.0060	n.a.	298
Ba^{2+}	0.2168	IO_3^-	0.0913	N_2O	-0.0085	-0.479	273-313
Mn^{2+}	0.1463	ClO_4^-	0.0492	NH_3	-0.0481	n.a.	298
Fe^{2+}	0.1523	IO_4^-	0.1464	CO_2	-0.0172	-0.338	273-313
Co^{2+}	0.1680	CN^-	0.0679	CH_4	+0.0022	-0.524	273-363
Ni^{2+}	0.1654	SCN^-	0.0627	C_2H_2	-0.0159	n.a.	298
Cu^{2+}	0.1675	$HCrO_4^-$	0.0401	C_2H_4	+0.0037	n.a.	298
Zn^{2+}	0.1537	HCO_3^-	0.0967	C_2H_6	+0.0120	-0.601	273-348
Cd^{2+}	0.1869	$H_2PO_4^-$	0.0906	C_3H_8	+0.0240	-0.702	286-345
Al^{3+}	0.2174	HSO_3^-	0.0549	n- C_4H_{10}	+0.0297	-0.726	273-345
Cr^{3+}	0.0648	CO_3^{2-}	0.1423	H_2S	-0.0333	n.a.	298
Fe^{3+}	0.1161	HPO_4^{2-}	0.1499	SO_2	-0.0817	+0.275	283-363
La^{3+}	0.2297	SO_3^{2-}	0.1270	SF_6	+0.0100	n.a.	298
Ce^{3+}	0.2406	SO_4^{2-}	0.1117				
Th^{3+}	0.2709	$S_2O_3^{2-}$	0.1149				
		PO_4^{3-}	0.2119				
		$[Fe(CN)_6]^{4-}$	0.3574				

Oxygen solubility [mmol/dm^3] in water and dilute sulphuric acid solutions as a function of temperature.

		H_2SO4 [mmol/dm^3]				
		25 g/l	50 g/l	100 g/l	150 g/l	200 g/l
T (°C)	Water	0.26 M	0.51 M	1.02 M	1.53 M	2.04 M
0	2.106	2.018	1.910	1.663	1.449	1.262
10	1.683	1.577	1.494	1.306	1.142	0.998
15	1.526	1.417	1.344	1.177	1.031	0.903
16	1.498	1.389	1.317	1.154	1.011	0.886
17	1.471	1.361	1.292	1.132	0.993	0.870
18	1.445	1.335	1.267	1.111	0.974	0.855
19	1.420	1.310	1.244	1.091	0.957	0.840
20	1.395	1.286	1.221	1.071	0.940	0.825
21	1.372	1.263	1.199	1.053	0.924	0.812
22	1.349	1.241	1.178	1.035	0.909	0.798
23	1.328	1.220	1.158	1.018	0.894	0.786
24	1.306	1.199	1.139	1.001	0.880	0.773
25	1.286	1.179	1.120	0.985	0.866	0.762
26	1.266	1.160	1.102	0.970	0.853	0.750
27	1.248	1.142	1.085	0.955	0.840	0.739
28	1.229	1.124	1.068	0.940	0.828	0.729
29	1.212	1.107	1.052	0.927	0.816	0.719
30	1.194	1.091	1.037	0.914	0.805	0.709
35	1.117	1.018	0.968	0.855	0.754	0.666
40	1.052	0.957	0.911	0.806	0.713	0.630
50	0.950	0.885	0.843	0.749	0.665	0.590
60	0.878	0.819	0.782	0.697	0.621	0.554
70	0.827	0.773	0.740	0.662	0.592	0.530
80	0.793	0.744	0.712	0.640	0.575	0.516
90	0.773	0.726	0.697	0.628	0.566	0.511
100	0.764	0.719	0.691	0.626	0.566	0.513

Oxygen solubility [mmol/dm^3] in sodium chlorine solutions and process solutions 1 and 2 as a function of temperature.

NaCl [mmol/dm^3]					Process 1	Process 2
T (°C)	0.43 M	0.86 M	1.28 M	1.71 M		
0	1.866	1.589	1.510	1.155	0.526	0.483
10	1.464	1.254	1.189	0.924	0.427	0.392
15	1.319	1.134	1.073	0.841	0.391	0.359
16	1.293	1.112	1.053	0.826	0.385	0.353
17	1.268	1.092	1.033	0.812	0.379	0.347
18	1.245	1.072	1.014	0.798	0.373	0.342
19	1.222	1.053	0.996	0.785	0.367	0.337
20	1.200	1.035	0.979	0.772	0.362	0.332
21	1.179	1.017	0.962	0.760	0.357	0.327
22	1.158	1.000	0.946	0.749	0.352	0.323
23	1.139	0.984	0.930	0.738	0.347	0.318
24	1.120	0.969	0.915	0.727	0.343	0.314
25	1.102	0.954	0.901	0.717	0.338	0.310
26	1.085	0.939	0.887	0.707	0.334	0.306
27	1.068	0.926	0.874	0.697	0.330	0.302
28	1.052	0.912	0.861	0.688	0.326	0.299
29	1.037	0.899	0.849	0.679	0.322	0.296
30	1.022	0.887	0.837	0.671	0.319	0.292
35	0.955	0.832	0.784	0.633	0.303	0.278
40	0.900	0.787	0.741	0.603	0.291	0.266
50	0.836	0.735	0.690	0.571	0.279	0.256
60	0.777	0.688	0.645	0.541	0.269	0.246
70	0.737	0.657	0.614	0.524	0.264	0.241
80	0.712	0.639	0.595	0.516	0.264	0.241
90	0.698	0.631	0.586	0.516	0.268	0.244
100	0.695	0.632	0.586	0.523	0.276	0.251

Oxygen solubility [mmol/dm^3] in zinc sulphate solutions as a function of temperature.

	$ZnSO_4$ [mmol/dm^3]						
T (°C)	0.385 M	0.8 M	1 M	1.15 M	1.3075 M	1.55 M	2 M
0	1.708	1.304	1.145	1.039	0.938	0.801	0.598
10	1.339	1.029	0.906	0.824	0.746	0.639	0.481
15	1.205	0.929	0.820	0.746	0.676	0.581	0.438
16	1.182	0.912	0.805	0.733	0.664	0.571	0.431
17	1.159	0.895	0.790	0.719	0.652	0.561	0.423
18	1.137	0.879	0.776	0.707	0.641	0.551	0.417
19	1.116	0.863	0.762	0.695	0.630	0.542	0.410
20	1.096	0.848	0.749	0.683	0.619	0.533	0.404
21	1.077	0.834	0.737	0.672	0.609	0.525	0.397
22	1.058	0.820	0.725	0.661	0.600	0.517	0.392
23	1.040	0.806	0.713	0.650	0.590	0.509	0.386
24	1.023	0.794	0.702	0.640	0.581	0.501	0.380
25	1.007	0.781	0.691	0.631	0.573	0.494	0.375
26	0.991	0.769	0.681	0.622	0.565	0.487	0.370
27	0.976	0.758	0.671	0.613	0.557	0.480	0.365
28	0.961	0.747	0.662	0.604	0.549	0.474	0.361
29	0.947	0.736	0.653	0.596	0.542	0.468	0.356
30	0.933	0.726	0.644	0.588	0.535	0.462	0.352
35	0.872	0.681	0.605	0.553	0.503	0.436	0.333
40	0.822	0.644	0.572	0.524	0.478	0.414	0.318
50	0.762	0.601	0.536	0.492	0.449	0.391	0.302
60	0.708	0.562	0.503	0.462	0.423	0.370	0.288
70	0.671	0.536	0.481	0.443	0.407	0.357	0.280
80	0.648	0.520	0.468	0.433	0.398	0.351	0.277
90	0.635	0.513	0.464	0.429	0.396	0.350	0.278
100	0.631	0.514	0.465	0.432	0.399	0.354	0.283

Appendix 2

Density values measured and reported

Perry (1976) Water				This work Water		Process 1		Process 2	
T (°C)	g/cm^3	T (°C)	g/cm^3	T (°C)	g/cm^3	T (°C)	g/cm^3	T (°C)	g/cm^3
20	0.998	55	0.985	25	0.997	82	1.378	84	1.393
21	0.997	56	0.985	35	0.994	78	1.381	81	1.394
22	0.997	57	0.984	36	0.993	77	1.382	80	1.396
23	0.997	58	0.984	38	0.992	74	1.385	78	1.398
24	0.997	59	0.983	45	0.991	69	1.388	76	1.4
25	0.997	60	0.983	50	0.989	66	1.391	73	1.402
26	0.996	61	0.982	54	0.987	64	1.392	70	1.404
27	0.996	62	0.982	56	0.986	62	1.393	67	1.405
28	0.996	63	0.981	62	0.982	60	1.395	65	1.407
29	0.995	64	0.981	65	0.981	59	1.396	61	1.41
30	0.995	65	0.98	69	0.98	57	1.397	58	1.414
31	0.995	66	0.98	71	0.978	55	1.398	55	1.415
32	0.995	67	0.979	74	0.977	54	1.399	54	1.416
33	0.994	68	0.978	75	0.976	51	1.4	52	1.418
34	0.994	69	0.978	81	0.972	50	1.401	50	1.419
35	0.994	70	0.977	85	0.97	48	1.402	48	1.42
36	0.993	71	0.977	86	0.97	46	1.403	47	1.421
37	0.993	72	0.976			45	1.404	45	1.422
38	0.992	73	0.976			42	1.405	42	1.423
39	0.992	74	0.975			40	1.406	40	1.424
40	0.992	75	0.974			38	1.408	39	1.425
41	0.991	76	0.974			34	1.41	37	1.426
42	0.991	77	0.973			33	1.41	35	1.427
43	0.991	78	0.973			32	1.411	33	1.428
44	0.99	79	0.972					31	1.429
45	0.99	80	0.971					30	1.429
46	0.989	81	0.971						
47	0.989	82	0.97						
48	0.988	83	0.969						
49	0.988	84	0.969						
50	0.988	85	0.968						
51	0.987	86	0.967						
52	0.987	87	0.967						
53	0.986	88	0.966						
54	0.986	89	0.965						
		90	0.965						

Composition of the solution examined and the formula of the fitted line and value of least square method R^2.

	Composition of the solutions						Formula of the fitted lines			
	H_2SO_4	$ZnSO_4$	Zn^{2+}	Fe^{3+}	Fe^{2+}	SO_4^{2-}	$y = Ax^2 + Bx + C$			
Solution	g/l	g/l	g/l	g/l	g/l	M	A*E-06	B*E-04	C	R^2
Water							-3.295	-0.7765	1.000	0.996
Solution 1	30						-2.635	-1.824	1.023	0.998
Solution 2	50						-1.270	-3.491	1.040	0.998
Solution 3	100						-2.603	-2.346	1.067	0.999
Solution 4	200						-2.027	-3.234	1.126	0.994
Solution 5	30			5			-2.415	-1.986	1.041	0.999
Solution 6	50			15			-1.020	-4.065	1.093	0.996
Solution 7		210					-1.970	-3.612	1.215	0.994
Process 1						3	-3.825	-2.140	1.421	0.999
Process 2						2.7	-4.074	-2.250	1.440	0.997

Density values calculated from fitted line for solutions at different temperature.

Temperature	(°C)	25	30	40	50	60	70	80	90	95
Water	(g/cm^3)	0.996	0.995	0.992	0.988	0.983	0.978	0.973	0.966	0.963
Solution 1	(g/cm^3)	1.017	1.015	1.011	1.007	1.003	0.997	0.992	0.985	0.982
Solution 2	(g/cm^3)	1.030	1.028	1.024	1.019	1.014	1.009	1.004	0.998	0.995
Solution 3	(g/cm^3)	1.060	1.058	1.053	1.049	1.044	1.038	1.032	1.025	1.021
Solution 4	(g/cm^3)	1.117	1.114	1.110	1.105	1.099	1.093	1.087	1.080	1.077
Solution 5	(g/cm^3)	1.035	1.033	1.029	1.025	1.020	1.015	1.010	1.004	1.000
Solution 6	(g/cm^3)	1.082	1.080	1.075	1.070	1.065	1.060	1.054	1.048	1.045
Solution 7	(g/cm^3)	1.205	1.202	1.197	1.192	1.186	1.180	1.173	1.167	1.163
Process 1	(g/cm^3)	1.413	1.411	1.406	1.401	1.394	1.387	1.379	1.371	1.366
Process 2	(g/cm^3)	1.432	1.430	1.424	1.419	1.412	1.404	1.396	1.387	1.382

Appendix 3

Surface tension values of different solutions

This work			Lange (1973)		Laine (1999)	
T (°C)	S (mN/m)	Std	T (°C)	S (mN/m)	T (°C)	S (mN/m)
20	71.58	0.04	0	75.83	0	76.12
30	69.68	0.29	5	75.09	5	75.30
60	65.82	0.03	10	74.39	10	74.47
70	65.1	0.03	15	73.62	15	73.64
			20	72.88	20	72.80
			21	72.73	25	71.97
			22	72.58	30	71.13
			23	72.43	35	70.29
			24	72.29	40	69.45
			25	72.14	45	68.61
			26	71.99	50	67.76
			27	71.84	55	66.91
			28	71.69	60	66.06
			29	71.55	65	65.21
			30	71.4	70	64.35
			35	70.66	75	63.49
			40	69.92	80	62.63
			45	69.18	85	61.77
			50	68.45	90	60.90
			55	67.71	95	60.03
			60	66.97	100	59.15
			65	66.23		
			70	65.49		
			75	64.75		
			80	64.01		
			85	63.28		
			90	62.54		
			95	61.8		
			100	61.8		

H_2SO_4	$ZnSO_4$	T (°C)	S (mN/m)	Std
25 g/l	25 g/l	25	67.99	0.05
		50	55.2	0.13
		75	50.81	0.17
	50 g/l	25	61.79	0.27
		50	58.17	0.3
		75	50.39	0.27
	100 g/l	25	70.79	0.09
		50	64.76	0.04
		75	53.64	0.34

Surface tension values measured for different solutions

H_2SO_4	$FeSO_4$	T (°C)	S (mN/m)	Std
25 g/l	25 g/l	25	73.24	0.03
		50	67.47	0.04
		75	63.52	0.28
	50 g/l	25	68.21	0.23
		50	64.12	0.18
		75	59.26	0.43
	100 g/l	25	69.41	0.35
		50	63.98	0.18
		75	57.85	0.45

$ZnSO_4$	H_2SO_4	T (°C)	S (mN/m)	Std
100 g/l	0 g/l	25	72.11	0.07
		50	67.6	0.08
		75	61.42	0.25
	25 g/l	25	70.79	0.09
		50	64.76	0.04
		75	53.64	0.34
	50 g/l	25	64.22	0.31
		50	60.67	0.23
		75	53.73	0.45
	100 g/l	25	64.07	0.38
		50	57.18	0.25
		75	50.83	0.18

	Process solution 1		Process solution 2		Process solution 3	
T (°C)	S (mN/m)	Std	S (mN/m)	Std	S (mN/m)	Std
60	71.19	0.52	65	0.13	66.2	0.09
70	72.31	0.61	46.84	0.15	51.38	0.13
80	60.32	3.19	40.4	0.37	47.51	0.34

Appendix 4

Viscosity values for different solutions

Lobo (1989) Water		This work Water		50 g/kg H_2SO_4		100 g/kg H_2SO_4		200 g/kg H_2SO_4	
T (°C)	(mm^2/s)	T (°C)	(mm^2/s)	T (°C)	(mm^2/s)	T (°C)	(mm^2/s)	T (°C)	(mm^2/s)
5	1.519	23	0.94	24	1.01	23	1.14	21	1.30
10	1.308	23	0.94	30	0.92	31	0.96	21	1.32
15	1.142	23	0.94			40	0.80	31	1.08
20	1.007	40	0.68					33	1.03
25	0.914	40	0.68					35	0.99
30	0.804	40	0.67					41	0.89
35	0.727	60	0.51					41	0.87
40	0.661	60	0.51					50	0.76
45	0.605	60	0.51					50	0.77
50	0.556	80	0.40					60	0.66
55	0.514	80	0.35					60	0.67
60	0.477	26	0.90						
65	0.444	30	0.84						
70	0.415	32	0.80						
75	0.390	33	0.79						
80	0.367	41	0.68						
85	0.346	41	0.67						
90	0.328	41	0.66						
95	0.311	50	0.58						
100	0.296	50	0.58						
		50	0.58						
		60	0.51						
		60	0.50						
		60	0.50						
		21	1.00						
		22	0.99						
		22	0.99						
		22	0.99						
		22	0.99						
		60	0.51						
		60	0.51						

This work			
Process 1		Process 2	
T (°C)	(mm^2/s)	T (°C)	(mm^2/s)
21	5.88	21	6.73
30	4.04	32	4.62
40	1.68	41	3.61
41	1.63		

Appendix 5

Bubble sauter mean diameters

Water, 0.04 l/min		Water, 0.03 l/min		DF 250	
T (°C)	Dsm (mm)	T (°C)	Dsm (mm)	T (°C)	Dsm (mm)
25	0.98	22	0.63	23	0.22
40	0.73	32	0.54	32	0.21
50	0.65	42	0.49	42	0.22
60	0.67	51	0.45	52	0.22
70	0.73	61	0.42	59	0.22
80	0.85	70	0.42	69	0.22
		79	0.44	79	0.24

Cumulative surface area as a function of bubble diameter for different liquids.

H_2O		30 g/l H_2SO_4		Process solution		O.003 M	
Diameter	Cum. surf. (%)	Diameter	Cum. surf. (%)	Diameter	Cum. surf. (%)	Diameter	Cum. surf. (%)
0.06	0.00	0.06	0.00	0.05	0.01	0.06	0.00
0.09	0.04	0.09	0.03	0.07	0.02	0.09	0.52
0.12	0.18	0.12	0.40	0.10	0.07	0.12	2.30
0.17	1.68	0.17	2.02	0.14	0.75	0.17	19.49
0.24	12.48	0.24	9.74	0.19	27.18	0.24	54.00
0.34	28.87	0.34	33.72	0.27	59.30	0.34	23.15
0.48	35.49	0.48	39.78	0.39	12.66	0.48	0.54
0.68	17.54	0.68	13.23	0.55	0.00	0.68	0.00
0.97	3.45	0.97	1.08	0.77	0.00	0.97	0.00
1.37	0.27	1.37	0.00	1.09	0.00	1.37	0.00
1.93	0.00	1.93	0.00	1.55	0.00	1.93	0.00
2.73	0.00	2.73	0.00	2.19	0.00	2.73	0.00
3.86	0.00	3.86	0.00	3.09	0.00	3.86	0.00

Appendix 6

Bubble sauter mean diameter in different liquids

NaCl	Diameter	ZnSO4	Diameter
mol/l	mm	mol/l	mm
0	4.53	0.00	4.53
0.05	3.59	0.02	3.10
0.1	2.79	0.04	1.99
0.15	1.97	0.06	1.18
0.2	1.17	0.08	0.96
0.4	1.00	0.10	0.73
		0.12	0.71
		0.14	0.73
		0.16	0.70
		0.18	0.72
		0.20	0.71

Bubble sauter mean diameter in different liquids

	Water				0.2 M NaCl	0.1 M $ZnSO_4$
RPM	0 l/min	1 l/min	2.5 l/min	5 l/min	2.5 l/min	2.5 l/min
354	1.40	2.66	3.63	4.00	1.04	1.12
400	1.72	2.54	3.83	3.98	1.11	0.95
500	3.02	3.00	4.24	4.34	1.07	0.78
600	4.19	4.21	4.61	4.39	1.17	0.73
700	4.33	4.48	4.47	4.80	1.24	0.69
800	4.27	4.37	4.42	4.51	1.27	0.67
900	4.47	4.38	4.55	4.74	1.29	0.68
981	4.38	4.51	4.61	4.71	1.28	0.68

Bubble sauter mean diameter and hold- up in zinc sulphate solutions in water model.

$ZnSO_4$		
mol/l	Hold-up%	Diameter
0.00	3.44	4.53
0.02	3.63	3.10
0.04	3.63	1.99
0.06	3.77	1.18
0.08	3.77	0.96
0.10	3.73	0.73
0.12	3.80	0.71
0.14	3.79	0.73
0.16	3.81	0.70
0.18	3.80	0.72
0.20	3.84	0.71

Appendix 7

Bubble sauter mean diameter in 0.1 $ZnSO_4$ solution.

	354 RPM	600 RPM	981 RPM
l/min	D (mm)	D (mm)	D (mm)
0	0.78	1.01	1.08
1	1.17	1.10	1.15
5	1.28	1.11	1.03
15	1.23	1.10	1.07
30	Flooding	1.06	1.02
45	Flooding	1.14	1.11

Gas hold-up in water with different mixing speeds and gas flow rates in water model.

	354 RPM	600 RPM	981 RPM
l/min	Hold-up %	Hold-up %	Hold-up %
0	0.46	3.44210997	5.7591623
1	0.96	3.73	5.80
2.5	1.16	3.73	5.80
5	1.50	3.68	5.71
15	1.60	4.06	6.57
30		4.20	7.71
45		4.85	8.23

Gas hold-up in water with different gas flow rates and mixing speeds in water model

	354 RPM	400 RPM	500 RPM	600 RPM	700 RPM	800 RPM	900 RPM	981 RPM
l/min	hold-up %	hold-up %	hold-up %	hold-up %	hold-up %	hold-up %	hold-up %	hold-up %
0	0.46	1.50	2.53	3.44	4.15	4.85	5.21	5.76
2.5	1.16	1.95	2.96	3.73	4.34	5.17	5.49	5.80
15	1.60			4.06				6.57
30	-			4.20				7.71
45	-			4.85				8.23

Surface aeration with different gas flow rates and mixing speeds in water model.

Gas flow	354 RPM	600 RPM	981 RPM
0	1.00	1.00	1.00
1	0.61	0.86	0.96
2.5	0.25	0.72	0.83
5	0.18	0.59	0.75
15	0.01	0.22	0.44
30		0.01	0.07
45		0.01	0.03

Surface aeration with different mixing speeds and liquid volumes.

	354 RPM	400 RPM	500 RPM	600 RPM	700 RPM	800 RPM	900 RPM	981 RPM
0-level	0.18	0.31	0.48	0.59	0.67	0.70	0.72	0.75
2cm level	0.09	0.13	0.33	0.46	0.58	0.64	0.67	0.69
4cm level	0.02	0.02	0.09	0.42	0.60	0.69	0.72	0.74
soap water	0.04	0.05	0.16	0.31	0.36	0.42	0.49	0.48

Relative power consumption with different mixing speeds and gas flow rates in water model.

l/min	354 RPM	600 RPM	981 RPM
0	1.000	1.000	1.000
1	0.963	0.996	0.997
2.5	0.960	0.979	0.997
5	0.957	0.968	0.997
15	0.957	0.957	0.972
30		0.936	0.920
45		0.872	0.829

Power consumption with different mixing speeds and gas flow rates in water model.

	354 RPM	400 RPM	500 RPM	600 RPM	700 RPM	800 RPM	900 RPM	981 RPM
l/min	w	w	w	w	w	w	w	w
0	80	94	130	169	223	297	385	453
15	76			161				440
30				158				416
45				147				375

Volumetric mass transfer values measured in water model.

Measuring place Number	Gas flow rate (l/min)	K_La (1/s)*10^{-3} 354 RPM (1/min)	600 RPM (1/min)	981RPM (1/min)
1	1	2.17	2.82	4.44
	2.5	2.85	3.82	6.26
	5	3.95	6.52	12.00
3	1	2.17	4.01	5.06
	2.5	3.22	5.03	7.46
	5	4.89	7.94	10.62
2	2.5		4.60	
			4.64	
			4.08	

Appendix 8

Reproducibility experiments with distilled water and 60 RPM.

Experiment Number	Result k_L (m/l)
1	17.20
2	17.80
3	17.81
4	17.88
5	18.09
6	18.12
7	18.17
8	18.21
9	18.68
10	18.75
11	19.10
12	19.15
13	19.20
14	20.02
15	20.07
16	20.34
17	21.07
18	21.37
19	21.65
20	22.02
Average	19.24
Stand.deviation	1.44
Confidence (95.0%)	0.63
Confidence/average (%)	3.28

Oxygen content in gas phase as a function of time.

Time (min)	$C(O_2)$ %
0	99.999
5	96.9
30	92.7
60	90.7
90	89.5
120	89
150	88.5
180	88.3

Mass transfer coefficient between oxygen and water.

H_2O k_L (m/s)	Hydrostatic pressure (pa)		
RPM	200	500	800
30		13.81	
45	16.49	16.70	17.59
60		19.16	

Mass transfer coefficient between oxygen and dilute sulphuric acid solutions.

	Sulpuric acid content					
	0	30 g/l	50 g/l	100 g/l	150 g/l	200 g/l
30 RPM	13.81	13.18	11.13	7.01	5.00	1.50
45 RPM	16.70	14.36	12.26	9.58	7.01	2.75
60 RPM	19.16	17.32	13.79	11.50	8.50	5.00

Mass transfer coefficient between oxygen and electrolytic solutions.

H_2SO_4	mol/l	0.00	0.51	1.02	1.53	2.04
	k_L (m/s)	16.70	15.22	10.37	7.01	3.45
$ZnSO_4$	mol/l	0.00	0.38	0.76	1.15	1.53
	k_L (m/s)	16.70	13.60	12.40	9.64	9.00
NaCl	mol/l	0.00	0.43	0.86	1.28	1.71
	k_L (m/s)	16.70	15.05	15.05	14.35	13.50

Mass transfer coefficient between oxygen and process solutions 1 and 2.

	Process 1 k_L (m/s)	Process 2 k_L (m/s)
30 RPM	4.72	1.50
45 RPM	7.00	2.50
60 RPM	11.32	3.78

Calculated O_2-H_20 composition as a function of temperature between 0 – 100 °C

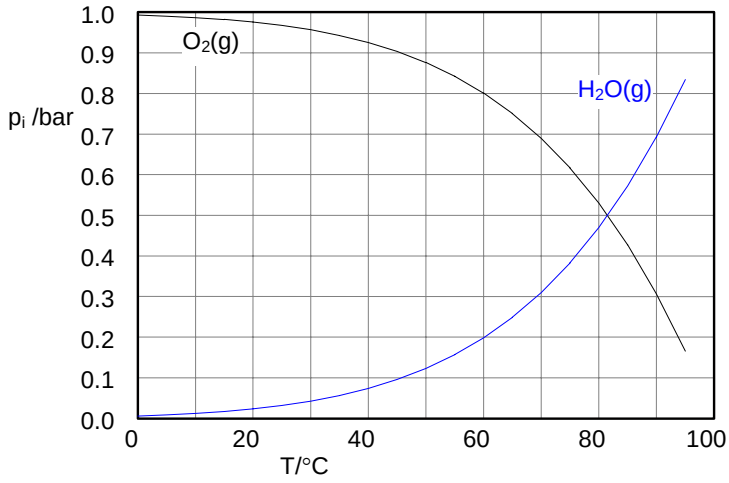

Calculated O_2-H_20 composition as a function of pressure between 1 – 3 bars, at 90 °C

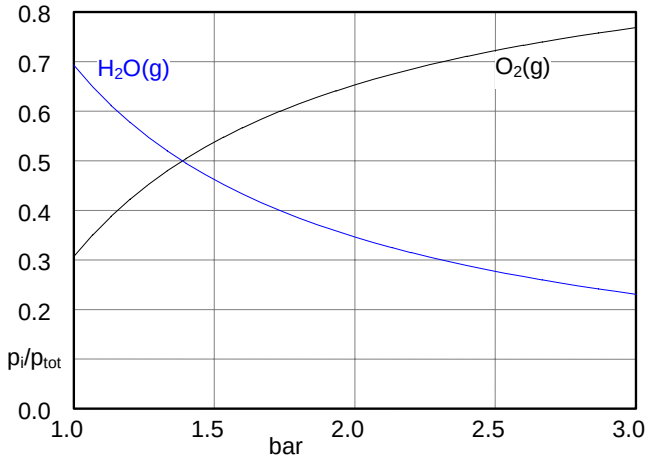

Appendix 9

Measurements of standard 200 RPM experiment

Day	Time	Hours	Minutes	Total Minutes	Container Pressure mbar	Corrected due sample mbar	Sample	Reactor pressure bar	Redox potential mV	Container Temp. °C	Room Temp. °C	Reactor Temp. °C
0	10.00	0.00	0	0	9470	9470		0.978	322	23	22.9	89.67
	10.05	0.08	5	5	9470	9470		0.994	327	23	22.9	89.92
	10.10	0.17	10	10	9466	9466		1.027	331	23	22.9	85.35
	10.16	0.27	16	16	9466	9466		1.033	333	23	23	85.97
	10.31	0.52	31	31	9468	9468		1.030	337	23	23	87.38
	10.43	0.72	43	43	9456	9469	1	1.013	338	23	23	88.03
	11.18	1.30	78	78	9456	9469		1.032	343	23	23	89.6
	11.39	1.65	99	99	9456	9469		1.003	344	23	23	90.17
	11.47	1.78	107	107	9445	9469	2	1.001	346	23	23	90.12
	12.12	2.20	132	132	9439	9463		0.990	347	23	23	89.64
	12.59	2.98	179	179	9424	9448		0.982	350	23	23	89.49
	14.40	4.67	280	280	9414	9438		0.980	349	23	23	89.29
	14.50	4.83	290	290	9401	9437	3	0.988	349	23	23	89.23
	15.47	5.78	347	347	9385	9421		1.007	361	23	22.7	89.25
	16.35	6.58	395	395	9377	9413		1.010	362	22.5	22.7	89.3
	16.44	6.73	404	404	9365	9412	4	1.013	362	23	22.9	89.19
	21.47	11	47	707	9349	9396		1.001	364	23.5	23.6	89.13
	21.55	11	55	715	9336	9395	5	1.009	366	23.5	23.6	88.99
1	7.52	21	52	1312	9267	9326		0.993	370	23	23.2	89.19
	11.40	25	40	1540	9247	9306		0.990	372	23.5	23.2	89.13
	11.47	25	47	1547	9236	9305	6	0.999	371	23.5	23.4	88.91
	13.52	27	52	1672	9233	9302		1.002	374	23.5	23.6	88.94
	15.30	29	30	1770	9233	9302		0.986	373	24	23.8	89.05
2	8.25	46	25	2785	9137	9206		0.987	381	24	24.1	89.25
	12.37	50	37	3037	9122	9191		0.992	384	24	24.3	88.94
	12.44	50	44	3044	9110	9190	7	0.994	385	24	24.3	89.09
3	11.02	73	2	4382	9001	9081		1.007	395	24.5	24.5	89.35
	11.16	73	16	4396	8648	8648		3.012	398	24.5	24.5	89.8
	11.27	73	27	4407	8640	8640	8	2.977	401	24.5	24.5	89.6
4	10.09	96	9	5769	8238	8238		3.006	450	24.5	24.3	89.96
	10.19	96	19	5779	8223	8235	9	2.969	451	24.5	24.5	90.05
	13.11	99	11	5951	8177	8189		2.993	455	25	24.7	90.1
	15.14	101	14	6074	8154	8166		2.992	457	25	25.1	90.15
5	10.01	120	1	7201	7830	7842		2.994	480	24.5	24.6	89.93
	10.12	120	12	7212	7801	7839	10	2.990	482	24.5	24.7	90.1
	12.30	122	30	7350	7762	7800		2.985	486	25	24.8	89.9
	15.27	125	27	7527	7717	7755		2.988	490	25	24.9	90.11
	16.42	126	42	7602	7695	7733		2.999	490	25	24.9	90.01
6	10.03	144	3	8643	7390	7428		2.987	517	24.5	24.2	90.05
	10.11	144	11	8651	7359	7426	11	2.987	517	24.5	24.3	89.98
	12.28	146	28	8788	7321	7388		2.999	519	24.5	24.4	89.73
	15.00	149	0	8940	7294	7361		2.984	521	24.5	24.8	90.11
7	10.00	168	0	10080	7049	7116		2.985	525	24.5	24.4	89.97
	10.09	168	9	10089	7025	7114	12	2.993	524	24.5	24.5	89.57
	11.45	169	45	10185	7020	7109		2.988	526	25	24.9	89.85
	13.37	171	37	10297	7006	7095		2.988	527	25	25	89.93
	16.10	174	10	10450	6991	7080		2.998	527	25.5	25.3	90.04
8	10.06	192	6	11526	6835	6924		3.007	537	24.5	24.5	89.65
	10.13	192	13	11533	6816	6923	13	2.987	537	24.5	24.7	90.02
	12.40	194	40	11680	6808	6915		2.998	539	25	25.1	89.61
	14.40	196	40	11800	6799	6906		3.006	540	25	25.3	89.63
	15.38	197	38	11858	6794	6901		3.007	541	25	25.1	89.79
9	11.09	217	9	13029	6672	6779		2.984	550	24.5	24.7	89.53
	11.15	217	15	13035	6643	6778	14	2.989	549	24.5	24.7	89.5
10	18.49	248	49	14929	6524	6659		2.998	558	24.5	25	89.5
	19.00	249	0	14940	6498	6658	15	2.985	558	24.5	25	89.63
	7.08	261	8	15668	6433	6593		3.009	561	23.5	23.7	90.15
11	10.07	264	7	15847	6419	6579		3.011	561	23.5	23.6	89.87
	10.17	264	17	15857	6400	6578	16	2.984	561	23.5	23.8	90.08

Measurements of ethanol 1.5% experiment

Day	Time	Hours	Minutes	Total Minutes	Container Pressure mbar	Corrected due sample mbar	Sample number	Reactor pressure bar	Redox potential mV	Container Temp. °C	Room Temp. °C	Reactor Temp. °C
0	10.01	0.017	1	1	9552	9552		1.008	271	24.1	24	84.58
	10.05	0.083	5	5	9555	9555		0.986	272	24.1	24	84.76
	10.10	0.167	10	10	9557	9557		0.984	274	24	24	84.9
	10.18	0.300	18	18	9558	9558		1.003	276	24	24.5	85.63
	10.32	0.533	32	32	9559	9559	1	1.032	281	24	24	87.13
	10.50	0.833	50	50	9549	9559		0.999	291	24	24.5	88.45
	11.26	1.433	86	86	9538	9548		1.016	297	24	24	88.79
	11.36	1.600	96	96	9537	9547	2	1.024	299	24	24	88.74
	11.44	1.733	104	104	9526	9546		1.033	299	24	24	88.76
	12.15	2.250	135	135	9519	9539		1.019	303	24	24	89.09
	12.44	2.733	164	164	9514	9534		1.026	307	24	24	89.13
	13.11	3.183	191	191	9510	9530		1.011	311	24	24	89.11
	14.10	4.167	250	250	9500	9520	3	1.007	318	24	24	89.14
	14.18	4.300	258	258	9488	9519		1.029	310	24.1	24	89.1
	15.24	5.400	324	324	9475	9506		1.024	325	23.9	24	89.33
	18.10	8.167	490	490	9453	9484	4	1.017	334	24	24	89.76
	18.23	8.383	503	503	9433	9482		1.017	326	24.1	24	89.78
1	6.15	20.000	15	1215	9346	9395		1.012	340	24	23.5	89.78
	9.42	23.000	42	1422	9311	9360	5	1.010	341	23.8	23.5	89.86
	9.52	23.000	52	1432	9305	9359		1.000	339	23.7	23.5	89.76
	16.31	30.000	31	1831	9249	9303		1.001	339	23.6	23.5	89.48
	20.54	34.000	54	2094	9226	9280		0.996	337	23.9	24	89.63
2	6.20	44.000	20	2660	9155	9209	6	1.007	335	23.6	23.5	89.38
	6.36	44.000	36	2676	9146	9207		0.995	334	23.6	23.5	89.73
	9.32	47.000	32	2852	9106	9167		1.009	332	23.1	23	89.73
	14.12	50.000	12	3012	9078	9139		1.004	335	23.2	23	89.64
3	8.00	70.000	0	4200	8970	9031	7	1.010	332	23.4	23.5	89.48
	8.02	70.000	2	4202	8967	9031		0.982	331	23.4	23.5	89.6
	9.40	71.000	40	4300	8960	9024		1.001	330	23.4	23.5	89.85
	10.00	72.000	0	4320	8649	8713		2.998	333	23.5	23.5	89.74
4	7.23	93.000	23	5603	8192	8192		2.995	366	23.3	23	89.66
	9.00	95.000	0	5700	8171	8171	8	3.001	369	23.3	23	89.58
	9.15	95.000	15	5715	8149	8168		2.998	365	23.3	23	89.79
5	6.40	116.000	40	7000	7725	7744		2.993	378	23.2	23	89.77
	9.30	119.000	30	7170	7681	7700	9	2.987	382	23.5	23	89.69
	9.45	119.000	45	7185	7658	7696		2.989	383	23.5	23	89.74
	11.15	121.000	15	7275	7637	7675		2.993	383	24	24	89.52
	14.45	124.000	45	7485	7591	7629		2.983	385	24.6	24.5	89.78
6	6.40	140.000	40	8440	7306	7344		2.980	400	24.3	24.5	89.81
	10.00	144.000	0	8640	7251	7289	10	2.994	404	24.3	24.5	90.05
	10.10	144.000	10	8650	7231	7286		2.985	404	24.3	24.5	90.1
	14.40	148.000	40	8920	7163	7218		2.980	408	25.1	25	90.13
7	6.15	164.000	15	9855	6864	6919		2.987	420	24.8	24.5	89.64
	10.04	168.000	4	10084	6807	6862	11	2.989	422	25.1	25	89.8
	10.14	168.000	14	10094	6786	6853		2.980	422	25.1	25	89.96
	12.11	170.000	11	10211	6765	6832		2.978	423	25.9	25.5	89.99
	14.31	172.000	31	10351	6733	6800		2.972	424	26.2	26	89.86
	15.29	173.000	29	10409	6718	6785		2.974	425	26.1	26	89.81
8	10.02	192.000	2	11522	6410	6477	12	2.975	434	25.5	25.5	90
	10.11	192.000	11	11531	6385	6476		2.980	433	25.6	25.5	90
	11.55	193.000	55	11635	6369	6460		2.975	435	26	26	90.06
	14.09	196.000	9	11769	6343	6434		2.969	436	26.3	26.5	89.79
	15.03	197.000	3	11823	6331	6422		2.969	436	26.4	26.5	89.84
9	6.45	212.000	45	12765	6087	6178		2.985	443	25.6	26	89.39
	10.10	216.000	10	12970	6038	6129	13	2.990	444	26	26	89.62
	10.12	216.000	12	12972	6015	6128.5		2.981	444	26	26	89.73
10	6.33	236.000	33	14193	5747	5860.5		2.983	450	26.1	27	89.78
	7.04	237.000	4	14224	5739	5852.5	14	2.969	449	26.1	26.5	89.8
	7.21	237.000	21	14241	5710	5848		2.998	450	26	26	89.58
11	7.30	261.000	30	15690	5430	5568		2.995	455	26.1	26	89.65
	8.00	262.000	0	15720	5426	5564	15	2.980	454	26.2	26	89.9
	8.16	262.000	16	15736	5401	5561		2.993	456	26.2	26	89.57
12	6.37	284.000	37	17077	5164	5324		2.994	459	25.5	25.5	89.71
	10.04	288.000	4	17284	5134	5294	16	2.974	458	26	26	89.76
	10.13	288.000	13	17293	5110	5293		2.987	459	26.1	26	89.55
	11.55	289.000	55	17395	5097	5280		2.975	459	25.9	26	89.71
	14.23	292.000	23	17543	5081	5264		2.987	459	26.3	26.5	89.68
13	9.52	311.000	52	18712	4875	5058	17	2.985	462	25.1	25.5	89.43
	10.00	312.000	0	18720	4856	5057		2.995	462	25.1	25.5	89.34
	12.05	314.000	5	18845	4843	5044		3.002	462	25.3	25.5	89.68
	14.00	316.000	0	18960	4833	5034		3.001	462	25.7	26	89.66

Measurements of octhene 1.5%experiment

Day	Time	Hours	Minutes	Total Minutes	Container Pressure mbar	Corrected due sample mbar	Sample number	Reactor pressure bar	Redox potential mV	Container Temp. °C	Room Temp. °C	Reactor Temp. °C
0	10.00	0.000	0	0	9765	9765		1.022	174	24.5	26	86.12
		0.083	5	5	9770	9770		0.962	162	24.5	26	86.68
		0.167	10	10	9765	9765		0.980	165	24.5	26	87.1
		0.300	18	18	9761	9761		1.001	173	24.5	26	87.6
		0.567	34	34	9757	9757	1	0.996	189	24.5	26	88.18
		0.733	44	44	9741	9755		0.997	169	24.5	26	88.24
		0.950	57	57	9736	9750		1.009	200	24.5	26.5	88.33
	11.28	1.467	88	88	9731	9745	2	1.002	323	24	26	88.92
	11.35	1.583	95	95	9719	9744		1.005	322	24	26.5	88.88
	12.57	2.883	173	173	9705	9730		1.006	318	24	26	89.35
	13.25	3.417	205	205	9703	9728	3	0.982	322	24	26	89.72
	13.36	3.517	211	211	9692	9727		0.996	403	24	26	89.65
	15.17	5.283	317	317	9681	9716		0.987	422	24	26	90.06
	16.24	6.400	390	384	9672	9707	4	0.996	435	24.5	26.5	90.1
	16.35	7	396	390	9664	9706		0.994	426	24.5	26.5	89.99
1	11.13	25	13	1513	9493	9535	5	0.980	286	24	26.5	90.17
	11.22	25	22	1522	9481	9534		0.987	285	24	26.5	90.06
	11.42	25	42	1542	9478	9531		1.022	284	24	26.5	89.86
2	11.41	49	41	2981	9331	9384	6	0.993	276	23.5	26	90.39
	11.48	49	48	2988	9322	9383		0.989	275	23.5	26	90.51
3	8.43	70	43	4243	9201	9262	7	0.977	304	23.5	25.5	90.2
	8.50	70	50	4250	9192	9253		0.993	305	23.5	25.5	90.09
	9.06	71	6	4266	8905	8966		3.026	308	23.5	25.5	90.38
	10.15	72	15	4335	8888	8949		3.026	316	23.5	25.5	90.46
	11.38	73	38	4418	8867	8928		3.023	322	23.5	25.5	90.53
	13.16	75	16	4516	8843	8904		3.035	327	23.5	25.5	90.21
	15.56	79	56	4796	8809	8870		3.021	335	23.5	26	90.5
4	9.16	95	16	5716	8537	8598	8	3.019	383	23.5	25.5	90.36
	9.26	95	26	5726	8511	8595		3.041	383	23.5	25.5	90.03
	12.58	98	58	5938	8463	8547		3.031	391	23.5	25.5	90.46
	16.17	102	17	6137	8412	8496		3.025	398	23	25	90.54
5	8.55	118	55	7135	8162	8246	9	3.030	416	23	25	90.39
	9.03	119	3	7143	8139	8248		3.031	416	23	25	90.33
	14.46	124	46	7486	8073	8182		3.022	421	23	25.5	90.64
6	6.20	140	20	8420	7830	7939		3.025	432	23	25	90.05
	9.01	143	1	8581	7796	7905	10	3.019	436	23	25	90.41
	9.08	143	8	8588	7770	7904		3.021	436	23	25	90.38
	15.59	150	59	9059	7689	7823		3.028	436	23	25	90.15
7	7.10	165	10	9910	7508	7642		3.028	454	23	25	90.04
	9.30	167	30	10050	7484	7618	11	3.028	455	23	25	90.29
	9.40	167	40	10060	7461	7616		3.014	455	23	25	90.35
	15.04	173	4	10384	7405	7560		3.008	436	23	26	90.4
9	16.57	222	57	13377	6925	7080	12	3.009	484	23.5	26	90.12
	17.04	223	4	13384	6900	7079		3.010	485	23.5	26	89.97
10	6.32	236	32	14192	6787	6966		3.031	511	23	24.5	89.71
	9.45	239	45	14385	6762	6941	13	3.035	518	23	25	89.54
	9.55	239	55	14395	6742	6940		3.026	518	23	25	89.85
	12.27	242	27	14547	6724	6922		3.020	521	23	25	89.88
	15.16	245	16	14716	6701	6899		3.038	518	23	25	89.64
11	6.30	260	30	15630	6579	6777		3.036	519	22.5	24.5	89.78
	9.04	263	4	15784	6561	6759	14	3.02	521	22.5	24	89.86
	9.13	263	13	15793	6537	6758		3.02	521	22.5	24	89.67
	13.54	267	54	16074	6500	6721		3.043	522	23	24.5	89.66
12	9.28	287	28	17248	6369	6590	15	3.044	519	23	24	90.1
	9.35	287	35	17255	6351	6589		3.024	519	23	24	90
	12.48	290	48	17448	6334	6572		3.042	521	24.5	24.5	89.97
	15.50	293	50	17630	6310	6548		3.048	522	22.5	24	89.7
13	6.35	308	35	18515	6222	6460		3.017	522	23	2	89.89
	9.24	311	24	18684	6203	6441	16	3.04	522	23	24	89.89
	9.31	311	31	18691	6182	6440		3.022	522	23	24	89.9
	12.04	314	4	18844	6151	6409		3.019	524	23	24	89.7
	15.17	317	17	19037	6123	6381		3.019	523	23	24.5	89.45
14	7.00	333	0	19980	6048	6306		3034	524	22.5	25.5	89.38
	8.46	334	46	20086	6035	6293		3.034	523	22.5	26	89.39

Measurements of 2% SO_2 experiment

Day	Time	Hours	Min.	Total Min.	Container Pressure mbar	Corrected due sample mbar	Sample number	Reactor pressure bar	Redox potential mV	Container Temp. °C	Room Temp. °C	Reactor Temp. °C
	10.00	0.0		0	9466	9466		-0.367	345	23.4	23.5	85.18
	10.02	0.0		2	9275	9275		1.018	346	23.4	23.5	85.35
		0.1		6	9267	9267		1.200	348	23.4	23.5	85.57
		0.2		11	9273	9273		1.129	350	23.4	23.5	85.97
		0.6		34	9273	9273	1	1.058	357	23.5	23.5	86.84
		0.7		44	9259	9259		1.020	359	23.6	23.5	87.39
		1.9		111	9243	9243	2	0.993	368	23.2	23	89.45
		2.0		120	9228	9228		1.002	369	23.2	23	89.56
	14.26	4.4		266	9214	9214	3	0.986	380	23.3	23.5	88.59
	14.45	4.8		285	9201	9201		0.986	381	23.3	23.5	88.88
	15.56	5.9		356	9179	9179	4	1.019	384	22.9	23	88.81
	16.03	6.1		363	9163	9163		1.028	384	22.9	23	88.77
1	15.26	29.0	20	1760	9016	9016	5	0.993	398	23.4	23	88.9
		29.0	26	1766	9002	9002		1.005	398	23.4	23	88.78
2	14.48	52.0	48	3168	8865	8865	6	0.980	405	23.5	23.5	88.9
	14.55	52.0	55	3175	8851	8851		1.003	406	23.5	23.5	88.58
		66.0	47	4007	8772	8772		1.026	408	23.6	23.5	88.95
3	9.50	71.0	50	4310	8410	8410	7	2.970	408	23.6	23.5	88.92
	10.11	72.0	11	4331	8392	8392		3.018	410	23.6	23.5	88.97
	10.54	72.0	54	4374	8378	8378		3.016	413	23.5	23.5	89.21
	12.05	74.0	5	4445	8354	8354		3.012	417	23.5	23.5	89.12
	13.51	75.0	51	4551	8318	8318		3.010	421	23.2	23.5	89.04
	14.24	76.0	24	4584	8301	8301		3.025	422	23	23.5	89.19
	15.14	77.0	14	4634	8276	8276		3.027	424	22.9	23	89.08
	16.43	78.0	43	4723	8259	8259		3.009	425	23.2	23	89.13
4	9.28	95.0	28	5728	8004	8004	8	3.012	440	23.5	23	89.24
	9.38	95.0	38	5738	7969	7969		3.012	441	23.5	23.5	89.16
	13.03	99.0	3	5943	7918	7918		3.026	444	23.6	23.5	88.99
	15.23	101.0	23	6083	7882	7882		3.010	447	23.6	23.5	89.16
	16.43	102.0	43	6163	7858	7858		3.027	448	23.5	23.5	89.05
	11.28	121.0	28	7288	7562	7562	9	3.026	468	23.6	23.5	88.92
5	11.34	121.0	34	7294	7531	7531		3.012	469	23.6	23.5	88.99
	14.22	124.0	22	7462	7485	7485		3.027	472	23.6	23.5	88.98
	16.45	126.0	45	7605	7443	7443		3.015	475	23.3	23.5	89.15
6	12.18	146.0	18	8778	7141	7141	10	3.025	497	23.7	23.5	89.2
	12.24	146.0	24	8784	7110	7110		3.012	498	23.7	23.5	89.21
	16.30	150.0	30	9030	7048	7048		3.027	503	23.6	23.5	88.99
7	9.32	167.0	32	10052	6803	6803	11	3.034	523	23.5	23.5	89.09
	9.40	167.0	40	10060	6776	6776		3.013	523	23.5	23.5	89.2
	16.52	174.0	52	10492	6675	6675		3.018	531	23.5	23.5	89.01
8	13.34	195.0	34	11734	6414	6414	12	3.033	546	23.3	23.5	89.18
	13.42	195.0	42	11742	6393	6393		3.010	548	23.3	23.5	89.28
10	6.57	236.0	57	14217	6071	6071	13	3.033	563	23.4	23	89.35
	7.08	237.0	8	14228	6045	6045		3.012	564	23.4	23.5	89.4
	11.12	241.0	12	14472	6021	6021		3.033	564	23.5	23.5	89.02
	17.43	247.0	43	14863	5988	5988		3.036	566	23.3	23	89.03
11	7.10	261.0	10	15670	5922	5922		3.036	567	23.1	23.5	89.3
	9.27	263.0	27	15807	5919	5919	14	3.019	569	23.2	23.5	88.97
	9.33	263.0	33	15813	5891	5891		3.010	569	23.3	23.5	88.96
	13.28	267.0	28	16048	5874	5874		3.032	571	23.3	23.5	89.2
	17.37	271.0	37	16297	5862	5862		3.025	573	23.4	23.5	89.26
12	10.25	288.0	25	17305	5805	5805	15	3.02	575	23.5	23.5	89.26
	10.33	288.0	33	17313	5772	5772		3	576	23.6	23.5	89.16
	16.14	294.0	14	17654	5744	5744		3.016	578	23.1	23.5	89.14
13	7.15	309.0	15	18555	5689	5689		3.012	579	23	23	89.38
	16.51	318.0	51	19131	5653	5653	16	3.016	579	22.9	23.5	88.95
	16.58	318.0	58	19138	5629	5629		3.003	579	23	23	89.02
14	10.26	336.0	26	20186	5584	5584	17	3.01	583	23.4	23.5	89.17

Measurements of standard 250 RPM experiment

Time	Hours	Min.	Total Min.	Container Pressure mbar	Corrected due sample mbar	Sample number	Reactor pressure bar	Redox potential mV	Room Temp. °C	Reactor Temp. °C
10.00	0.00		0	9774	9774		-0.443	367	22.6	84.28
10.03	0.05		3	9600	9600		1.126	340	22.6	84.32
10.07	0.12		7	9607	9607		1.028	346	22.6	84.55
10.10	0.17		10	9600	9600		1.033	342	22.6	84.72
10.28	0.47		28	9579	9579		1.036	349	22.6	85
10.38	0.63		38	9562	9567	1	1.054	355	22.5	87.3
11.03	1.05	3	63	9559	9564		1.054	350	22.6	88.27
11.44	1.73	44	104	9557	9562		1.030	366	22.6	89.89
11.57	1.95	57	117	9555	9560		1.026	368	22.8	89.87
12.13	2.22	13	133	9540	9557	2	1.041	361	22.8	89.51
13.32	3.53	32	212	9523	9540		1.031	367	22.8	89.65
15.48	5.80	48	348	9487	9504	3	1.032	371	22.5	89.36
16.07	6.12	7	367	9474	9499		1.035	367	22.6	89.64
17.07	7	7	427	9462	9487		1.031	374	22.4	89.63
22.07	12	7	727	9429	9454	4	1.034	371	23.1	89.5
22.14	12	14	734	9421	9453		1.017	373	23.1	89.73
7.32	21	32	1292	9352	9384	5	1.013	384	22.9	89.62
7.43	21	43	1303	9340	9382		1.027	377	22.9	89.49
9.42	23	42	1422	9329	9371		1.027	380	22.7	89.66
11.36	25	36	1536	9303	9345		1.024	383	22.2	89.73
12.50	26	50	1610	9286	9328		1.026	379	22.4	89.39
14.34	28	34	1714	9288	9330		1.016	383	22.5	89.36
16.34	30	34	1834	9275	9317		1.025	382	22.2	89.52
10.09	48	9	2889	9206	9248	6	1.020	387	23	89.55
10.23	48	23	2903	9193	9247		1.016	386	23	89.76
10.52	72	52	4372	9082	9136	7	1.011	391	22.9	89.38
11.09	73	9	4389	9071	9135		1.015	390	23	89.66
11.52	73	52	4432	8789	8853		3.035	395	23.1	89.61
10.41	96	41	5801	8337	8337	8	3.009	410	22.7	89.79
10.55	96	55	5815	8307	8332		3.027	410	22.8	89.62
17.08	103	8	6188	8137	8162		3.016	410	21.6	89.5
10.52	120	52	7252	7785	7810	9	3.006	412	22.5	89.96
11.05	121	5	7265	7756	7805		3.025	411	22.5	89.71
16.24	126	24	7584	7623	7672		3.023	413	22.1	89.79
19.10	129	10	7750	7562	7611		3.025	414	22.4	89.75
6.24	140	24	8424	7346	7395		3.005	421	22.9	89.8
10.44	144	44	8684	7249	7298	10	3.010	424	22.3	89.99
10.52	144	52	8692	7221	7295		3.015	424	22.2	89.73
12.48	146	48	8808	7173	7247		3.022	423	22	89.59
21.37	154	37	9277	7004	7078		3.017	433	23	89.7
21.40	154	40	9280	7003	7077		3.021	432	22.5	89.7
10.29	168	29	10109	6718	6792	11	3.014	445	22.1	90.05
10.39	168	39	10119	6678	6789		3.012	447	22.1	89.75
6.11	188	11	11291	6275	6386		3.007	481	23.3	89.77
9.14	191	14	11474	6204	6315		2.996	494	22.9	89.68
10.33	192	33	11553	6179	6290	12	3.013	489	22.9	89.79
10.40	192	40	11560	6150	6287		3.007	489	22.9	89.6
13.51	195	51	11751	6084	6221		3.002	504	23.3	89.62
14.17	220	17	13217	5554	5691	13	2.994	518	24.3	89.76
14.24	220	24	13224	5524	5688		2.998	519	24.3	89.59
17.32	247	32	14852	5125	5289	14	3.015	565	24.2	89.76
17.40	247	40	14860	5102	5287		2.999	566	24.2	89.7
6.48	260	48	15648	5016	5201		3.029	580	23.1	89.66
9.58	263	58	15838	5008	5193		3.03	582	23.2	89.68
11.31	265	31	15931	5005	5190	15	3.04	583	23.2	89.61

Measurements of ethanol 3% experiment

Day	Time	Hours	Minutes	Total Minutes	Container Pressure mbar	Corrected due sample mbar	Sample number	Reactor pressure bar	Redox potential mV	Room Temp. °C	Reactor Temp. °C
0	10.00	0.000	0	0	10120	10120		1.172	351	23	84
	10.03	0.050	3	3	10130	10130		1.129	352	23	85
	10.06	0.100	6	6	10130	10130		1.104	352	23	85
	10.10	0.167	10	10	10130	10130		1.080	352	23	85.2
	10.15	0.250	15	15	10140	10140		1.056	352	23	85.52
	10.30	0.500	30	30	10140	10140	1	1.037	353	23	86.11
	10.43	0.717	43	43	10120	10129		1.070	355	23.1	87.02
	11.05	1.083	65	65	10120	10129		1.057	357	23.1	88
	11.26	1.433	86	86	10120	10129		1.047	358	23.1	88.35
	11.39	1.650	99	99	10110	10119		1.041	359	23	88.35
	11.55	1.917	115	115	10110	10119	2	1.060	358	23	88.4
	12.05	2.083	125	125	10100	10118		1.066	359	23	88.9
	12.10	2.167	130	130	10090	10108		1.067	359	23	89.1
	12.42	2.7	162	162	10090	10108		1.053	362	23	89.34
	13.12	3.2	192	192	10080	10098		1.055	362	22.9	89.96
	13.30	3.5	210	210	10080	10098		1.042	363	22.9	89.9
	15.05	5.0	5	305	10060	10078		1.043	365	22.9	90.4
	15.56	5.0	56	356	10050	10068	3	1.045	366	22.9	90.06
	16.05	6.0	5	365	10040	10066		1.048	367	22.9	90.01
	21.57	11.0	57	717	9995	10021	4	1.055	370	23.3	89.55
	22.03	12.0	3	723	9987	10020		1.040	369	23.3	89.72
	6.41	20.0	41	1241	9921	9954		1.051	373	23	89.6
	9.12	23.0	12	1392	9915	9948		1.053	371	23	89.68
	9.55	23.0	55	1435	9913	9946	5	1.050	372	23	89.55
1	10.04	24.0	4	1444	9908	9945		1.035	370	23	89.77
	11.41	25.0	41	1541	9894	9931		1.055	371	23	89.55
	15.07	29.0	7	1747	9872	9909		1.041	374	23	89.52
	7.10	45.0	10	2710	9810	9847		1.049	375	23	89.84
	9.42	47.0	42	2862	9805	9842	6	1.052	375	22.9	89.76
2	9.51	47.0	51	2871	9798	9842		1.025	375	22.9	89.72
	15.43	53.0	43	3223	9786	9830		1.047	377	23.3	89.55
	6.54	68.0	54	4134	9732	9776		1.035	379	23.1	89.54
3	11.16	73.0	16	4396	9712	9756	7	1.046	379	22.8	89.73
	11.28	73.0	28	4408	9707	9755		1.020	379	22.8	89.48
	11.36	73.0	36	4416	9400	9448		3.027	379	22.8	89.42
	12.43	74.0	43	4483	9375	9423		3.038	388	22.8	89.83
	13.17	75.0	17	4517	9359	9407		3.037	392	22.8	89.73
	15.44	77.0	44	4664	9300	9348		3.028	397	22.7	90
	7.17	93.0	17	5597	8972	9020	8	3.016	409	23.2	89.82
	7.30	93.0	30	5610	8949	9015		3.040	407	23.3	89.8
4	9.30	95.0	30	5730	8907	8973		3.030	409	23.2	90.21
5	14.39	124.0	39	7479	8297	8363	9	3.019	423	23.6	89.71
	14.45	124.0	45	7485	8278	8361		3.033	423	23.7	89.73
	8.45	142.0	45	8565	7890	7973		3.020	435	22.1	89.71
6	10.20	144.0	20	8660	7871	7954	10	3.021	436	22.4	89.91
	10.31	144.0	31	8671	7839	7952		3.029	436	22.5	89.71
	12.20	146.0	20	8780	7815	7928		3.017	438	22.6	89.91
	9.16	167.0	16	10036	7426	7539		3.018	447	22.6	89.88
7	10.27	168.0	27	10107	7408	7521	11	3.034	447	22.7	89.72
	10.35	168.0	35	10115	7385	7519		3.034	447	22.8	89.92
	12.23	170.0	23	10223	7360	7494		3.041	447	23.2	89.81
	15.16	173.0	16	10396	7316	7450		3.035	449	23.4	89.9
	6.30	188.0	30	11310	7028	7162		3.038	452	23.2	90.01
8	10.07	192.0	7	11527	6981	7115	12	3.039	453	23.4	89.91
	10.15	192.0	15	11535	6962	7112		3.035	453	23.4	90.02
	12.14	194.0	14	11654	6928	7078		3.036	453	23.3	90.16
	9.25	215.0	25	12925	6565	6715		3.022	458	23.6	90.05
10	10.31	216.0	31	12991	6542	6692	13	3.024	458	23.1	89.78
	10.40	216.0	40	13000	6519	6690		3.035	457	23	89.87
	12.22	218.0	22	13102	6480	6651		3.031	458	22.7	89.72
	14.47	220.0	47	13247	6435	6606		3.023	458	22.3	89.67
	6.38	236.0	38	14198	6192	6363		3.035	461	22.5	89.71
11	10.06	240.0	6	14406	6146	6317	14	3.02	461	22.9	89.64
	10.14	240.0	14	14414	6125	6315		3.033	461	22.9	89.72
	13.29	243.0	29	14609	6076	6266		3.027	461	22.7	90.12
	14.35	244.0	35	14675	6058	6248		3.018	462	22.7	89.91
13	8.42	286.0	42	17202	5507	5697		3.03	465	23.2	89.6
	10.01	288.0	1	17281	5485	5675	15	3.03	465	23.1	89.8
	10.11	288.0	11	17291	5468	5673		3.023	465	23	89.9
	15.42	293.0	42	17622	5418	5623		3.023	466	23.1	89.8
	6.24	308.0	24	18504	5247	5452		3.028	467	23.1	89.75

Measurements of octhene 3% experiment

Day	Time	Hours	Minutes	Total Minutes	Container Pressure mbar	Corrected due sample mbar	Sample number	Reactor pressure bar	Redox potential mV	Room Temp. °C	Reactor Temp. °C
0	10.00	0.000	0	0	9615	9615		0.962	353	23	82.73
	10.05	0.083	5	5	9588	9588		1.257	354	23	83.31
	10.10	0.167	10	10	9491	9491		1.013	360	23.1	83.8
	10.21	0.350	21	21	9496	9496		1.006	362	23.1	84.67
	10.30	0.500	30	30	9496	9496	1	1.004	365	23.1	85.69
	10.45	0.750	45	45	9481	9495		1.027	368	23.1	86.88
	11.00	1.000	60	60	9480	9480		1.038	371	22.9	87.65
	11.22	1.367	82	82	9480	9480		1.016	373	23	88.23
	11.36	1.600	96	96	9480	9480		1.028	374	23	88.47
	11.53	1.883	113	113	9478	9478		1.020	375	22.9	89.09
	12.09	2.150	129	129	9476	9476	2	1.002	377	22.8	89.33
	12.18	2.300	138	138	9460	9475		1.034	377	22.8	89.3
	13.01	3.017	181	181	9456	9471		1.017	380	22.8	90.01
	13.34	3.567	214	214	9454	9469		1.026	380	22.9	90.32
	14.11	4.183	251	251	9455	9470	3	1.017	382	23.2	90.42
	14.21	4.517	271	271	9445	9469		1.031	382	23.3	90.59
	15.36	5.600	336	336	9444	9468		1.023	384	23.4	90.98
	16.00	6.000	360	360	9441	9465		1.015	384	23.4	90.63
	19.10	7.167	430	430	9418	9442	4	1.033	384	23.6	90.21
	19.18	7.300	438	438	9410	9440		1.022	385	23.6	90.33
	8.50	22.000	50	1370	9297	9327	5	1.019	393	23.2	90.05
1	9.09	23.000	9	1389	9286	9325		1.039	394	23.3	90.15
	11.00	25.000	0	1500	9272	9311		1.047	395	23.2	90.15
	12.52	26.000	52	1612	9259	9298		1.043	396	23.2	90.25
	14.07	28.000	7	1687	9251	9290		1.031	397	23.2	90.34
2	7.44	45.000	44	2744	9139	9178		1.035	401	23.5	90.17
	9.36	47.000	36	2856	9125	9164	6	1.034	402	23.3	90.3
	9.44	47.000	44	2864	9116	9163		1.029	402	23.4	90.25
	11.04	49.000	4	2944	9105	9152		1.043	402	23.3	90.11
	12.39	50.000	39	3039	9081	9128		1.023	400	22.8	90.21
	14.07	52.000	7	3127	9063	9110		1.043	403	22.6	90.32
3	8.48	70.000	48	4248	9004	9051		1.037	405	23.3	90.16
	10.25	72.000	25	4345	8996	9043	7	1.048	405	23.4	90.12
	10.35	72.000	35	4355	8699	9042		3.024	406	23.4	90.41
	12.02	74.000	2	4442	8670	9013		3.013	420	23.6	90.42
	12.37	74.000	37	4477	8661	9004		3.016	424	23.6	90.52
	14.35	76.000	35	4595	8623	8966		3.012	432	23.9	90.48
4	9.00	95.000	0	5700	8227	8570	8	3.016	474	23.7	90.29
	9.15	95.000	15	5715	8203	8565		3.020	471	23.7	90.36
5	8.55	118.000	55	7135	7643	8005	9	3.012	518	23.5	90.3
	9.02	119.000	2	7142	7623	8003		3.028	518	23.5	90.35
	6.15	140.000	15	8415	7162	7542		3.010	562	23.3	90.49
6	9.14	143.000	14	8594	7113	7493	10	3.021	566	23.3	90.3
	9.24	143.000	24	8604	7090	7490		3.025	566	23.4	90.36
	11.10	145.000	10	8710	7063	7463		3.034	569	23.2	90.29
	13.27	147.000	27	8847	7037	7437		3.020	572	23.4	90.58
7	9.14	167.000	14	10034	6835	7235	11	3.020	584	23.3	90.42
	9.26	167.000	26	10046	6810	7233		3.026	584	23.4	90.29
	11.24	169.000	24	10164	6799	7222		3.022	584	23.3	90.27
	13.06	171.000	6	10266	6787	7210		3.013	585	23.2	90.5
8	9.27	191.000	27	11487	6647	7070	12	3.028	586	22.8	90.53
	9.39	191.000	39	11499	6624	7068		3.022	586	22.9	90.48
	11.43	193.000	43	11623	6604	7048		3.023	586	22.8	90.37
	13.17	195.000	17	11717	6606	7050		3.034	586	23	90.62
	15.09	197.000	9	11829	6593	7037		3.027	586	22.6	90.49
	7.55	213.000	55	12835	6531	6975		3.027	583	23.5	90.34
9	9.32	215.000	32	12932	6513	6957	13	3.04	583	23	90.43
	9.41	215.000	41	12941	6492	6956		3.024	583	23	90.48
	11.58	217.000	58	13078	6480	6944		3.023	583	23.1	90.21
	14.52	220.000	52	13252	6471	6935		3.034	583	23.3	90.16
	8.03	238.000	3	14283	6406	6870		3.036	580	23.3	90.44
10	9.23	239.000	23	14363	6405	6869	14	3.022	580	23.5	90.41
	9.32	239.000	32	14372	6384	6869		3.032	580	23.5	90.2
	11.02	241.000	2	14462	6377	6862		3.032	580	23.5	90.47
	13.39	243.000	39	14619	6376	6861		3.032	580	23.7	90.54
11	10.10	264.000	10	15850	6315	6800	15	3.039	576	23.7	90.23
	10.20	264.000	20	15860	6297	6799		3.023	576	23.7	90.38
12	9.52	287.000	52	17272	6211	6713	16	3.034	572	23.4	90.62
	10.03	288.000	3	17283	6190	6712		3.019	572	23.5	90.51
13	6.00	308.000	0	18480	6136	6658		3.034	569	22.8	90.25
	9.24	311.000	24	18684	6119	6641	17	3.035	569	22.6	90.44

Measurements of 0 g/l $ZnSO_4$ experiment

Day	Time	Hours	Minutes	Total Minutes	Container Pressure mbar	Corrected due sample mbar	Sample number	Reactor pressure bar	Redox potential mV	Reactor Temp. °C
0	13.50	0	0	0	9785	9785		-0.582	339	80
	13.51	0.01666667	1	1	9538	9538		1.027	336	80
	13.55	0.08333333	5	5	9568	9568	1	0.966	342	80
	14.02	0.2	12	12	9561	9569		1.02	342	80
	14.07	0.28333333	17	17	9560	9568		1.017	352	80
	14.13	0.38333333	23	23	9553	9561		1.012	360	81
	14.24	0.56666667	34	34	9553	9561		1.012	365	82
	14.27	0.61666667	37	37	9551	9559	2	1.011	366	82
	14.30	0.66666667	40	40	9542	9558		0.952	367	82
	14.42	0.86666667	52	52	9537	9553		1.009	369	83.5
	14.59	1	9	69	9525	9541	3	1.002	371	84.5
	15.02	1	12	72	9512	9539		0.939	371	84.5
	15.24	1	34	94	9491	9518		1.001	375	85
	15.40	1	50	110	9476	9503		1.001	377	85.32
	16.00	2	10	130	9458	9485	4	1.001	379	85.7
	16.10	2	20	140	9440	9476		1.003	382	85.8
	17.00	3	10	190	9397	9433	5	1.001	386	86.43
	17.10	3	20	200	9385	9425		1	387	86.5
	18.00	4	10	250	9342	9382	6	0.996	394	86.6
	18.10	4	20	260	9329	9374		1.004	394	86.7
	19.01	5	11	311	9289	9334		1.001	402	86.89
	20.00	6	10	370	9241	9286	7	1.001	409	87
	20.07	6	17	377	9228	9280		0.998	410	87.17
	23.00	9	10	550	9090	9142	8	0.997	425	87.36
	23.03	9	13	553	9080	9140		0.996	426	87.3
	23.12	9	22	562	9073	9133		1.002	426	87.222
	2.00	12	10	730	8957	9017	9	1	440	87.46
	2.04	12	14	734	8946	9014		0.995	440	87.48
1	6.59	17	9	1029	8749	8817	10	0.997	456	87.62
	7.06	17	16	1036	8735	8812		0.997	455	87.51
	10.50	21	0	1260	8615	8692		0.996	470	87.58
	12.25	22	35	1355	8548	8625		0.997	472	87.56
	15.25	25	35	1535	8422	8499		0.99	478	87.51
	17.40	27	50	1670	8353	8430		0.991	483	87.72
	18.30	28	40	1720	8326	8403	11	0.989	485	87.75
	18.35	28	45	1725	8312	8400		0.992	485	87.69
2	7.19	41	29	2489	7794	7882	12	0.995	511	87.83
	7.28	41	38	2498	7782	7876		0.992	511	87.94
	11.25	45	35	2735	7628	7722		0.993	518	87.66
	11.40	45	50	2750	7606	7700		0.993	518	87.93
	13.50	48	0	2880	7541	7635		0.99	520	87.65
	16.35	50	45	3045	7450	7544	13	0.986	528	87.99
	16.50	51	0	3060	7431	7536		0.99	525	88.02
	9.02	67	12	4032	6848	6953	14	0.99	550	88.06
3	9.20	67	30	4050	6829	6944		0.992	549	88.11
	13.17	71	27	4287	6706	6821		0.993	554	88.15
	13.44	71	54	4314	6692	6807		0.995	560	87.89
	14.17	72	27	4347	6679	6794		0.998	556	88.06
	15.06	73	16	4396	6657	6772		0.987	556	88.02
	16.31	74	41	4481	6617	6732		0.993	558	88.12
	17.33	75	43	4543	6587	6702		0.99	559	88.03
	17.54	76	4	4564	6577	6692		0.997	564	88.06
	18.54	77	4	4624	6552	6667		0.995	565	88.18
	19.30	77	40	4660	6536	6651		0.999	567	87.97
	20.27	78	37	4717	6511	6626		0.999	567	88.09
4	11.31	93	41	5621	6200	6315	15	0.994	578	88
	11.50	94	0	5580	6191	6325		1.001	578	88
5	7.08	113	18	6798	5978	6112		0.994	604	88.06
	10.16	116	26	6986	5961	6095	16	0.997	608	87.93
	10.36	116	46	7006	5952	6089		0.986	606	88.07
	10.58	117	8	7028	5945	6082		0.997	607	87.74
	12.38	118	48	7128	5929	6066		0.993	608	87.79
	13.50	120	0	7200	5914	6051		1	609	88.05
	16.31	122	41	7361	5893	6030		0.989	606	88
	18.04	124	14	7454	5883	6020		0.989	608	88
6	7.55	138	5	8285	5761	5898		0.997	626	88
	9.42	139	52	8392	5763	5900	17	0.994	626	88
	9.57	140	7	8407	5755	5899		0.976	619	88
	12.50	143	0	8580	5730	5874		0.999	628	88
	14.30	144	40	8680	5719	5863	18	0.997	629	88
	14.50	145	0	8700	5710	5860		0.98	622	88

Measurements of 60 g/l $ZnSO_4$ experiment

Time	Hours	Minutes	Total Minutes	Container Pressure mbar	Corrected due sample mbar	Sample number	Reactor pressure bar	Redox potential mV	Reactor Temp. °C
9.05	0.00	0	0	9908	9908		-0.462	345	84
9.07	0.00	2	2	9705	9705		1.179	345	84
	0.05	3	3	9715	9715	1	1.163	346	84
	0.08	5	5	9715	9722		1.098	346	84
	0.12	7	7	9716	9723		1.111	347	84
	0.15	9	9	9718	9725		1.099	348	84
	0.20	12	12	9719	9726		1.093	349	84
	0.30	18	18	9720	9727		1.095	351	84
	0.42	25	25	9721	9728		1.096	352	84.5
	0.50	30	30	9722	9729	3	1.093	353	85.3
	0.67	40	40	9723	9731		1.02	353	86.3
	0.92	55	55	9722	9730		1.013	351	88.1
	1	0	60	9721	9729		1.012	351	88.3
	1	5	65	9718	9726		1.009	349	88.45
	1	22	82	9713	9721		1.007	346	88.41
	1	30	90	9709	9717	4	1.006	344	88.31
	1	42	102	9692	9711		1.03	341	88.2
	1	50	110	9691	9710		1.036	339	88.19
12.00	2	55	175	9671	9690		0.989	303	89.6
12.05	3	0	180	9665	9684	4	1.01	298	89.6
12.13	3	8	188	9653	9679		1.015	291	89.12
12.22	3	17	197	9652	9678		1.01	285	89
12.30	3	25	205	9652	9678		1.011	279	89.6
12.40	3	35	215	9651	9677		1	275	90.21
12.52	3	47	227	9647	9673		0.988	269	90.45
13.00	3	55	235	9643	9669		0.986	268	90.54
13.15	4	10	250	9636	9662		0.984	265	90.37
13.25	4	20	260	9631	9657		0.984	265	90
13.41	4	36	276	9623	9649		0.993	264	89.57
14.00	4	55	295	9615	9641		1.004	263	90.19
14.18	5	13	313	9610	9636		0.994	260	90.8
14.33	5	28	328	9605	9631		0.986	259	90.8
14.59	5	54	354	9593	9619		0.984	260	90
15.11	6	6	366	9588	9614	5	0.992	260	90
15.20	6	15	375	9579	9612		1.008	260	90
15.42	6	37	397	9577	9610		1.005	257	91
15.58	6	53	413	9573	9606		0.994	254	91
16.17	7	12	432	9567	9600		0.989	250	91
20.00	10	55	655	9525	9558	6	1.021	246	91
20.10	11	5	665	9522	9556		0.984	246	91
20.40	11	35	695	9512	9546		0.988	247	91
6.10	21	5	1265	9414	9448	7	1.016	253	91
6.20	21	15	1275	9407	9447		0.992	252	91
7.40	22	35	1355	9400	9440		1.025	253	91
9.05	24	0	1440	9399	9439		1.01	254	90.7
10.18	25	13	1513	9392	9432		1.007	256	90.2
11.25	26	20	1580	9387	9427		0.971	253	90.2
12.16	27	11	1631	9381	9421		0.99	254	91
14.05	29	0	1740	9364	9404		0.973	253	
15.03	29	58	1798	9360	9400		0.994	255	90
16.56	31	51	1911	9344	9384	8	0.97	255	
17.05	32	0	1920	9328	9382		0.993	257	
5.30	44	25	2665	9195	9249	9	0.97	262	
5.40	44	35	2675	9184	9248		0.983	263	
8.05	47	0	2820	9178	9242		0.986	269	
9.47	48	42	2922	9169	9233		0.97	266	
11.00	49	55	2995	9160	9224		0.972	267	
12.05	51	0	3060	9152	9216		0.986	271	
13.00	51	55	3115	9139	9203		1.004	270	
13.45	52	40	3160	9135	9199		0.97	270	
14.05	53	0	3180	9130	9194		0.965	292	
14.25	53	20	3200	9128	9192		0.992	295	90
14.40	53	35	3215	9125	9189		0.984	294	
15.00	53	55	3235	9120	9184		0.966	301	
16.05	55	0	3300	9102	9166	10	0.986	316	
16.15	55	10	3310	9092	9164		0.972	308	
8.40	71	35	4295	8779	8851	11	0.988	323	
8.50	71	45	4305	8773	8849		0.98	329	
9.30	72	25	4345	8760	8836		0.972	331	
15.00	77	55	4675	8664	8740		0.97	335	
11.37	98	32	5912	8277	8353	12	0.983	375	91

Measurements of 100 g/l $ZnSO_4$ experiment

Time	Hours	Minutes	Total Minutes	Container Pressure mbar	Corrected due sample mbar	Sample number	Reactor pressure bar	Redox potential mV	Reactor Temp. °C
10.00	0.000	0	0	9677	9677		0.991	345	82.6
10.02	0.033	2	2	9496	9496		1.017	345	82.88
	0.117	7	7	9494	9494		1.013	347	83.25
	0.167	10	10	9493	9493		1.009	346	83.54
	0.333	20	20	9489	9489		1.004	342	84
	0.417	25	25	9487	9487		1.004	337	84.28
	0.583	35	35	9485	9485		1.001	326	84.52
	0.700	42	42	9484	9484		1.005	313	84.63
	0.867	52	52	9494	9494		1.017	263	84.92
	0.950	57	57	9495	9495	1	1.016	235	85.29
11.03	1	3	63	9494	9494		1.013	221	85.69
	1	21	81	9466	9491		1.006	207	86.42
	1	53	113	9458	9483	2	1.021	210	86.95
13.01	3	1	181	9455	9480		1.003	213	88.35
13.16	3	16	196	9447	9479		0.981	210	88.81
15.23	5	23	323	9427	9459		0.984	214	89.78
	5	53	353	9414	9446	3	1.033	217	89.36
17.01	7	1	421	9411	9443		0.980	216	89.38
	7	20	440	9394	9441		1.017	214	89.8
6.15	20	15	1215	9256	9303		1.002	211	90.4
9.28	23	28	1408	9234	9281	4	1.002	211	90.26
9.53	23	31	1411	9232	9279		0.986	213	90.08
10.07	24	7	1447	9221	9278		1.005	215	89.79
12.30	26	30	1590	9201	9258		1.014	213	90.05
15.24	29	24	1764	9183	9240		1.002	215	89.8
16.21	30	21	1821	9179	9236	5	0.992	211	89.96
6.30	44	30	2670	9113	9170		1.018	205	89.9
9.45	47	45	2865	9112	9177		1.020	203	89.98
10.10	48	10	2890	9110	9175		0.989	203	89.9
14.10	52	10	3130	9096	9161	6	1.022	202	90.2
15.41	77	41	4661	9075	9140		1.028	164	90.4
15.55	77	55	4675	9072	9145		0.975	166	90.17
14.08	100	8	6008	9052	9125	7	1.099	132	90.5
14.2	100	20	6020	9052	9133		1.049	130	90.5
8.48	118	48	7128	9040	9121		1.171	99	90.77
9.36	119	36	7176	9040	9121	8	1.198	100	90.93
9.50	119	50	7190	9039	9120		1.000	100	90.93
13.02	123	2	7382	9042	9123		1.045	96	90.78
14.16	124	16	7456	9043	9124		1.043	98	90.85
6.25	140	25	8425	9063	9144		1.300	87	92.5
9.07	143	7	8587	9062	9143	9	1.309	86	92.36
9.21	143	21	8601	9062	9143		1.022	87	92.8
12.00	146	0	8760	9064	9145		0.999	89	90.43
13.25	147	25	8845	9065	9146		0.997	86	90.28
13.43	147	43	8863	8693	8774		3.055	233	90.13
13.52	147	52	8872	8692	8773		3.045	232	90.23
15.02	149	2	8942	8674	8755		3.026	232	90.13
16.15	150	15	9015	8650	8731	10	3.037	237	89.8
9.57	167	57	10077	8277	8358		3.022	244	89.9
10.11	168	11	10091	8253	8355		3.026	249	89.95
13.24	171	24	10284	8189	8291		3.017	247	89.95
16.26	174	26	10466	8117	8219	11	3.012	260	89.77
11.44	193	44	11624	7678	7780		3.009	255	89.82
11.57	193	57	11637	7649	7775		3.021	255	89.82
16.52	198	52	11932	7524	7650	12	3.008	261	89.65
11.04	217	2	13022	7083	7209		2.998	261	89.78
11.15	217	15	13035	7048	7203		3.028	261	89.63
12.02	218	2	13082	7028	7183		3.002	263	89.7
14.42	220	42	13242	6954	7109	13	3.007	263	89.58
11.20	241	20	14480	6432	6587		3.011	263	90
11.32	241	32	14492	6409	6582		3.015	268	89.92
18.30	272	30	16350	5624	5797	14	3	276	89.8
18.45	272	45	16365	5599	5791		3.009	279	89.8
6.00	284	0	17040	5322	5514		3.013	276	90
10.04	288	4	17284	5215	5407	15	3.015	276	89.65
10.16	288	16	17296	5194	5402		3.001	279	89.55

Measurements of process solution 1 experiment

Time	Hours	Minutes	Total Minutes	Container Pressure mbar	Corrected due sample mbar	Reactor pressure bar	Redox potential mV	pH	Reactor Temp. °C
10.06	0.000	0	0	9791	9791	-0.491	395	-0.4	52
10.08	0.033	2	2	9480	9480	1.110	395	-0.4	52
10.09	0.050	3	3	9483	9483	1.105	395	-0.4	52
10.10	0.067	4	4	9496	9496	1.108	395	-0.4	52
10.11	0.083	5	5	9510	9510	1.109	395	-0.4	52
10.12	0.100	6	6	9513	9513	1.108	395	-0.4	52
10.14	0.133	8	8	9515	9515	1.107	395	-0.44	52
10.16	0.167	10	10	9516	9516	1.106	394.5	-0.44	52
10.29	0.383	23	23	9517	9517	1.097	394	-0.44	52
10.36	0.500	30	30	9518	9518	1.093	394	-0.45	52
10.40	0.567	34	34	9518	9518	1.090	394	-0.45	52
10.45	0.650	39	39	9518	9518	1.087	394	-0.44	52
10.50	0.733	44	44	9518	9518	1.050	393.5	-0.45	51.7
10.56	0.833	50	50	9518	9518	1.049	393	-0.45	
11.06	1.000	0	60	9518	9518	1.048	393	-0.44	51.5
11.45	1.000	39	99	9513	9513	1.060	393	-0.45	51.5
12.31	2.000	25	145	9510	9510	1.051	387	-0.44	52.2
13.09	3.000	3	183	9507	9507	1.040	391	-0.44	52
14.13	4.000	7	247	9500	9500	1.052	392	-0.43	51.4
15.06	5	0	300	9497	9497	1.048	385	-0.43	52.3
16.10	6	4	364	9490	9490	1.035	388	-0.42	
16.38	6	32	392	9487	9487	1.042	387	-0.42	
20.36	10	30	630	9472	9472	1.038	384	-0.42	
6.30	20	24	1224	9425	9425	1.035	379	-0.42	
8.30	22	24	1344	9431	9431	1.040	375	-0.42	
10.21	24	15	1455	9438	9438	0.017	370	-0.58	70
10.25	24	19	1459	9270	9270	1.069	367	-0.59	70.7
10.27	24	21	1461	9274	9274	1.070	370	-0.59	
10.30	24	24	1464	9276	9276	1.072	368	-0.59	71.3
10.42	24	36	1476	9276	9276	1.076	367	-0.6	71.9
10.46	24	40	1480	9276	9276	1.069	369	-0.6	71.96
11.00	24	54	1494	9274	9274	1.056	371	-0.61	71.85
11.15	25	9	1509	9272	9272	1.042	371	-0.61	71.77
11.30	25	24	1524	9269	9269	1.029	371	-0.61	71.27
11.46	25	40	1540	9268	9268	1.033	370	-0.61	71.02
12.00	25	54	1554	9268	9268	1.028	366	-0.6	71.02
13.00	26	54	1614	9264	9264	1.035	370	-0.61	70.28
14.00	27	54	1674	9260	9260	1.022	371	-0.61	70.37
14.09	28	3	1683	9259	9259	1.025	371	-0.61	70.17
16.06	30	0	1800	9250	9250	1.035	368	-0.61	70.79
5.00	43	54	2634	9179	9179	1.015	369	-0.6	70.34
5.15	44	9	2649	9175	9175	1.027	367	-0.6	71.09
7.45	46	39	2799	9197	9197	0.213	366	-0.66	82.7
9.44	48	38	2918	9195	9195	0.285	368	-0.71	88.6
9.48	48	40	2920	9195	9195	0.023		-0.71	88.6
9.51	48	45	2925	9031	9031	1.116	366	-0.72	88.78
9.54	48	48	2928	9040	9040	1.117	364	-0.72	88.8
10.00	48	54	2934	9041	9041	1.107	363	-0.72	89
10.15	49	9	2949	9040	9040	1.092	359	-0.73	89.64
10.30	49	24	2964	9040	9040	1.081	364	-0.72	89.72
10.45	49	39	2979	9039	9039	1.086	363	-0.72	89.99
11.00	49	52	2992	9039	9039	1.076	357	-0.71	90.32
11.48	49	42	2982	9037	9037	1.037	358	-0.73	90.37
13.03	50	57	3057	9030	9030	1.027	352	-0.74	90.57
13.50	51	44	3104	9024	9024	1.035	347	-0.79	90.23
14.17	52	11	3131	9022	9022	1.019	343	-0.75	90.52
18.04	55	58	3358	9000	9000	1.031	328	-0.75	90.27
12.06	74	0	4440	8927	8927	1.006	313	-0.75	90.52
12.45	74	39	4479	8922	8922	1.018	315	-0.76	90.44
12.57	74	51	4491	8910	8910	1.025	313	-0.75	90.47
13.45	99	39	5979	8742	8742	1.016	306	-0.72	89.85
13.56	99	50	5990	8588	8588	2.002	309	-0.74	90.37
14.12	100	6	6006	8590	8590	2.021	316	-0.74	90.1
14.37	100	31	6031	8578	8578	2.075	315	-0.76	90.6
14.40	100	34	6034	8577	8577	2.078	315	-0.76	90.6
21.11	107	5	6425	8502	8502	2.068	320	-0.71	90.38
21.24	107	18	6438	8499	8499	2.072	323	-0.74	90.17
12.34	122	28	7348	8337	8337	2.065	325	-0.7	90.47
12.40	122	34	7354	8185	8185	3.029	327	-0.71	90.47
12.57	122	51	7371	8191	8191	3.033	330	-0.72	90.47
13.22	123	16	7396	8189	8189	3.008	329	-0.69	90.76

Measurements of process solution 2 experiment

Time	Hours	Minutes	Total Minutes	Container Pressure mbar	Corrected due sample mbar	pH	Reactor pressure bar	Redox potential mV	Room Temp. °C	Reactor Temp. °C
13.00	0.000	0	0	9836	9836	-0.15	0.000	460	49	22.4
13.01	0.017	1	1	9571	9571	-0.16	1.112	459	49	22.4
13.04	0.067	4	4	9580	9580	-0.15	1.109	459	49	22.4
13.26	0.433	26	26	9583	9583	-0.16	1.097	459	49.8	22.4
13.57	0.950	57	57	9583	9583	-0.15	1.081	459	50.3	22.4
14.42	1	42	102	9583	9583	-0.16	1.073	459	50.8	22.4
15.13	2	13	133	9583	9583	-0.16	1.065	460	52	22.4
16.23	3	23	203	9583	9583	-0.16	1.022	460	52	22.3
8.41	19	41	1181	9520	9520	-0.16	1.033	462	53.5	22.8
11.14	22	14	1334	9503	9503	-0.28	1.037	461	51.9	22.4
16.32	27	32	1652	9470	9470	-0.19	1.040	462	51.6	22.1
5.31	40	31	2431	9430	9430	-0.2	1.033	463	51.34	22.5
7.13	42	13	2533	9425	9425	-0.38	1.028	465	70.2	22.5
8.19	43	19	2599	9424	9424	-0.42	1.038	465	75.05	22.5
9.44	44	44	2684	9414	9414	-0.38	1.007	465	72.4	22.6
14.18	49	18	2958	9380	9380	-0.38	1.018	465	71.1	22.4
8.58	67	58	4078	9300	9300	-0.39	1.001	466	70.4	22.9
11.06	70	6	4206	9297	9297	-0.45	1.021	462	87.87	23
12.07	71	7	4267	9300	9300	-0.5	1.065	457	88.3	23.1
13.06	72	6	4326	9297	9297	-0.48	1.041	455	88.8	22.8
14.24	73	24	4404	9290	9290	-0.54	1.020	452	88.9	22.7
15.31	74	31	4471	9284	9284	-0.54	1.004	452	89.2	22.6
16.57	75	57	4557	9275	9275	-0.54	1.011	451	89.2	22.4
7.36	90	36	5436	9216	9216	-0.65	0.995	441	89.1	23
8.44	91	44	5504	9216	9216	-0.61	0.999	442	88.9	23
8.54	91	54	5514	9075	9075	-0.61	2.036	442	89	22.5
9.44	92	44	5564	9078	9078	-0.61	2.038	443	89.1	23
11.11	94	11	5651	9068	9068	-0.61	2.048	443	89.5	23
13.00	96	0	5760	9049	9049	-0.62	2.040	443	89.1	23
14.30	97	30	5850	9037	9037	-0.58	2.035	443	89.57	23
16.56	99	56	5996	9015	9015	-0.61	2.027	443	89.37	23
13.08	120	8	7208	8869	8869	-0.64	2.048	449	89.32	22.5
13.17	120	17	7217	8715	8715	-0.63	3.024	449	89.32	22.5
13.37	120	37	7237	8730	8730	-0.7	3.022	448	89.32	22.5
20.03	151	3	9063	8364	8364	-0.68	3.021	459	89.44	22.9
8.34	163	34	9814	8163	8163	-0.65	2.996	463	89.91	23.3
8.43	163	43	9823	8160	8160	-0.66	2.993	463	89.91	23.3
10.34	165	34	9934	8142	8142	-0.658	3.015	464	89.88	22.5
13.00	168	0	10080	8111	8111	-0.69	2.999	463	89.79	22.5
14.08	169	8	10148	8097	8097	-0.69	2.999	462	89.79	22.5
16.04	171	4	10264	8077	8077	-0.69	3.017	462	89.79	22.5
7.30	186	30	11190	7888	7888	-0.69	3.002	462	92	22.8
8.06	187	6	11226	7881	7881	-0.7	2.997	462	89.6	23.1
11.30	190	30	11430	7797	7797	-0.71	2.997	462	89	
12.53	191	53	11513	7794	7794	-0.71	3.028	463	89	
6.30	209	30	12570	7583	7583	-0.7	2.995	463	89	
9.41	212	41	12761	7554	7554	-0.7	2.993	464	89	
15.10	218	10	13090	7479	7479	-0.73	2.997	466		
17.04	220	4	13204	7455	7455	-0.73	3.010	468		
6.27	233	27	14007	7289	7289	-0.73	2.997	469	89.2	
14.54	241	54	14514	7180	7180	-0.75	3.02	471		
15.06	242	6	14526	7140	7140	-0.77	3.011	472		
6.10	257	10	15430	6937	6937	-0.76	3.005	473	90	
12.00	263	0	15780	6878	6878	-0.83	3.017	478	94	
15.45	266	45	16005	6830	6830	-0.75	2.995	476	91	
13.00	288	0	17280	6557	6557	-0.83	2.993	480	90	
13.10	288	10	17290	6529	6529	-0.83	3.007	480	90	
11.47	310	47	18647	6233	6233	-0.89	2.995	489	89.56	
12.02	311	2	18662	6183	6183	-0.87	3	489		
6.45	329	45	19785	5940	5940	-0.9	2.996	498		
7.00	330	0	19800	5908	5908	-0.9	3.001	498		

Sample analysis of standard 200 RPM experiment

Sample	Time Hour	Solid g	Liquid ml	Conc. g/l	pH	Zinc mg/l	Iron mg/l
1	0.5	3.13	190	16	0.38	92664	8920
2	2	5.01	232	22	0.35	90200	8567
3	5	4.62	220	21	0.32	100675	9258
4	7	4.42	210	21	0.31	98601	8906
5	11	3.75	198	19	0.30	99454	8973
6	25	4.35	200	22	0.29	99258	8921
7	50	4.17	230	18	0.28	100434	8928
8	73	2.99	185	16	0.33	95928	8650
9	96	3.74	228	16	0.33	103044	9000
10	120	3.79	225	17	0.35	103793	9171
11	144	3.34	220	15	0.34	100708	9081
12	168	2.44	185	13	0.37	102802	8963
13	192	2.72	190	14	0.38	103595	9176
14	217	3.21	197	16	0.41	102171	9504
15	248	2.34	183	13	0.40	98292	9154
16	264	2.82	212	13	0.41	101636	9598

Sample analysis of ethanol 1.5% experiment

Sample	Time hour	Solid g	Liquid ml	Conc. g/l	pH	Zinc mg/l	Iron mg/l
1	0.5	3.69	187	20	0.45	93821	8836
2	1.67	4.78	210.00	23	0.35	92091	8713
3	4.17	4.52	206.00	22	0.30	95538	8985
4	8.17	3.31	200.00	17	0.33	94964	8699
5	23.00	4.68	156.00	30	0.31	92432	8613
6	44.00	4.65	177.00	26	0.29	96429	8929
7	70.00	4.18	160.00	26	0.27	96275	8789
8	95.00	4.58	200.00	23	0.26	96624	8908
9	119.00	2.72	144.00	19	0.28	93811	8488
10	144.00	3.83	170.00	23	0.30	96186	8610
11	168.00	3.60	200.00	18	0.31	103997	9421
12	192.00	3.46	212.00	16	0.35	98901	9536
13	216.00	4.49	180.00	25	0.39	97008	9399
14	237.00	2.64	147.00	18	0.39	96818	9271
15	262.00	2.70	145.00	19	0.41	95813	9187
16	288.00	3.01	166.00	18	0.39	99479	9610
17	311.00	3.03	175.00	17	0.39	100341	9747
18	335.00	3.37	190.00	18	0.40	100301	9509
19	357.00	3.99	212.00	19	0.40	100634	9615

Sample analysis of octhene 1.5% experiment

Sample	Time hour	Solid g	Liquid ml	Conc. g/l	pH	Zinc mg/l	Iron mg/l
1	0.567	3.84	215	18	0.46	93152	9280
2	1.47	3.92	208	19	0.46	90932	8819
3	3.42	3.47	179	19	0.50	91647	8846
4	6	3.56	167	21	0.44	92961	9082
5	25	3.71	191	19	0.48	93039	8985
6	49	2.87	186	15	0.49	95862	9106
7	70	2.98	175	17	0.50	96132	9314
8	95	2.72	178	15	0.52	96298	9139
9	119	2.41	176	14	0.54	94949	9167
10	143	2.42	180	13	0.56	93906	9331
11	167	1.95	190	10	0.60	92160	8881
12	222	1.86	180	10	0.59	99629	9853
13	239	1.61	186	9	0.62	97414	9831
14	263	1.41	190	7	0.68	96855	9737
15	287	0.96	170	6	0.68	98895	9483
16	311	0.81	175	4.63	0.68	96516	9037
17	333	0.82	185	4.43	0.58	97433	9580

Sample analysis of 2% SO_2 experiment

Sample	Time hour	Solid g	Liquid ml	Conc. g/l	pH	Zinc mg/l	Iron mg/l
1	0.5	4.0	219	18.26	0.41	88316	8768
2	2	3.8	195	19.38	0.43	86980	8695
3	5	3.9	202	19.06	0.49	89477	8926
4	6	3.9	215	18.19	0.42	91114	8973
5	3	3.7	199	18.54	0.44	90806	8797
6	52	3.9	223	17.49	0.46	88494	8617
7	71	3.9	232	16.85	0.45	90786	8983
8	95	3.5	220	15.68	0.50	92939	9029
9	121	3.1	216	14.40	0.54	90066	8986
10	146	2.7	197	13.86	0.50	92640	8970
11	167	2.7	215	8.19	0.49	96045	9439
12	195	1.8	143	14.90	0.56	90599	8791
13	236	2.1	175	13.89	0.55	93109	8855
14	263	2.4	216	9.17	0.55	100189	9386
15	288	2.0	220	8.00	0.64	97781	9312
16	318	1.8	200	8.80	0.64	98359	9209
17	336	2.0	199	10.05	0.62	98487	9455

Sample analysis of standard 250 RPM experiment

Sample	Time hour	Solid g	Liquid ml	Conc. g/l	Zinc mg/l	Iron mg/l
1	0.5	3.65	150	24	84119	9262
2	2.00	7.04	200	35	78670	9134
3	6.00	4.82	170	28	67507	8887
4	12.00	4.86	160	30	85976	8905
5	21.00	4.43	165	27	85881	8637
6	48.00	4.42	210	21	92550	9306
7	72.00	3.68	205	18	88309	8510
8	96.00	3.65	165	22	92978	8984
9	120.00	3.03	190	16	95750	9315
10	144.00	4.70	175	27	100367	9246
11	168.00	2.48	175	14	101284	9877
12	192.00	3.84	185	21	104699	10049
13	220.00	3.76	205	18	103117	10291
14	247.00	3.91	200	20	104014	10457
15	265.00	3.60	210	17	106287	10297

Sample analysis of ethanol 3% experiment

Sample	Time hour	Solid g	Liquid ml	Conc. g/l	pH	Zinc mg/l	Iron mg/l
1	0.5	3.7	138	27	0.09	87510	9194.66
2	2	3.70	230.00	16	0.12	91140	9447.11
3	5	3.00	170.00	18	0.15	89397	9442.66
4	11	3.50	196.00	18	0.14	91945	9364.67
5	23	3.50	175.00	20	0.14	91354	9708.18
6	47	3.50	205.00	17	0.15	91354	9451.16
7	73	3.00	174.00	17	0.14	92482	9627.29
8	93	2.00	160.00	13	0.16	91550	9552.84
9	124	2.00	145.00	14	0.19	94776	9373.06
10	144	2.80	168.00	17	0.20	95419	9923.87
11	168	2.50	184.00	14	0.21	96955	9470.82
12	192	2.40	169.00	14	0.23	95732	9627.31
13	210	2.40	179.00	13	0.23	97310	9957.55
14	240	2.20	200.00	11	0.25	93909	9988.40
15	288	2.30	155.00	15	0.27	96167	9403.88
16	311	2.20	213.00	10.33	0.26	100084	9796.40
17	336	2.00	195.00	10.26	0.27	96919	9213.03
18	361	1.50	208.00	7.21	0.27	96919	9473.79
19	383	2.00	185.00	10.81	0.28	100695	9388.63

Sample analysis of octhene 3% experiment

Sample	Time hour	Solid g	Liquid ml	Conc. g/l	pH	Zinc mg/l	Iron mg/l
1	1	3.47	185	18.8	0.03	100152	9528
2	2	4.59	205	22.4	0.04	95703	8732
3	4	3.90	185	21.1	0.05	95389	8721
4	7	3.83	180	21.3	0.05	96290	8730
5	22	4.81	235	20.5	0.05	103122	8815
6	47	4.77	222	21.5	0.06	101627	8785
7	72	4.46	215	20.7	0.08	100634	8817
8	95	2.70	156	17.3	0.08	98077	8527
9	118	2.96	144	20.6	0.09	93922	8557
10	143	3.45	195	17.7	0.09	103357	9079
11	167	3.33	195	17.1	0.09	104900	9366
12	191	3.08	194	15.9	0.1	101500	9516
13	215	2.61	195	13.4	0.09	102614	9647
14	239	2.89	185	15.6	0.1	105237	9856
15	264	2.20	193	11.4	0.1	101173	10233
16	287	2.11	200	10.6	0.11	104465	10210
17	311	1.51	185	8.2	0.04	106438	10423
18	312	1.40	187	7.5	0.05	103795	9847

Sample analyses of 0 g/l $ZnSO_4$ experiment

Sample	Time hour	Zinc mg/l	Iron mg/l	Sample	Time hour	Solid g	Liquid ml	Conc. g/l	pH
1	0.2	8098	248	1	0.2	1.41	0.15	0.106	0.15
3	1.2	10535	470	2	0.66	1.24	0.161	0.130	0.13
6	4.3	9931	1048	3	1.2	1.26	0.171	0.136	0.04
8	9.2	9017	1636	4	2.3	1.29	0.166	0.129	0.1
10	17.2	10114	2958	5	3.3	3.23	0.19	0.059	0.12
11	28.6	9987	4337	6	4.3	2.46	0.165	0.067	0.1
12	41.5	10287	6291	7	6.2	1.95	0.146	0.075	0.06
13	50.75	10370	7492	8	9.2	1.64	0.172	0.105	0.012
14	67.5	10579	8906	9	12.2	2.01	0.16	0.080	0.07
15	93.66	11425	9743	10	17.2	1.9	0.188	0.099	0.05
16	116.75	10723	10110	11	28.6	2.3	0.172	0.075	0.14
18	145	10951	9895	12	41.5	2.29	0.193	0.084	0.14
19	168	11074	9881	13	50.75	13.07	0.21	11.000	0.13
				14	67.5	2.4	0.214	0.089	0.17
				15	93.66	1.92	0.187	0.097	0.2
				16	116.75	1.63	0.222	0.136	0.2
				17	140.2	1.21	0.168	0.139	0.17
				18	145	1.21	0.211	0.174	0.22
				19	168	1.23	0.215	0.175	0.19

Sample analyses of 60 g/l $ZnSO_4$ experiment

Sample	Time hour	Zinc mg/l	Iron mg/l
1	0.05	55861	8579
2			
3	1	61088	9326
4	3	61951	9534
5			
6	10	63814	9951
7	21	65398	9061
8	31	66741	9430
9			
10	55	67096	9673
11	71	66343	9864
12	98	70800	9941
13	116	70133	9734
15	166	75104	10264
16	189	74967	10557
17	213	75699	11179
18	241	76027	10006

HELSINKI UNIVERSITY OF TECHNOLOGY DOCTORAL THESES IN MATERIALS AND EARTH SCIENCES

TKK-ME-DT-1 Ranki-Kilpinen, T.,
Sulphation of Cuprous and Cupric Oxide Dusts and Heterogeneous Copper Matte Particles in Simulated Flash Smelting Heat Recovery Boiler Conditions. 2004.

TKK-ME-DT-2 Söderberg, O.,
Novel Ni-Mn-Ga alloys and their Magnetic Shape Memory Behaviour, 2004.

TKK-ME-DT-3 Kaskiala, T.,
Studies on Gas-Liquid Mass Transfer in Atmospheric Leaching of Sulphidic Zinc Concentrates, 2005.

ISBN 951-22-7664-X
ISBN 951-22-7665-8 (electronic)
ISSN 1795-0074